NASA Contractor Report 182207

/

97772

LDV Measurements in an Annular Combustor Model

Dean A. Barron
Purdue University
West Lafayette, Indiana

September 1996

Prepared for
Lewis Research Center
Under Contract NAS3–24350

National Aeronautics and
Space Administration

LDV MEASUREMENTS IN AN ANNULAR COMBUSTOR MODEL

A Thesis
Submitted to the Faculty

of

Purdue University

by

Dean A. Barron

In Partial Fulfillment of the
Requirements for the Degree

of

Master of Science in Aeronautics and Astronautics

August 1986

ACKNOWLEDGEMENTS

The author would like to thank Dr. John P. Sullivan for being his major professor. His guidance and instruction during work on this project has been invaluable.

Thanks are also foregoing to Dr. S. N. B. Murthy and Dr. W. A. Gustafson for being on the authors advisory committee.

The help of the technical staff Bob Sanders, Bill Bader, Jack Davis, Dave Reagan, and Scott Kepner is thanked for its support along the way.

Special thanks are also in order for NASA Lewis and Diesel Allison for their development and funding of a very challenging and interesting project.

TABLE OF CONTENTS

APPENDIX

LIST OF FIGURES

Figure Page

Figure Page

Appendix Figure
Figure

ABSTRACT

Barron, Dean A., M.S.A.A., Purdue University, August 1986. LDV Measurements in an Annular Combustor Model. Major Professor: John P. Sullivan.

This thesis covers the design and setup of a LDV system used to take velocity measurements in an annular combustor model. The annular combustor model is of contemporary design using 60 degree flat vane swirlers, producing a strong recirculation zone. Detailed measurements are taken of the swirler inlet air flow and of the downstream enclosed swirling flow.

The laser system used is a two color, two component system set up in forward scatter. Detailed are some of the special considerations needed for LDV use in the confined turbulent flow of the combustor model.

LDV measurements in a single swirler rig indicated that the flow changes radically in the first duct height. After this, a flow profile is set up and remains constant in shape. The magnitude of the velocities gradually decays due to viscous damping.

INTRODUCTION

This research is conducted as part of the NASA Lewis Research Center HOST (Turbine Engine Hot Section Technology) program. As the desire to fly further and faster at greater economy is being pushed there is a need to enhance the efficiency, life, and maintenance costs of the turbine engine hot section. The goal of the program is to upgrade the total existing technology of the operating conditions of the hot section.

In the past, design of the combustor was primarily accomplished by trial and error. Recently there has been much emphasis on the need for improved numerical codes for the design of efficient combustors. For the development of improved computational codes there is a need for an experimentally obtained data base to be used as test cases for the accuracy of the computations. As part of this effort, this thesis deals with the set-up and development of an LDV system to obtain bench-mark quality velocity measurements of the flow interaction of primary jets in a confined swirling flow typical of that in the dome region of an annular combustor [6]. This is to establish the primary cold flow patterns to be used as a test for improved aerothermal modeling codes.

The flow interaction is the result of two primary sources. The first of these two sources is that of the annular swirler. In the combustor the highly swirling flow produces a toroidal region of reverse flow. This recirculation region has several beneficial aspects for combustion [4]. It provides for improved flame stability by recirculation of the hot gases near the jet exit. This recirculation and strong mixing near the exit promote shorter combustion chamber lengths. Also, with the recirculation and burning occurring in the central toroidal zone, hot gases are kept away from the walls.

The second source of air is the primary jets. This primary air aerodynamically alters the swirling flow as well as provides additional air for mixing and combustion.

The author's objective in this research is to construct the flow interaction rig and set up a two color, two component LDV system to take mean and RMS values of velocity. Also, laser measurements are to be taken in a single swirler rig with no primary air.

Chapter 1 deals with the design of the rig and its operation. This design is to incorporate the ability to take data with varying configurations of primary jet flow. Of interest is the ability to vary downstream location, number of jets, position relative to swirl axis, and mass flow ratio relative to the swirlers. Finally, the rig must be accessible with the laser for LDV measurements.

Chapter 2 details the LDV setup used. This system is to be a two color, two component system being able to measure all three components of velocity in the regions of interest in the flow.

The LDV data taken in the single swirler boundary condition rig is presented in chapter 3 with the summary and conclusions of the work done being presented in the final chapter.

CHAPTER 1

RIG DESIGN AND OPERATION

The design of the test rig is such that it adequately models the swirling, primary jet, and channel flow of a modern gas turbine annular combustor. Figure 1.1 is a cross section of the Allison 570-k annular combustor. Part of the design criterion is that the swirlers have large enough swirl numbers to produce a recirculation zone typically used as mixing areas in the combustor. Also it is required that the annular and primary jet flows be fully developed upon entry into the test section.

1.1 TEST SECTION

The test section is of rectangular cross-section [7.62 x 38.10 cm (3.0 x 15.0 in)] and extends 10 duct heights [76.2 cm (30.0 in)] downstream from the head plate. The top, bottom, and sides are constructed of glass and plexiglass to facilitate easy access with the laser. Figure 1.2 is an illustration of the test section geometry. Air is drawn into the test section through the swirlers and primary jets by a centrifugal fan.

Five swirlers are mounted to the front face. The center swirler region is that of interest for taking data. The two swirlers on either side of the center are to remove side-wall effects inherent to our model but not in an actual combustor.

To determine the effect of different jet configurations on the flow, the primary jets are to be located at various downstream locations and in different positions relative to the swirler axis. The different jet configurations are accomplished using replaceable upper and lower plates. Each of these 1.27 cm (0.5 in) thick plexiglass plates have holes drilled in them to accommodate the desired primary jet configurations. The various test configurations are illustrated in figures 1.3 and 1.4.

These tests are designed to determine the effect of jet downstream location, number of jets, mass flow ratio, and position relative to the swirl axis. Tests one and two are for the baseline configurations. Test 1 is that of just the annular flow and no swirl or jet flow. For this case the usual swirler is replaced with a dummy swirler having no vanes. Test 2 is that of swirl only and no jets. Tests 3, 4, and 7 are at 3.81 cm (1.5 in) downstream with varying number of jets and positions relative to the swirl axis. Tests 5, 6, 8, 9, and 10 are at 7.62 cm (3.0 in) downstream with varying number of jets and position relative to the swirl axis.

1.2 DESIGN OF SWIRLERS AND PRIMARY JETS

In the combustor it is desirable that the annular swirler produce a strong recirculation zone. This area of reverse flow holds the hot gases in the center of the chamber away from the liner. It also produces large amounts of fuel air mixing near the swirler exit and shortens the needed combustor length.

Each swirler consists of an actual swirler from the production of the Allison 570-k turboshaft gas turbine engine (figure 1.5). These are 60 degree angle flat vane swirlers with 12 vanes. They have an outer flow diameter of 3.706 cm (1.459 in) and inner flow diameter of 2.753 cm (1.084 in). For configuration 1, the normal swirler is replaced with a dummy swirler having no vanes.

A measure of the strength of the swirling flow produced is the swirl number. The most commonly accepted definition is [1,4]:

$$\text{Swirl Number } S = \frac{G_\phi}{G_x R_2} \qquad (1.1)$$

Where: G_ϕ = angular momentum flux
G_x = axial momentum flux
R_2 = outer radius of swirl generator

For vane swirlers the swirl number can be approximated by [1,5]:

$$S = \frac{2}{3}\left[\frac{1-(R_1/R_2)^3}{1-(R_1/R_2)^2}\right]\tan\theta \qquad (1.2)$$

Where: R_1 = inner flow radius
R_2 = outer flow radius
θ = swirler vane angle

From the geometry of the swirlers, and using equation (1.2), the swirl number is calculated to be 1.52. Swirl generators producing swirl numbers greater than 0.6 produce recirculation regions along the swirling axis near the exit [1,4]. It is expected that the swirlers used will produce a very strong recirculation region.

The annular swirler inlet tubes are made of stainless steel and have diameters equivalent to the flow diameters of the swirlers. Each inlet tube is 25 effective diameters 49.649 cm (9.547 in) long. Where the effective diameter is defined by:

$$D_E = \text{outer diameter} - \text{inner diameter}$$

Initially the swirlers were mounted at the end of the inlet annulus flush with the head plate. However, in doing some preliminary smoke flow visualization an unexpected flow phenomenon occurred (figure 1.6). The flow would leave the swirler and make a sharp 90° bend and hug the head plate all the way out to the side walls. At the side walls the flow would then proceed downstream. This phenomenon has also been observed by Gore and Ranz [3] when high degrees of swirl are generated flush with the orifice exit.

It was not believed that this type of flow profile accurately modeled the intended combustor flow. Therefore, the swirlers were recessed 0.635 cm (0.25 in) back from the head plate. The annulus with the recessed swirler is shown in figure 1.7.

The primary jets provide cool additional air for mixing and combustion with the swirling air. Each primary jet is made of stainless steel and is 25 diameters long. The diameters vary for the different configurations. The necessary jet diameters were determined using the required mass flow ratios and number of jets as given in figure 1.3. Referring to figure 1.8, the mass flow ratio is given by:

$$\frac{M_j}{M_S} = \frac{N_j \bar{V}_j (\pi/4) d_j^2}{N_S \bar{V}_S (A_t N_b)/N_b} \tag{1.3}$$

Imposing the condition that $\bar{V}_j$ is equal to $\bar{V}_S$ and solving (1.3) for d_j yields:

$$d_j = \sqrt{\frac{4 M_j N_S A_t}{\pi M_S N_j}} \tag{1.4}$$

From the geometry of the swirler A_t is 2.361 cm^2 (0.366 in^2). Thereby, the needed diameter for configurations 3 through 9 is 10.6 mm (0.418 in). The actual jet being used has an inner diameter of 10.92 mm (0.43 in) with an outer diameter of 12.7 mm (0.5 in). For configuration 10 the calculated diameter is 15.0 mm (0.591 in). Actual inner and outer diameters are 14.99 mm (0.591 in) and 19.05 mm (0.75 in) respectively. The primary jet is shown in figure 1.9.

To determine the losses through the rig a single swirler rig was built. This rig is shown in figure 1.10. Pressure taps were installed on the swirler annular pipe, primary jet, and main duct downstream of the mixing region. Velocity measurements were taken with a hot wire downstream of the mixing region before entrance into the plenum. From these measurements the loss coefficients were calculated for the primary jets, annular pipe, and swirler. A summary of the measured losses is shown in figure 1.11. In this figure K is the loss coefficient in reference to the mean annular or primary jet velocity. Also, the measured values of static pressure and test section velocity are indicated.

Using the loss coefficient of 11.78 for the annulus and swirler a pressure drop of 2.19 psi would be required to obtain a design velocity of 45.72 m/sec (150 ft/sec). For the primary jets a pressure drop of 1.20 psi would be required for a desired velocity of 91.44 m/sec (300 ft/sec) through the jets. Considering a configuration having four jets per swirler and using a conservative value of 2.0 psi, there is a required volume flow of 591 cfm through the test section. Therefore, a fan is needed that can maintain a 2 psi pressure drop in the test section with almost 600 cfm of flow. To meet this requirement a 30 hp Chicago turbo-pressure blower was selected.

1.3 MASS FLOW BALANCE SYSTEM

Throttle cones are used on the entrance of each swirler and primary jet to adjust the mass flow in each section. This is to ensure that there is a mass flow balance between all of the primary jets and all of the swirlers. Since pressure drop along the length of the inlet tubes is proportional to mass flow squared, a series of pressure taps were installed on each swirler and those jets used for tests 3 thru 9.

For the swirlers the first tap is set 5.08 cm (2.0 in) downstream of the annular entrance. The second is located at 21.59 cm (8.5 in). For the primary jets the taps are located at 3.175 cm (1.25 in) and 22.225 cm (8.75 in) downstream of the jet entrance. These pressure tap locations were chosen for maximum distance between the taps, for maximum measurable pressure difference, but still be within the geometric restrictions imposed by support brackets.

Calibration of the primary jet and annular pressure taps is achieved by taking pitot measurements in the individual pipes. Details of this procedure are presented in the appendix. The results of the mass flow calibration are shown in figures 1.12 and 1.13. Figure 1.12 is a plot of annular pressure drop across the taps versus annular mean velocity for standard atmospheric conditions. An equivalent plot for the primary jets is shown in figure 1.13.

During rig operation the mass flow and balance are monitored using an Apple III minicomputer. The Apple controls a scanivalve which continuously feeds the various pressure tap readings to a Datametrics 590 pressure transducer. Voltage readings from the pressure transducer are monitored by a Fluke 3340A multimeter and sent to the computer via a general purpose interface buss. The computer then sends the pressure tap readings to the console for display. Thus, continuous monitoring of the rig's operation is provided. This system is shown schematically in figure 1.14.

1.4 RIG CHECKOUT

To test the operation of the rig, jet configuration 9 was set up. Static pressure measurements were made in the test section and hot wire measurements were taken to determine the mean velocity in the test section. It was found that for this configuration the test section was operating at 1.48 psi with a bulk mean velocity of 20.65 ft/sec. This yields a volume flow of 387 cfm. The design velocities of 150 ft/sec through the annulus and 300 ft/sec through the primary jet should produce a volume flow of 410 cfm. Thus the bulk mass flow is very near design. However, this bulk flow is achieved at much lower pressure than the original calculations had indicated.

For the measured mean velocity given above, the test section bulk Reynolds number is calculated to be 55,000.

1.5 COM3D COMPUTATIONAL CODE

A three dimensional code called COM3D is used to get a preliminary idea of the flow profiles that are involved. This is used to determine areas of strong velocity gradients were measurements would want to be taken. The COM3D code is a Navier-Stokes tridiagonal solver utilizing the k-e model for turbulence.

The 32x25x25 grid that is used for configuration 9 is shown in figures 1.15 and 1.16. In the y and z directions the 25 nodal points are evenly spaced forming a uniform grid. The x axis nodal points are spaced closer together upstream and further apart downstream. The upstream points are spaced closer together to facilitate accurate computation in areas where there are large velocity gradients.

Figure 1.17 is a vector plot at a plane 1.7 inches from the swirler. The interaction of the swirling air and primary flow produce four circulation regions. At x=3.0 inches, figure 1.18, the flow is driven primarily by the primary jet flow, with a stagnation region being produced from the impingement of the two jets. Figure 1.19 is a plane at z=0.0 inches or along the plane of intersection between adjoining swirlers. The saddle produced by the impingement of the primary jet flows is clearly seen. Finally figure 1.20 is along the swirl axis. The presence of the primary jet flow terminates the length of the recirculation region and helps feed the flow reversal.

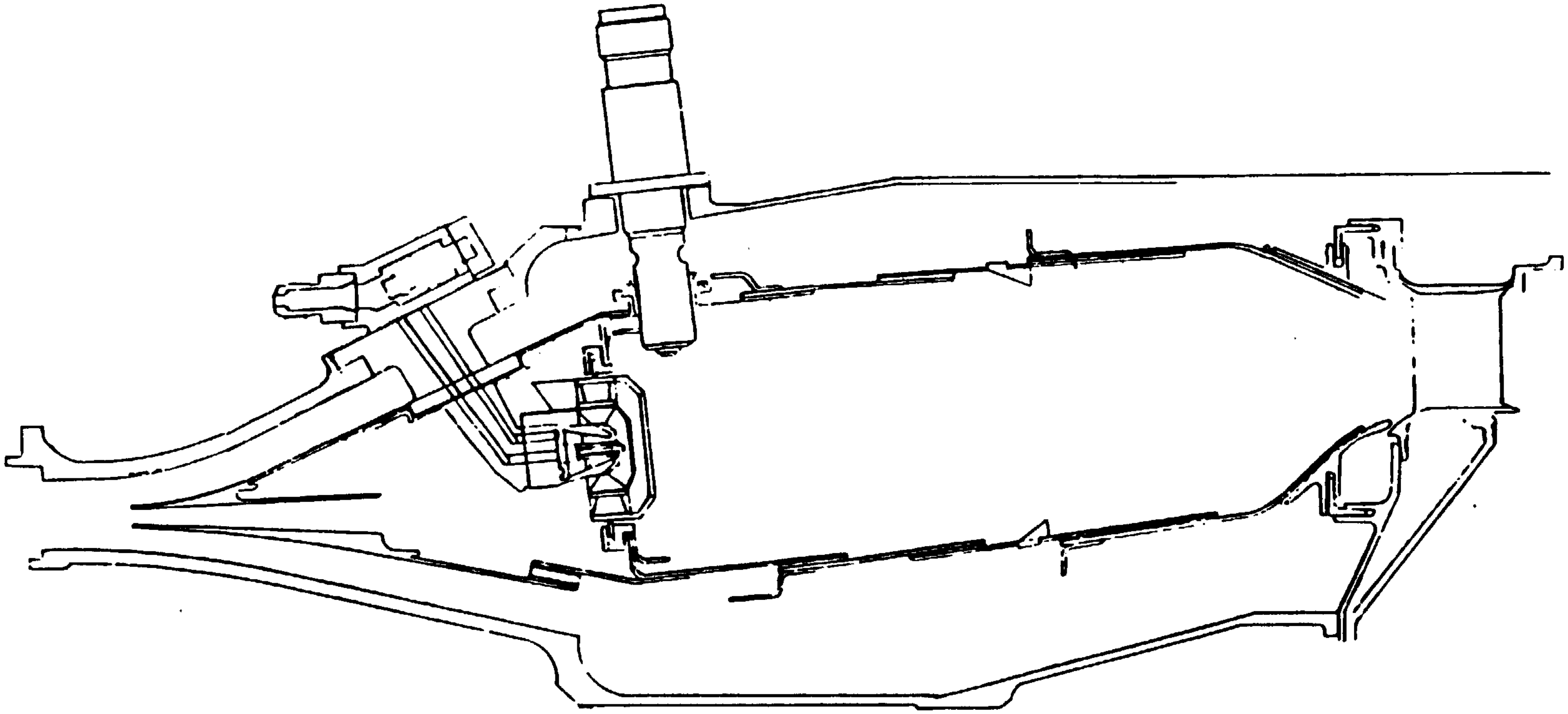

Figure 1.1 Cross Section of Allison's 570-k Annular Combustor

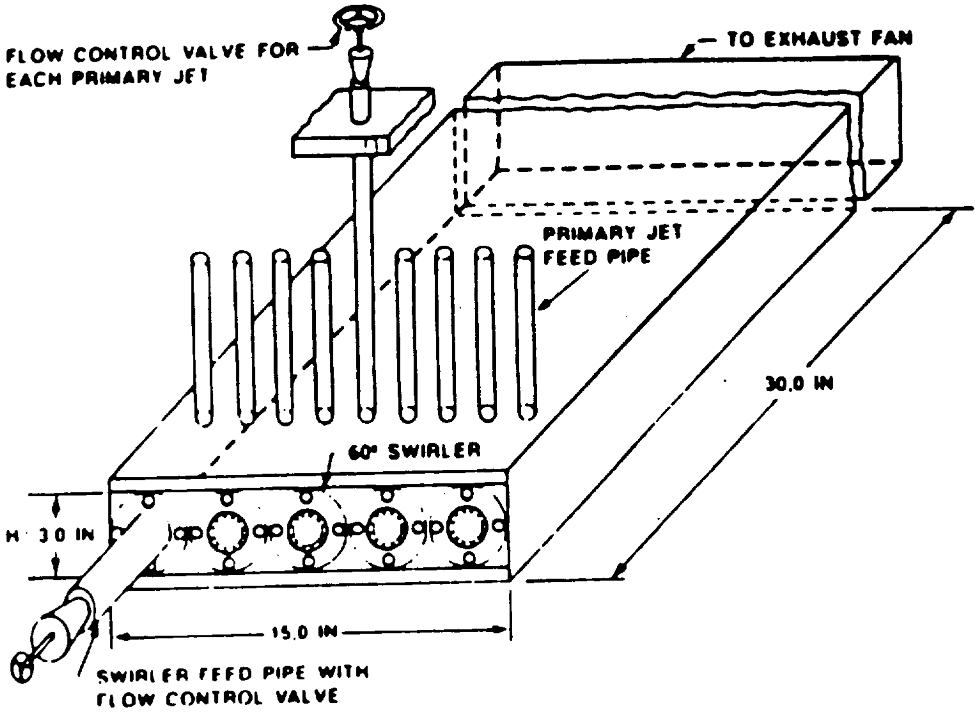

Figure 1.2 Test Section Geometry

TEST NO.	CONFIGURATION	$\frac{X_j}{h}$	$\frac{M_j}{M_s}$	$\frac{\text{JETS}}{\text{SWIRLER}}$	JET O.D. (inches)
1	BC1	-	-	-	-
2	BC2	-	-	-	-
3	C	0.5	1.5	4	0.5
4	D	0.5	1.5	4	0.5
5	D	1.0	1.5	4	0.5
6	C	1.0	1.5	4	0.5
7	A	0.5	0.75	2	0.5
8	B	1.0	0.75	2	0.5
9	A	1.0	0.75	2	0.5
10	A	1.0	1.5	2	0.75

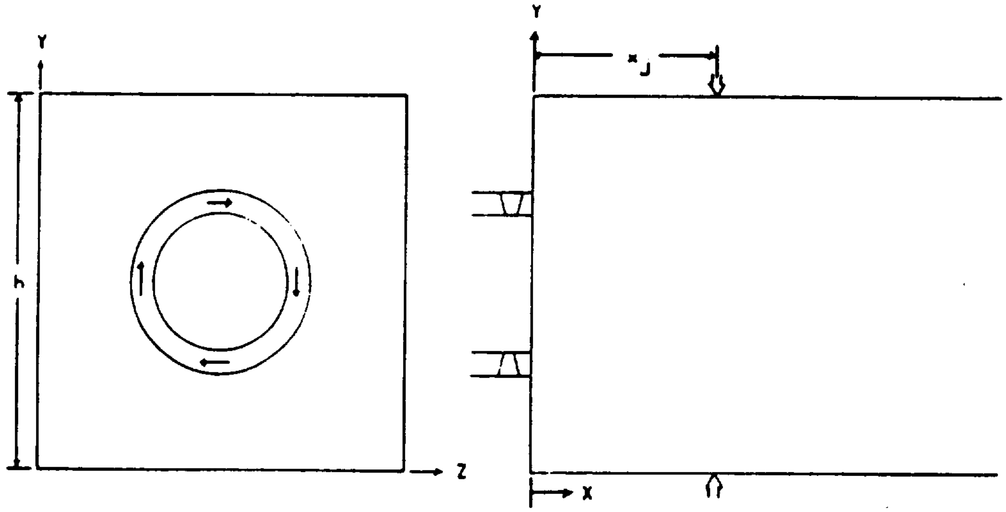

Figure 1.3 Primary Jet Test Matrix

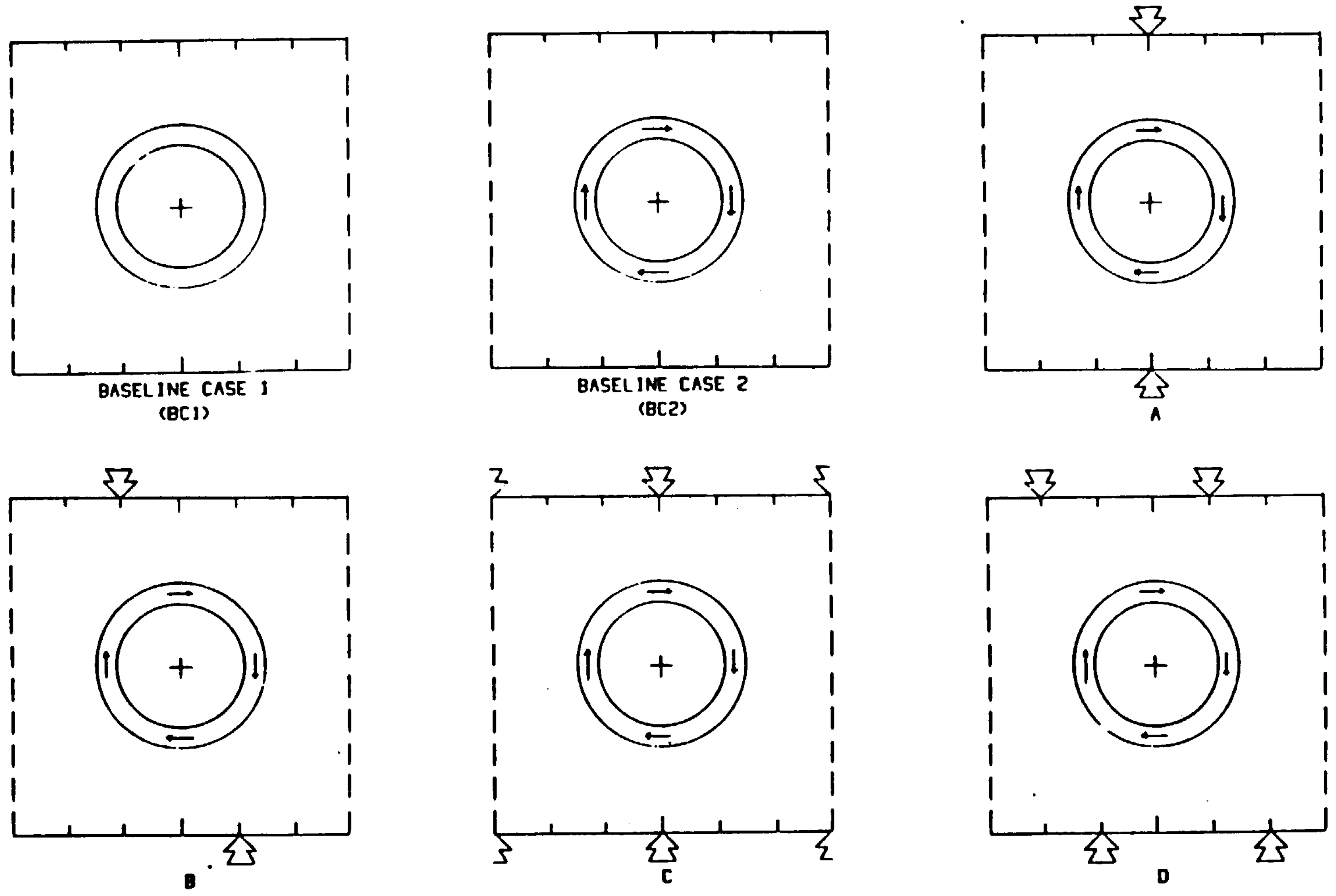

Figure 1.4 Primary Jet Flow Configurations

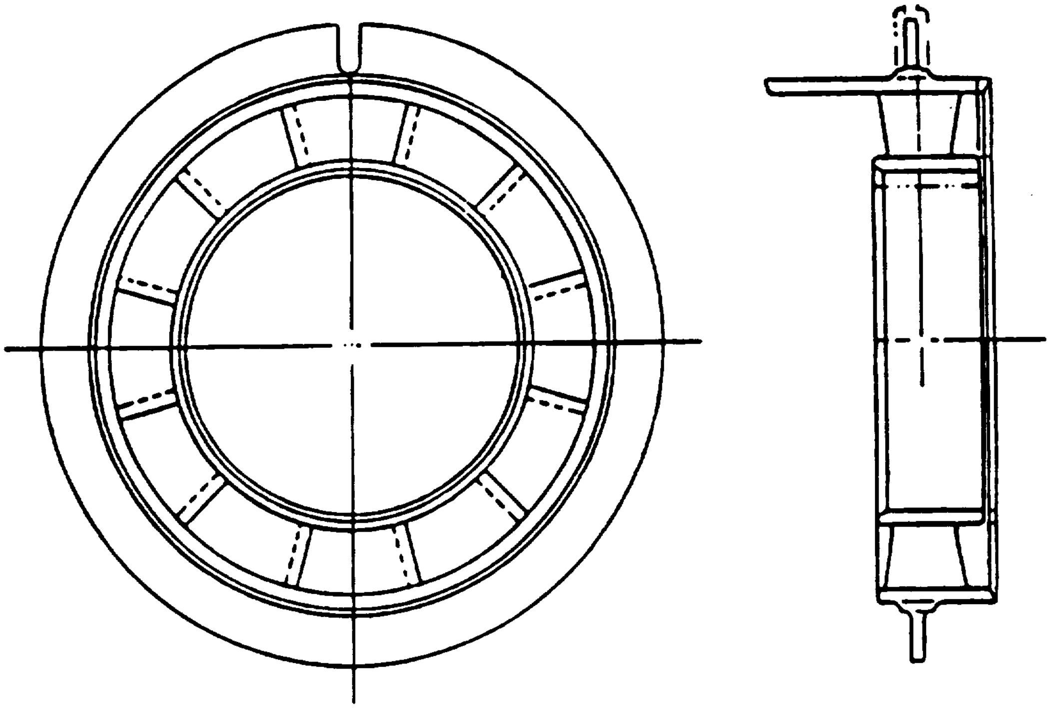

Figure 1.5 Diagram of Vane Swirler

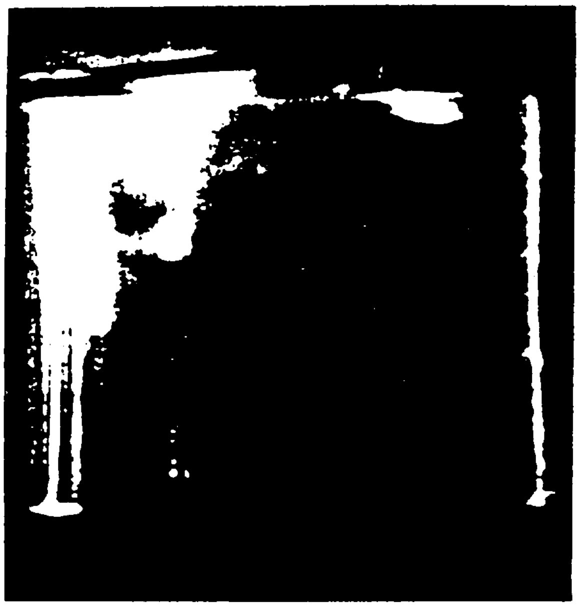

Figure 1.6 Radial Exit Flow with Flush Swirler

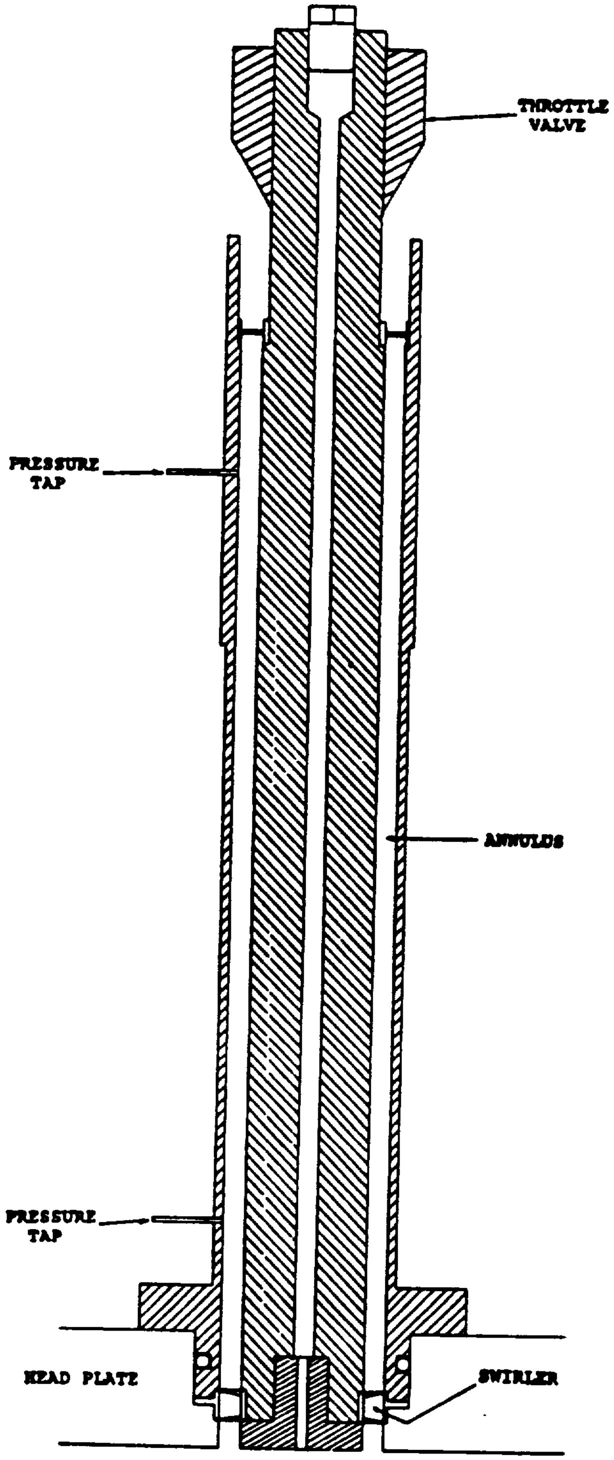

Figure 1.7 Drawing of Annular Swirler Inlet

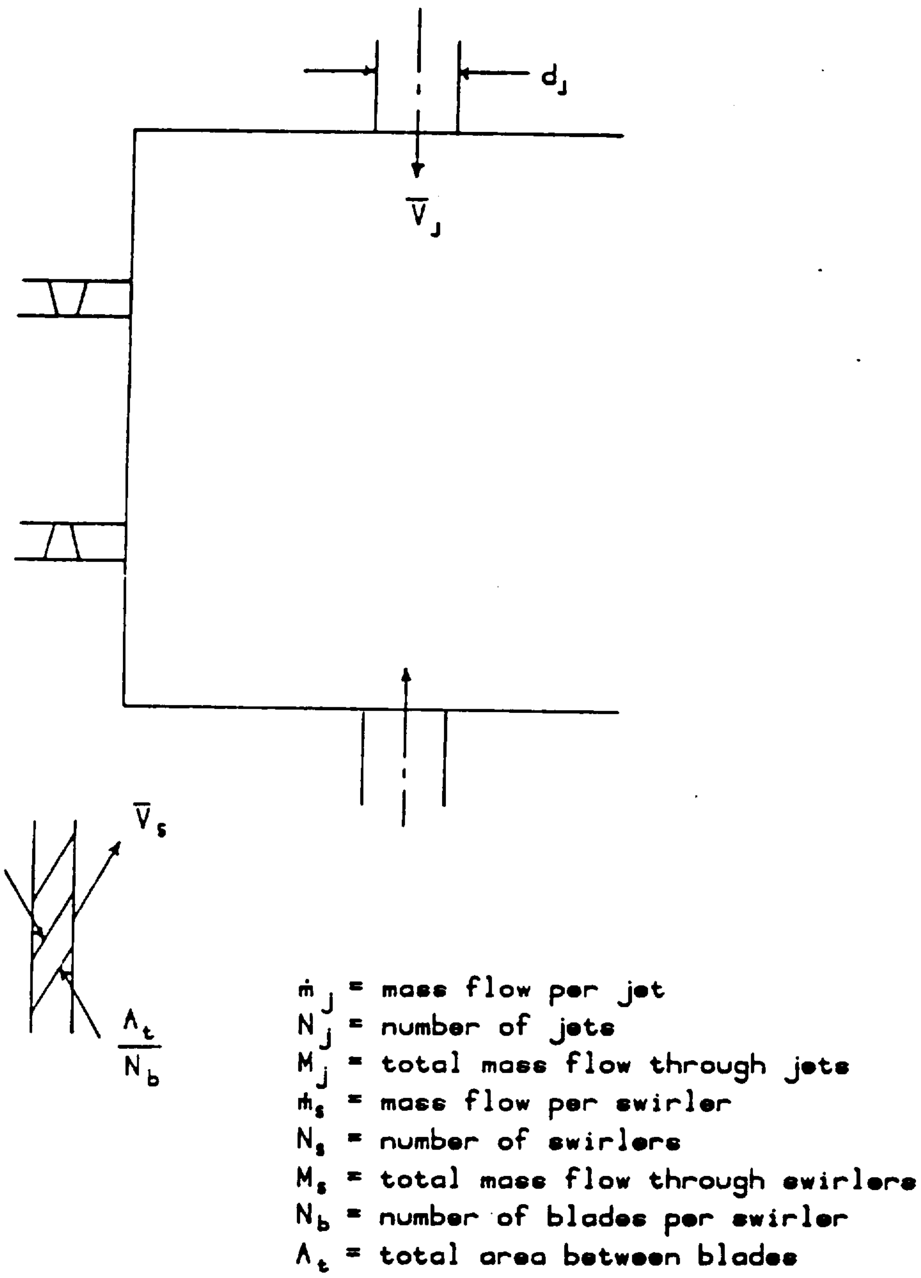

Figure 1.8 Determination of Primary Jet Diameters

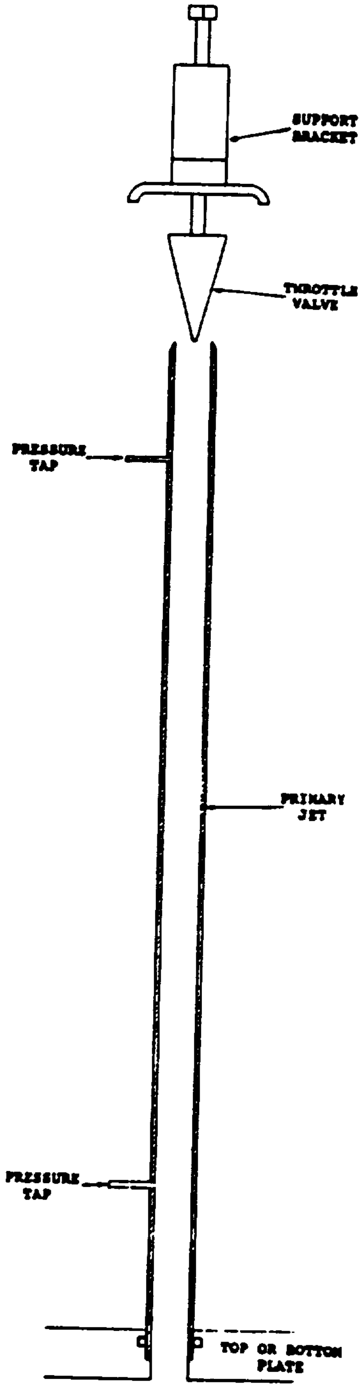

Figure 1.9 Drawing of Primary Jet

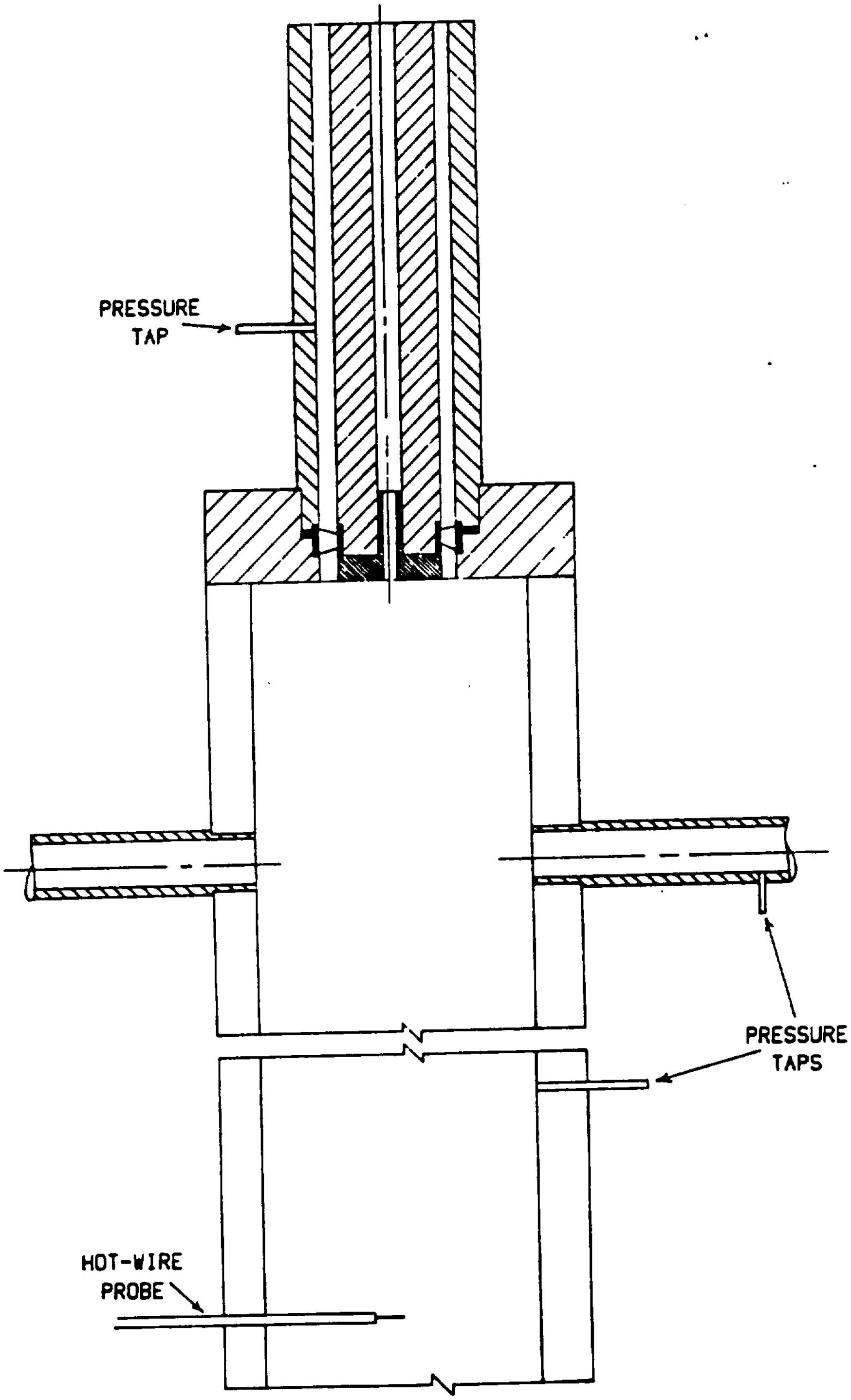

Figure 1.10 Single Swirler Loss Test Rig

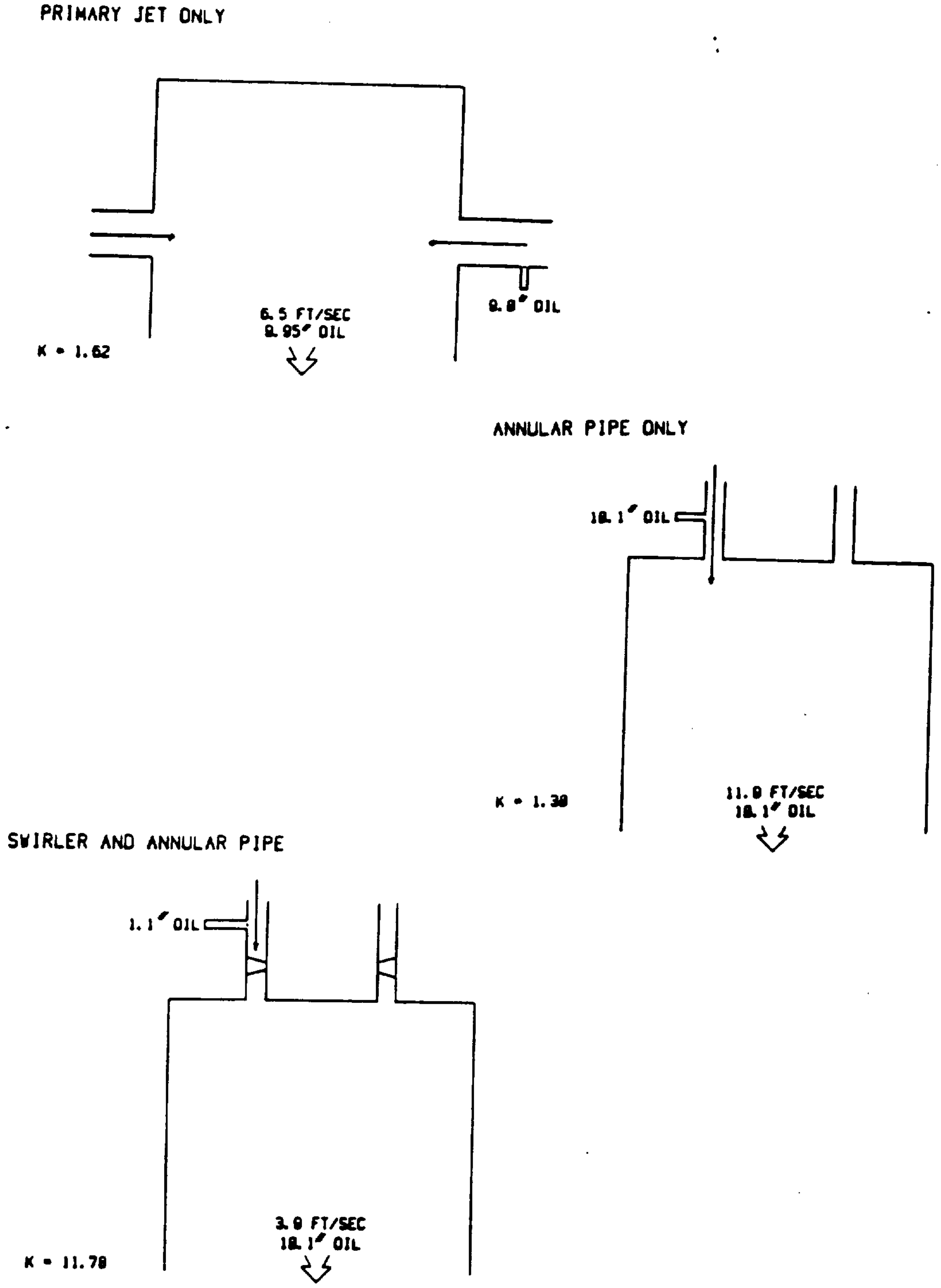

Figure 1.11 Results of Swirler Loss Tests

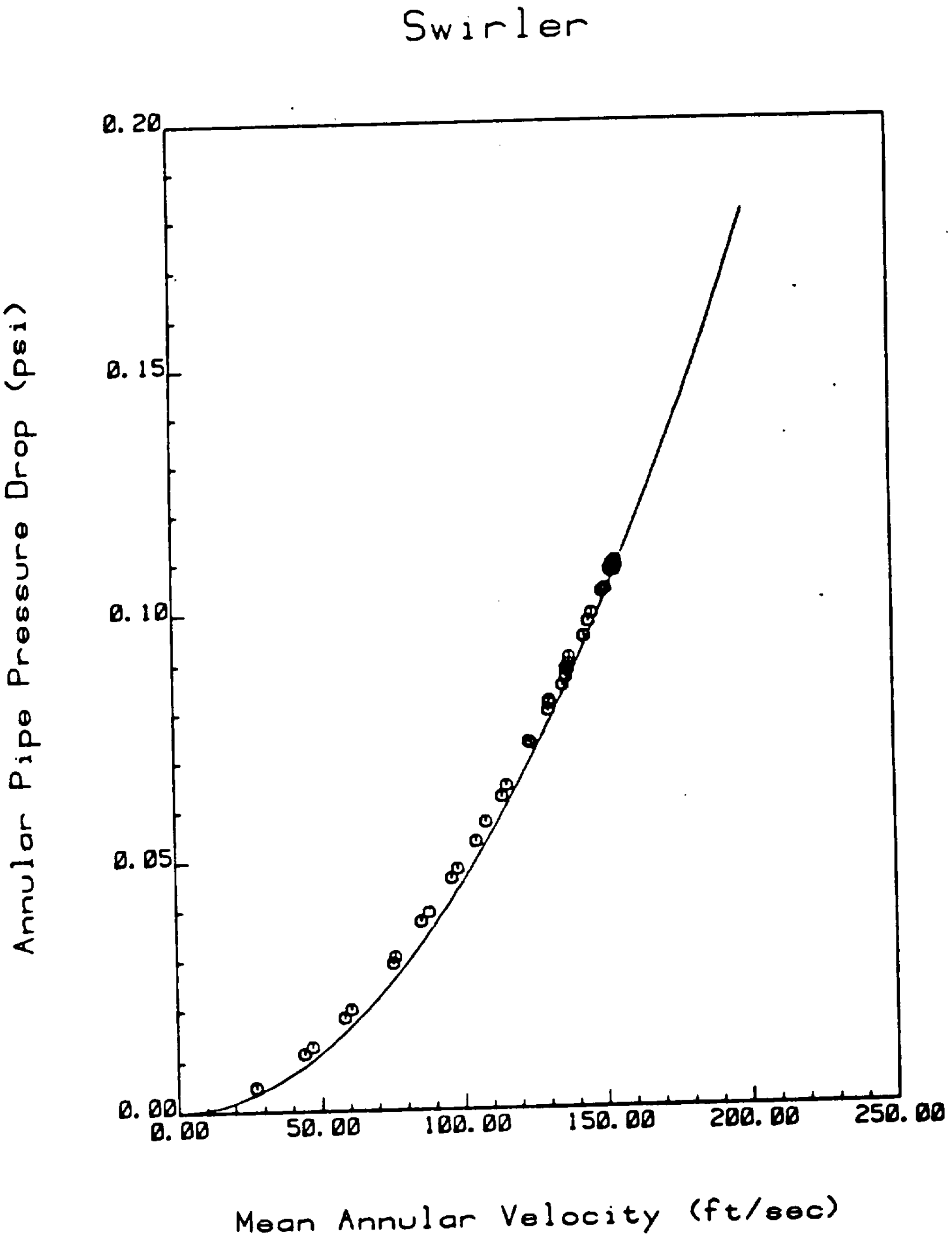

Figure 1.12 Swirler Calibration Curve

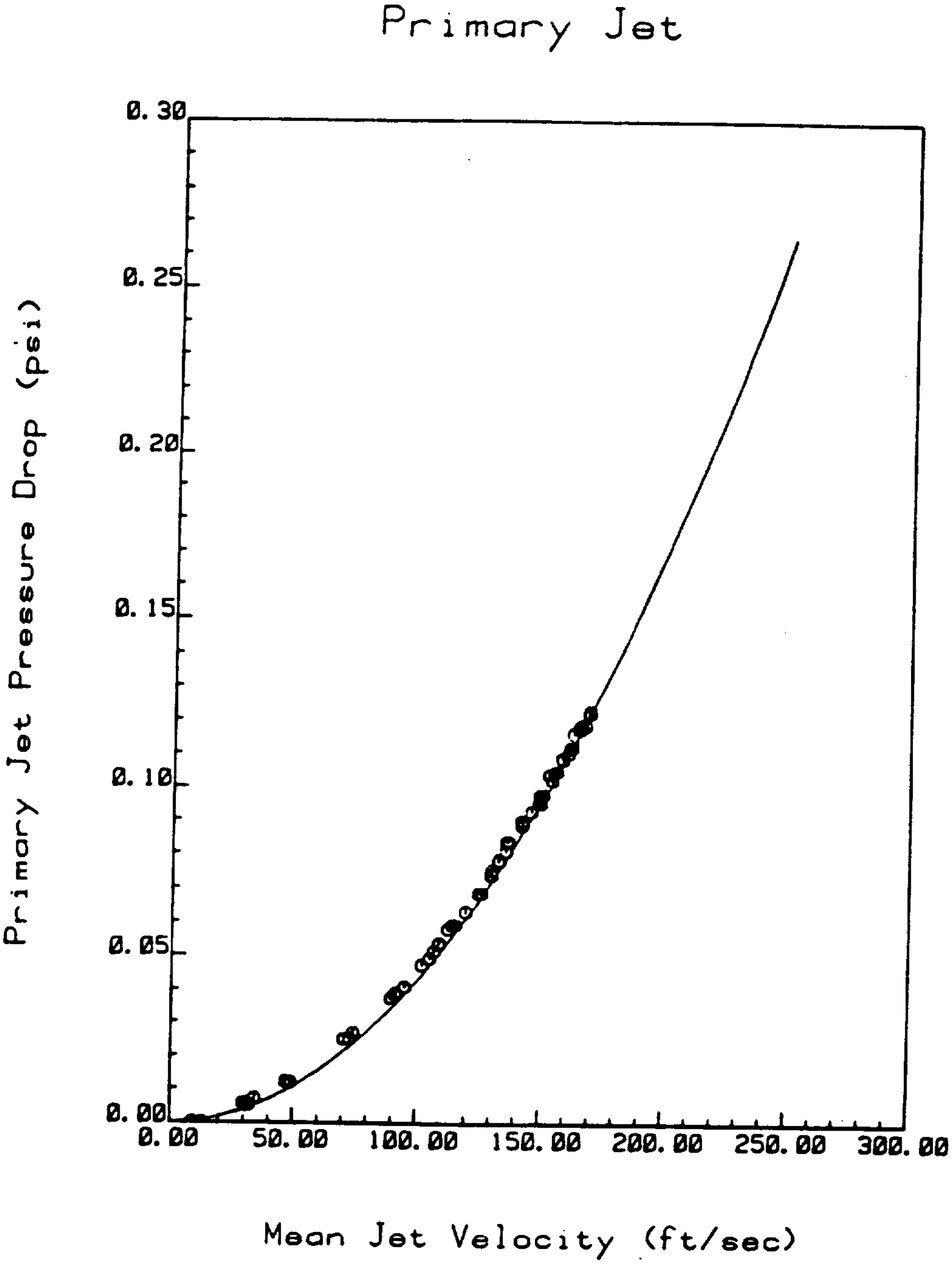

Figure 1.13 Primary Jet Calibration Curve

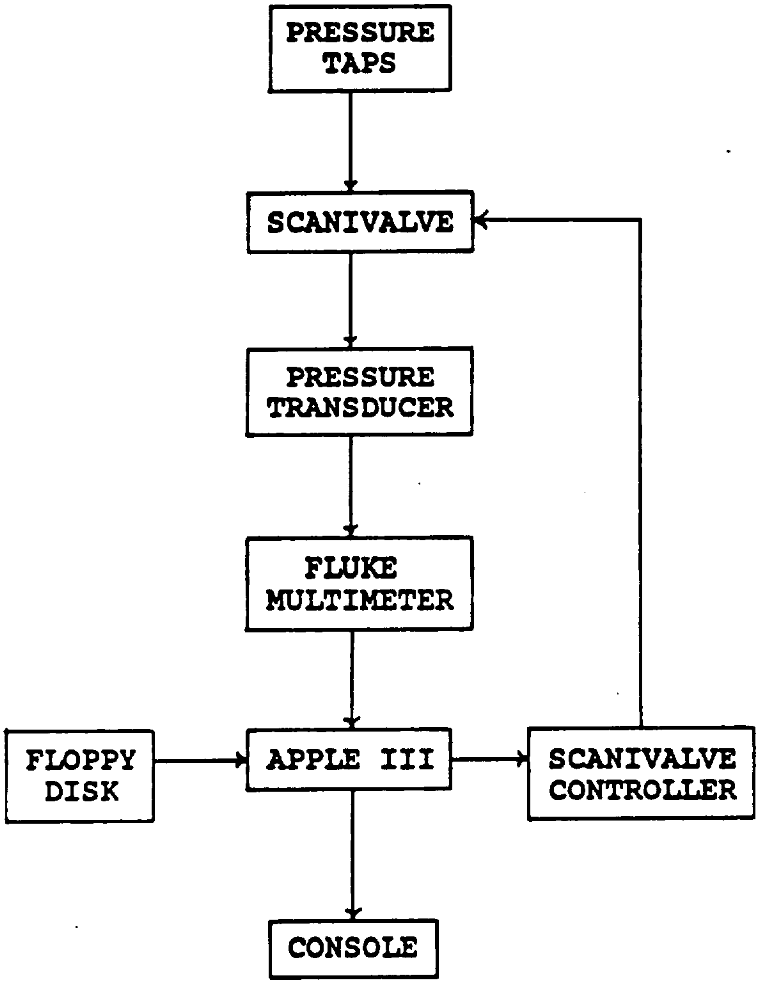

Figure 1.14 Diagram of Pressure Tap Monitoring System

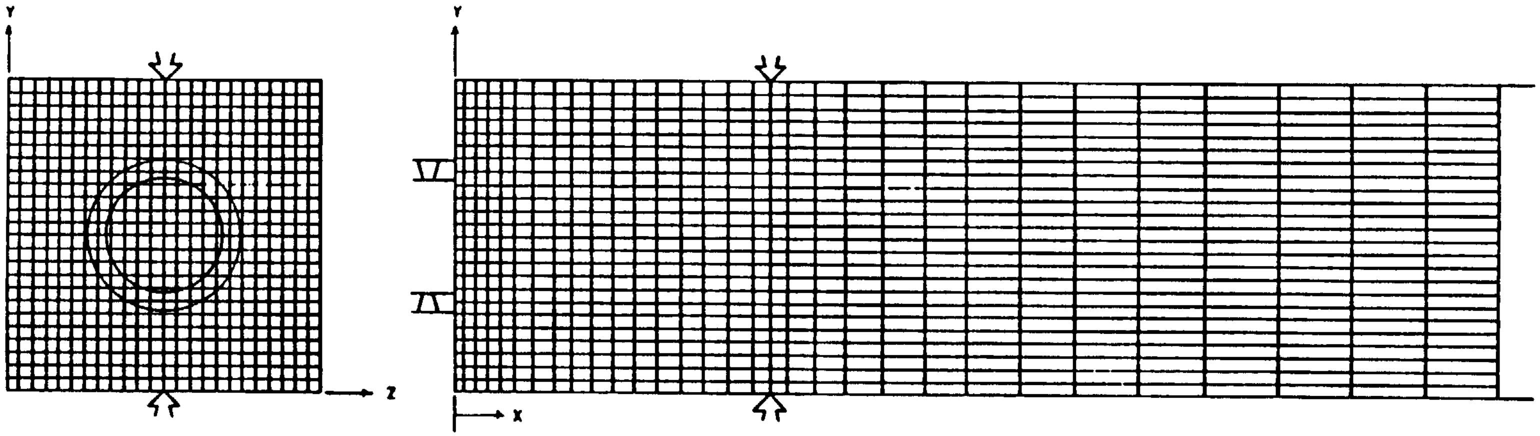

Figure 1.15 Com3d Grid for Test 9

NODAL POINTS	X POSITIONS (inches)	Y AND Z POSITIONS (inches)
1	0.000	0.000
2	0.090	0.125
3	0.190	0.250
4	0.305	0.375
5	0.435	0.500
6	0.580	0.625
7	0.740	0.750
8	0.950	0.875
9	1.105	1.000
10	1.300	1.125
11	1.500	1.250
12	1.700	1.375
13	1.920	1.500
14	2.140	1.625
15	2.360	1.750
16	2.590	1.875
17	2.825	2.000
18	3.000	2.125
19	3.175	2.250
20	3.450	2.375
21	3.750	2.500
22	4.100	2.625
23	4.500	2.750
24	4.900	2.875
25	5.400	3.000
26	5.950	
27	6.550	
28	7.200	
29	7.900	
30	8.600	
31	9.300	
32	10.000	

Figure 1.16 Com3d Nodal Point Locations

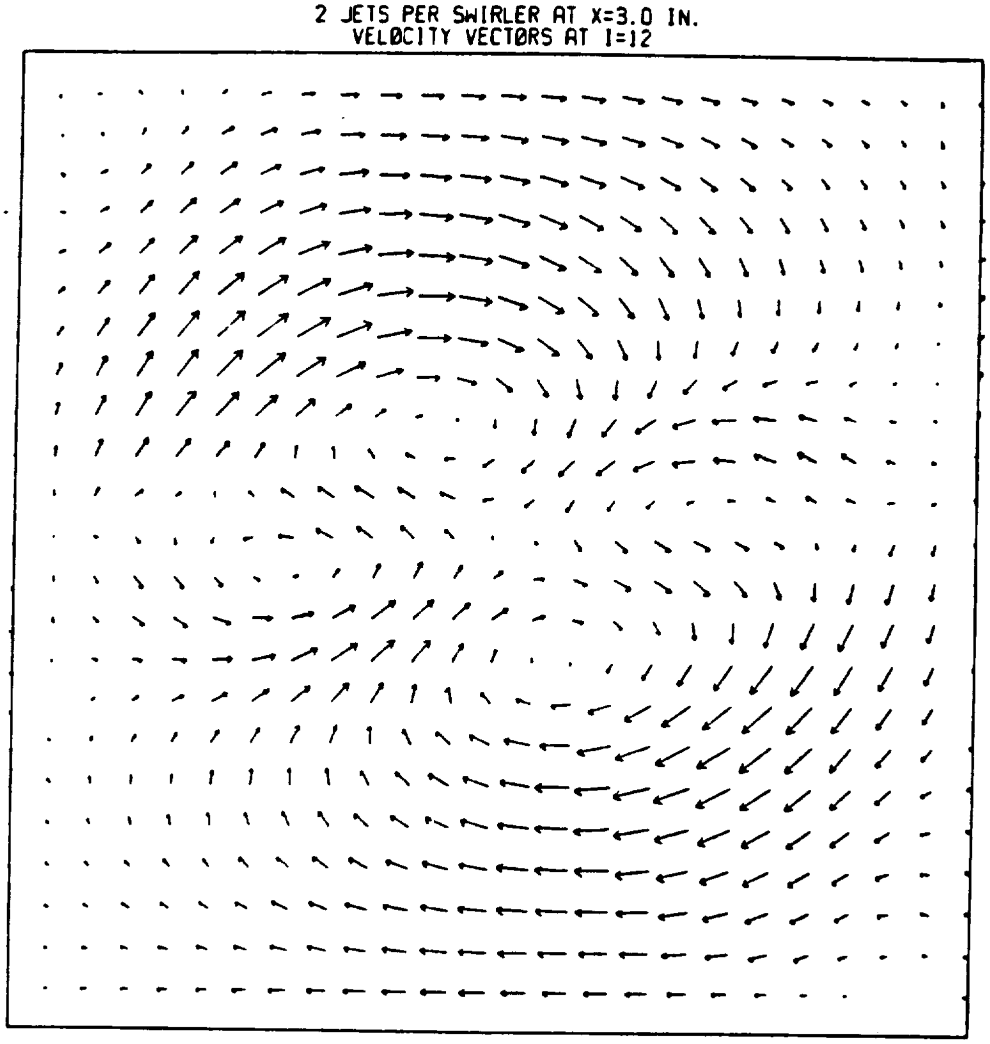

Figure 1.17 Com3d Vector Plot at x=1.70 inches

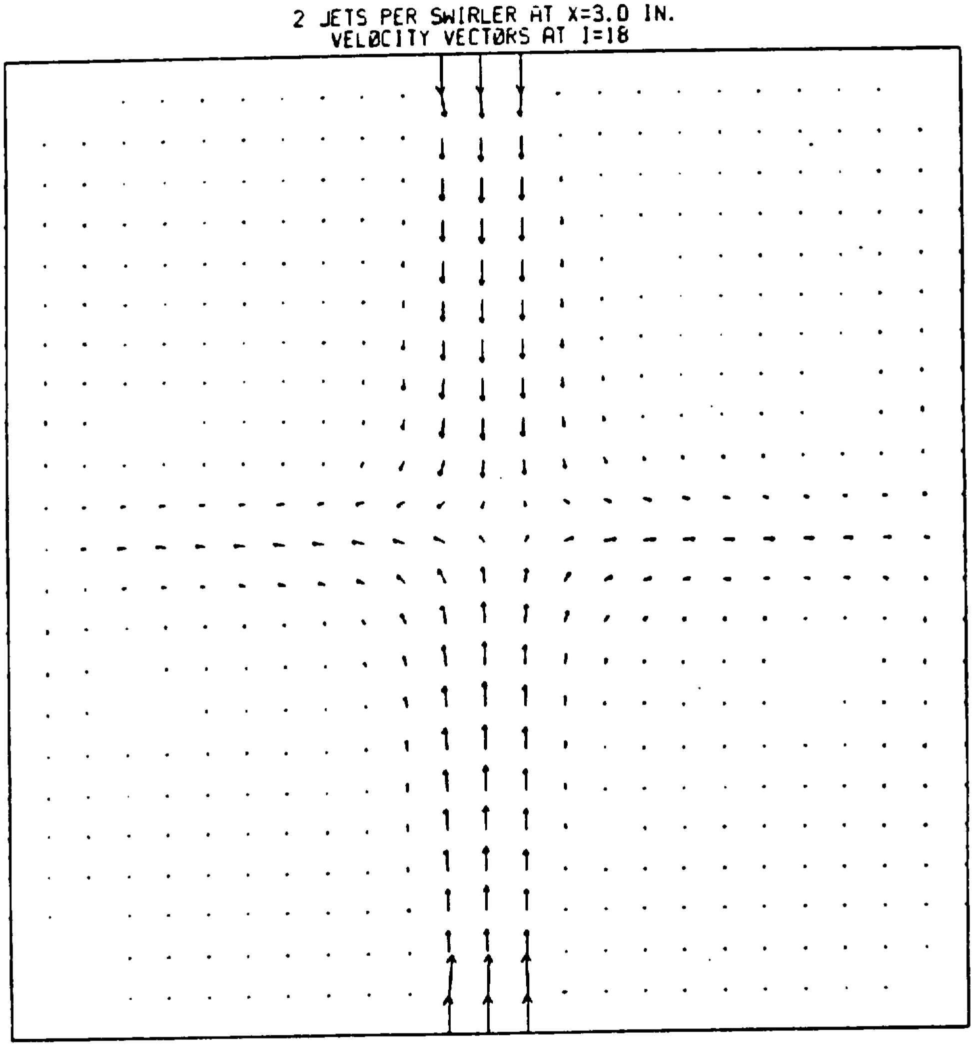

Figure 1.18 Com3d Vector Plot at x=3.00 inches

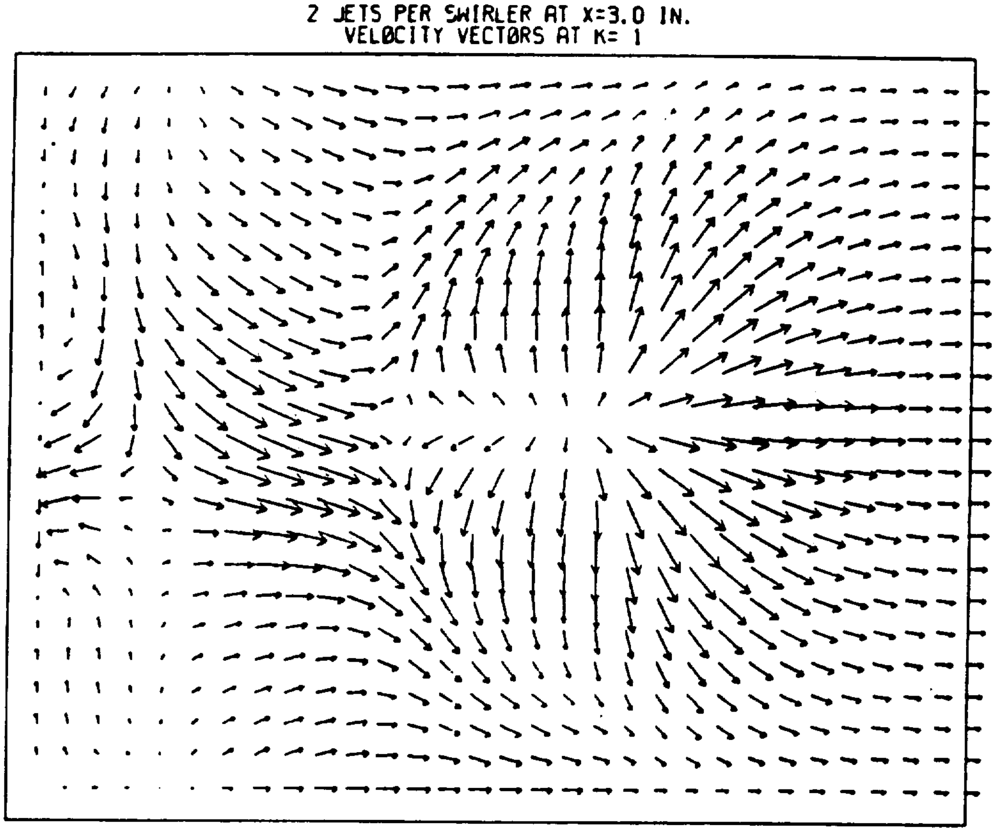

Figure 1.19 Com3d Vector Plot at z=0.00 inches

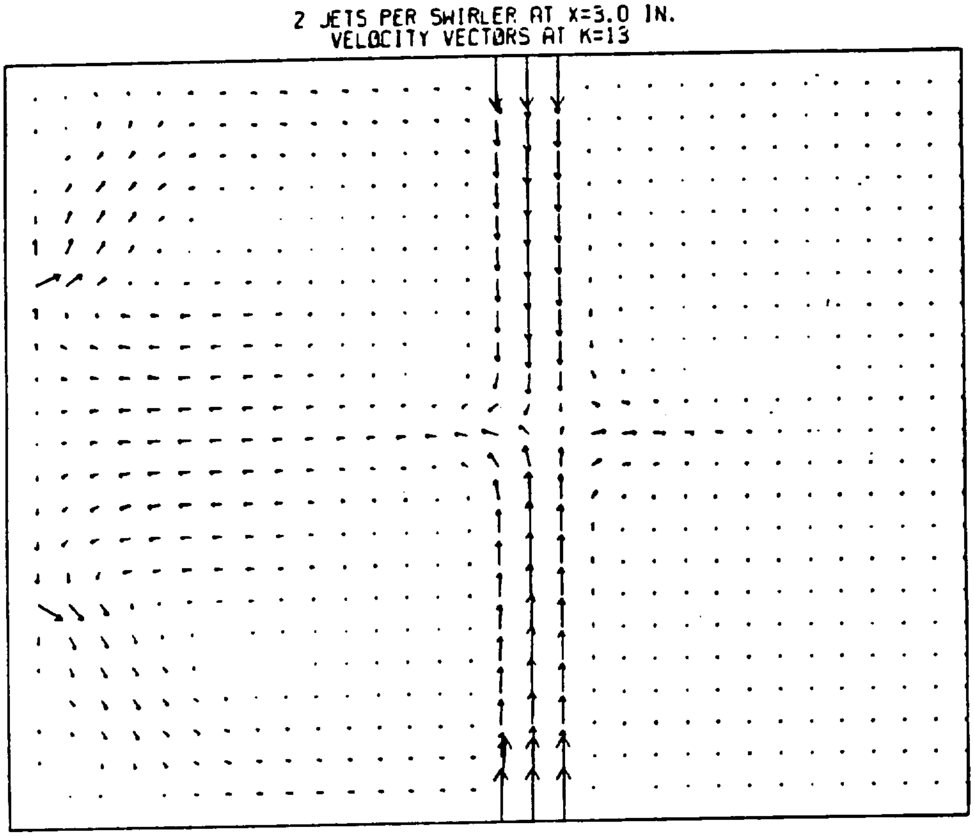

Figure 1.20 Com3d Vector Plot at z=1.50 inches

CHAPTER 2

LDV SYSTEM

The laser doppler velocimeter (LDV) system utilizes a Spectra Physics model 165 Argon-ion laser. It lases predominantly in the blue line of 4880 angstroms and green line of 5145 angstroms. These two color lines are used to produce a two color, two component system to take non-intrusive velocity measurements.

2.1 OPTICS

The optics package is made up primarily of Disa 55X components for a two color LDV system. Figure 2.1 is a sketch of the system used. The components of the transmitting optics is detailed below.

1) 1/4 wave plates: Due to the necessity to rotate the optics to take measurements near the various walls it is necessary to use the 1/4 wave plates. Figure 2.2 depicts the rotation of the optics to facilitate measurements near the walls. The first wave plate is mounted to the laser and converts the linearly polarized light of the laser to circularly polarized

light. The second wave plate is mounted to the entrance of the transmitting optics and converts the circularly polarized light back to linearly polarized light. The color splitter (described below) is sensative to the plane of polarization. Therefore, the second wave plate is mounted to the optics and rotates with the optics to ensure correct polarization for the color splitter.

2) Beam waste adjuster: The beam waste adjusts the beam diameter such that it is a minimum at the point of measurement.

3) Beam splitter: The beam splitter splits the single beam into two parallel beams of equal intensity containing both color lines. One of the beams is along the optical axis, and the other is offset 30 mm from the optical axis.

4) Bragg cell: The bragg cell accousto-optically shifts the frequency of the beam traveling along the optical axis by 40 Mhz. The result is that the interference fringes at the point of beam crossing move at 40 Mhz. Thereby, measurement of direction as well as magnitude is possible. The system was tested both with and without the bragg cell. However, due to the strong velocity gradients, high turbulence, and flow

reversals data acquisition with out the bragg cell is impractical if not impossible.

5) Color splitter: The color splitter splits the frequency shifted beam along the optical axis into the individual blue and green beams. Each beam is translated out 30 mm from the optical axis on either side of the axis.

6) Beam translator: The translator translates the three parallel beams closer to the optical axis to facilitate entrance into the beam expander. Also there are adjustment screws on the translator to adjust the beams so they meet at one common point. This common point of intersection is called the probe volume.

7) Second beam splitter: The bragg cell is not 100% efficient in transferring the laser intensity to the frequency shifted beam. There is still visible intensity in the unshifted and secondary mode beams. Therefore the frequency shifted beams of each color are of less intensity than the blue-green beam. The intensity level of two beams meeting at a common point is given by [2]:

$$I = |\vec{E}_{01}|^2 + |\vec{E}_{02}|^2 + 2\vec{E}_{01}\cdot\vec{E}_{02}\cos 2\pi \left[\frac{2y\sin(\theta/2)}{\lambda}\right] \qquad (2.1)$$

I is the total intensity at the intersection of the two beams. $\bar{E}_{01}$ and $\bar{E}_{02}$ are the intensities of the individual beams. I has a maximum intensity distribution when the two beams are of equal intensity. That is $\bar{E}_{01} = \bar{E}_{02}$. This is illustrated in figure 2.3. Since the frequency shifted beams are of much lower intensity than the unshifted blue-green beam it is necessary to add an additional beam splitter to the path of the blue-green beam. This splitter separates the blue-green beam into two beams of equal power and 1/2 as strong as the original beam. One of these beams is used and the other is wasted. The use of this splitter is depicted in figure 2.4.

8) Beam expander: The beam expander enlarges the beam diameters and translates the three beams radially outward from the optical axis by a ratio of 3.75/1. As can be seen from equations (2.1) and (2.2), probe volume size is inversely proportional to the expansion ratio. Thus, a large expansion ratio yields a small probe volume.

9) Field lens: The field lens focuses the three expanded, parallel beams to one common point. As presented by Sundar [8], the field lens is an astronomical lens and is designed, for minimal chromatic aberration, to be

mounted with the side having the greatest curvature to be facing the incoming parallel light.

The receiving optics were tried in back scatter, side scatter, and forward scatter. However, due to the very small size of the seeding particles (detailed in section 2.3) and proximity of walls only forward scatter yielded sufficient scattered light. The components of the receiving optics are described below.

1) Receiving lens: The receiving lens converts the scattered light from the probe volume to parallel light.

2) Beam expander: The beam expander in the receiving optics works in reverse of that in the transmitting section. That is it reduces the parallel light from the receiving lens to parallel light of a diameter necessary to enter the first spatial filter.

3) First spatial filter: The first spatial filter (pinhole) blocks out room light and other sources of unwanted light so that only the scattered light from the probe volume is passed. This pinhole is several times larger than the probe volume, and does let a small amount of stray light through.

4) Splitter plates: The splitter plates are placed at a 45 degree angle to the optical axis and reflect only the desired color to its respective photomultiplier (PM) tube. That is, the blue splitter reflects the blue scattered light towards the blue PM tube and lets the green light pass on to the green plate where it is then reflected towards the green PM tube.

5) Second spatial filter: The second spatial filters serve the same purpose as the first spatial filter except that they are considerably smaller than the first filter and let only the light from the probe volume pass.

6) Photomultipliers: There is one photomultiplier for each color line. They are sensitive to light and generate an electrical signal proportional to light intensity. That is, they convert light energy to electrical energy for data processing.

The simulated combustor flow with its walls, sharp velocity gradients, and turbulent reversals present a difficult flow for the LDV system. For these reasons the laser optics have been presented in detail. Of special importance are the use of the 1/4 waveplates for optics rotatability, bragg cell for adequate handling of the turbulent flow reversals, additional beam splitter for equal beam power levels, and forward scatter for a suitable signal.

As mentioned in section 1.1 the walls are made of glass and plexiglass. Originally the walls were manufactured entirely of 1.27 cm (0.5 in) thick plexiglass. However, this proved to be unacceptable for LDV measurements. The plexiglass varied in its thickness. This affects the laser system in three ways.

1] loss of beam overlap at probe volume

2] loss of focal distance to receiving lens

3] loss of pinhole alignment

All three of these effects cause deterioration or complete loss of Doppler signal. This made it possible to take data only at one position. When the probe volume moved, loss of signal would occur due to the above reasons. For these reasons, the areas of laser access were replaced with standard 0.635 cm (0.25 in) glass plate. The glass plate worked very well and provided movement of the probe volume without loss of signal.

2.2 SYSTEM GEOMETRY

In order to obtain good spatial resolution a field lens system was chosen with a short focal length. Probe volume dimensions are given by:

$$\text{Length} \quad l = \frac{4\lambda f}{2b\pi\sin(\theta_\beta/2)} \qquad (2.2)$$

$$\text{Diameter} \quad 2b_o = \frac{4\lambda f}{2b} \qquad (2.3)$$

Where: λ = wavelength
f = field lens focal length
$2b$ = diameter of beam entering field lens
θ_β = beam intersection angle

Therefore decreasing the field lens focal length decreases probe volume size. The field lens is actually a combination of two lenses. One of the lenses has a focal length of 7620 mm (30.0 in) and the other has a focal length of 12192 mm (48.0 in). The net focal length is computed using the standard thin lens formula.

$$f = \frac{1}{1/f_1 + 1/f_2} \qquad (2.4)$$

The two lenses provide a resultant focal length of 4689 mm (18.46 in).

The beam angles were measured using simple triangulation as depicted in figure 2.5. The beams were shown onto a wall perpendicular to the optical axis. The distances between the beam centers and the distance between the probe volume and wall were measured. From this, the beam angles are computed using basic trigonometry. The angles were computed to be:

Beam Intersection angle; GREEN: 9.36 deg.
BLUE: 9.60 deg.

Using the equations 2.2 and 2.3 the probe volume dimensions were calculated to be:

Probe Volume Length; GREEN: 0.376 mm (0.015 in)
BLUE: 0.348 mm (0.014 in)
Probe Volume Diameter; GREEN: 0.0307 mm (0.0012 in)
BLUE: 0.0291 mm (0.0011 in)

A summary of the LDV geometry is presented in figure 2.6.

2.3 SEEDING PARTICLE

As a seed particle crosses the interference fringes in the probe volume, set up by the intersecting beams, it scatters light that is modulating in intensity. It is this intensity modulation that is received by the PM tubes and processed by the electronics.

The seed particle is drawn into the rig at the entrance to the swirlers and primary jets. However, due to the high swirling nature of the flow it was necessary to develop a special particle for this flow. As the flow leaves the swirlers it travels radially outward towards the walls. At the walls the smoke particles would accumulate very rapidly, and make laser transmission or data sampling impossible.

Many seeding particles were tried. Of those tried, the solid particles (salt crystals and titanium tetrachloride) provided the worst results. Data acquisition typically was impossible after only five to ten minutes of run time. After this time there would be a large deposit of particles on the walls. Although slightly better, the liquid particles (water, fog juice, dioctyl pthylate, propylene glycol) would also accumulate and run down the rig in a short time.

Of the seeds tried, fog juice yielded the best results. However, the particles were still too large. Therefore, a system was devised to eliminate this problem. The TSI atomizer used, generates approximately a 2 μm size particle. A 1% mixture of fog juice to ethyl alcohol is atomized then sent through a series of evaporation chambers. Here the alcohol is given time to evaporate, and a resulting submicron size particle of fog juice is left. This setup is shown in figure 2.7. The first chamber is a five gallon drum and the second is a 8 ft. section of 6 in. PVC pipe. With this setup we are able to achieve 8 to 10 hours of run time before rig cleaning is needed.

2.4 DATA ACQUISITION SYSTEM

The data acquisition system is shown in figure 2.8. Signal from the PM tubes contains the 40 Mhz signal from the Bragg cell + or - the doppler signal. PM signal is greater than 40 Mhz if the flow is into the direction of fringe movement and less than 40 Mhz if the flow is with the fringe movement.

Since the signal frequency is higher than that allowable for the processors it is sent through a frequency mixer. The mixer heterodynes this signal with a selected mix frequency ranging from 31 to 49 Mhz.

Output from the mixer is sent to the TSI counter processors (one for each color line). The processor initially provides gain and high and low pass filtering. The filtering eliminates noise from being processed. Each particle generates a burst as it passes through the probe volume. At the onset of a burst a timer is started. If the burst contains a set minimum number of cycles the clock is stopped. If the burst contains less than the required number of cycles the burst is considered invalid and the processor resets to accept another burst. This step eliminates particles that pass along the edge of the probe volume which provide a signal burst with a small number of cycles. For this experiment the cycles/burst were set at

8. Finally the time for the passage of the cycles/burst is compared to that for 1/2 cycles/burst. If the two values do not compare within a certain percentage the sample is discarded. A 7% comparison was used for the data acquisition. This step eliminates signal that would be generated when two particles cross through the probe volume at the same time.

The data is then sent to the computer. The computer utilized is a DEC 11/23 minicomputer. Besides taking the data the computer also controls the probe volume movement. The laser table is movable in two directions via computer controlled stepping motors. The third direction of movement is accomplished by movement of the field lens. Also done with a stepping motor. this provides full three dimensional movement of the probe volume in the flow field. The axis movement sensitivities are listed below.

Horizontal Table Movement: 1/1000 inch/pulse
Vertical Table Movement: 1/22574 inch/pulse
Field Lens Movement: 1/1000 inch/pulse

To accommodate the use of forward scatter, as mentioned earlier, a sliding boom was used between the transmitting and receiving optics. The boom was bolted to the bottom of the laser table and extended under the rig to the opposite side. Bolted to the top of the boom was a sliding beam with one end attached to the field lens and the other to the receiving optics. This provided full 3 dimensional movement of the receiving optics with the probe volume. The boom is shown in figure 2.9.

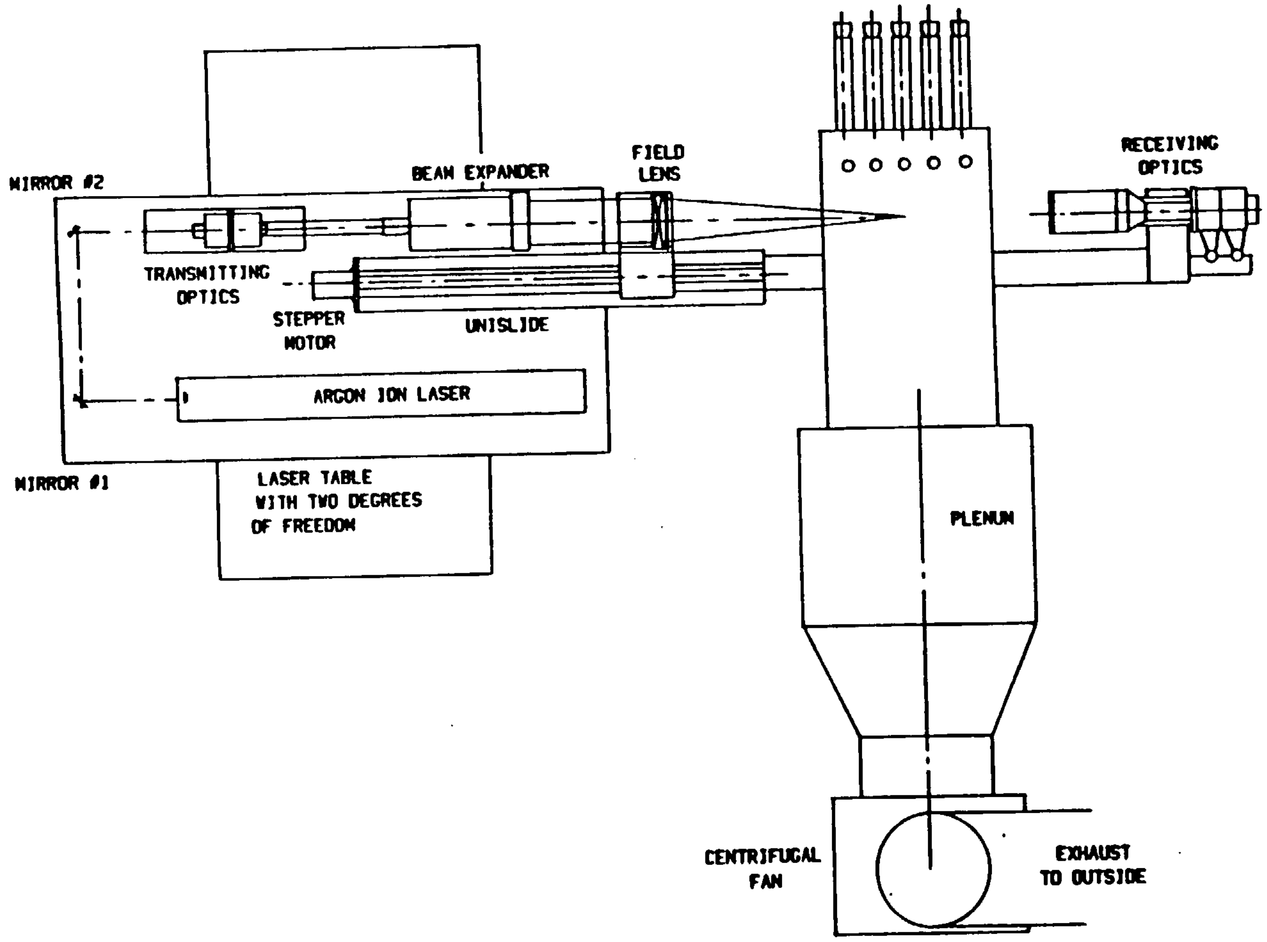

Figure 2.1 Arrangement of LDV Optics

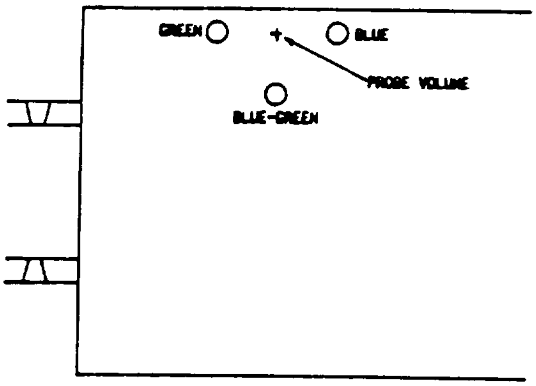

DATA TAKEN NEAR UPPER WALL

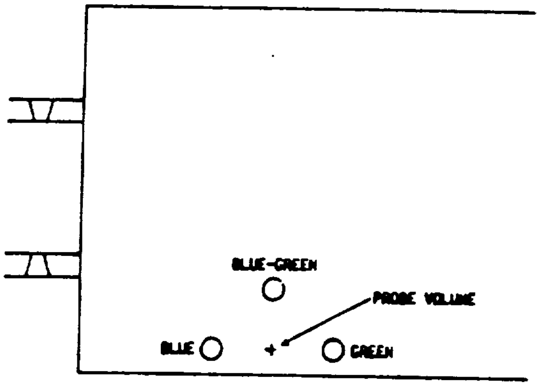

DATA TAKEN NEAR BOTTOM WALL

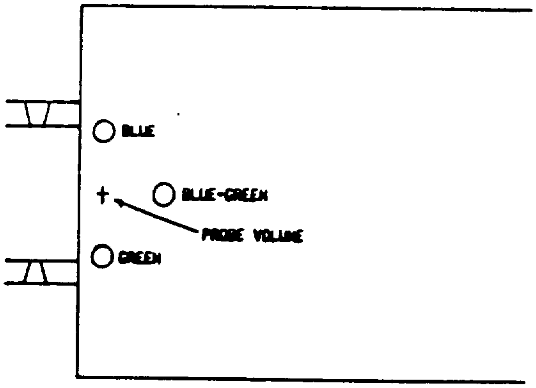

DATA TAKEN NEAR HEAD PLATE

Figure 2.2 Rotation of Optics

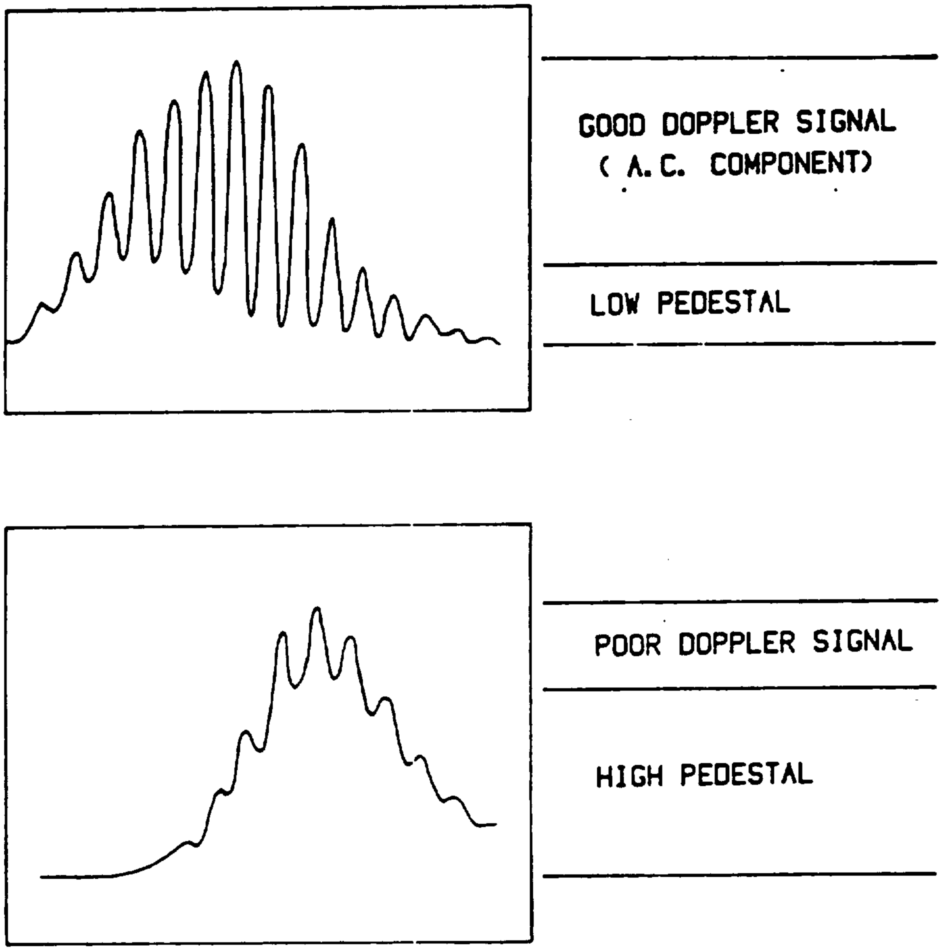

Figure 2.3 Effect of Unequal Beam Intensities

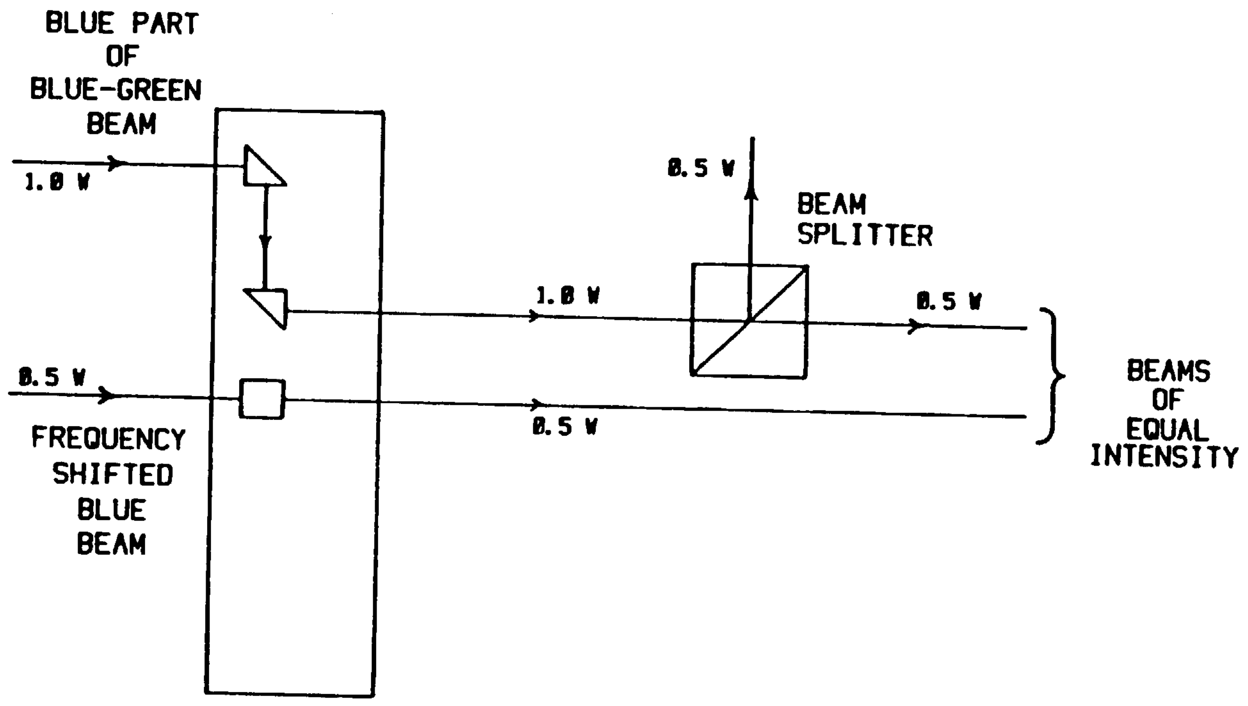

Figure 2.4 Use of Additional Beam Splitter

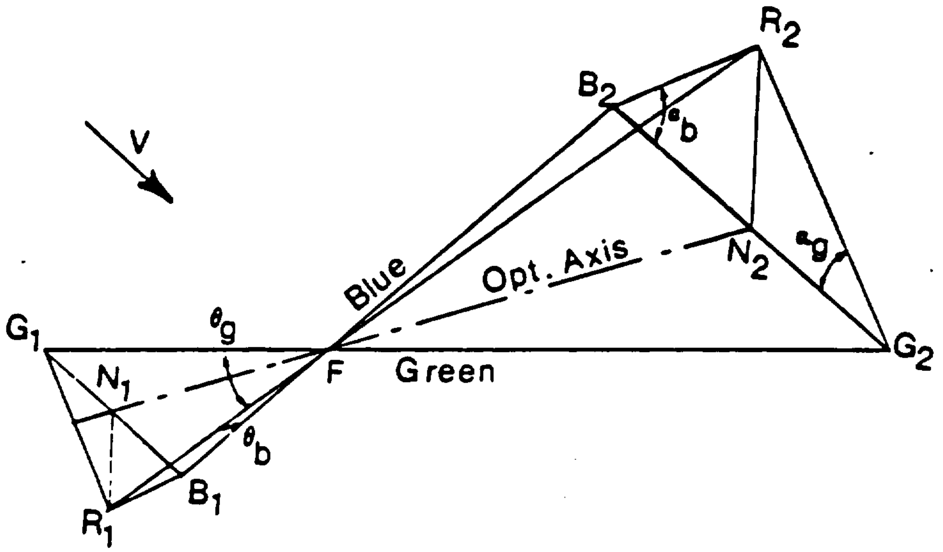

α_b = 43.0° ± 0.1°

α_g = 44.4° ± 0.1°

G_2R_2 = 11.16" ± 0.01"

N_2F = 68.19" ± 0.01"

B_2R_2 = 11.44" ± 0.01"

B_2G_2 = 16.39" ± 0.01"

Figure 2.5 Details of Beam Geometry for LDV System

	GREEN	BLUE
BEAM INTERSECTION ANGLE (deg.)	9.36	9.60
PROBE VOLUME LENGTH (mm)	0.376	0.348
PROBE VOLUME DIAMETER (mm)	0.0307	0.0291
PROPORTIONALITY CONSTANT (ft/sec/Mhz)	10.34	9.56

FIELD LENS FOCAL LENGTH (mm)	468.88
RECEIVING LENS FOCAL LENGTH (mm)	310.00

Figure 2.6 Summary of LDV Geometry

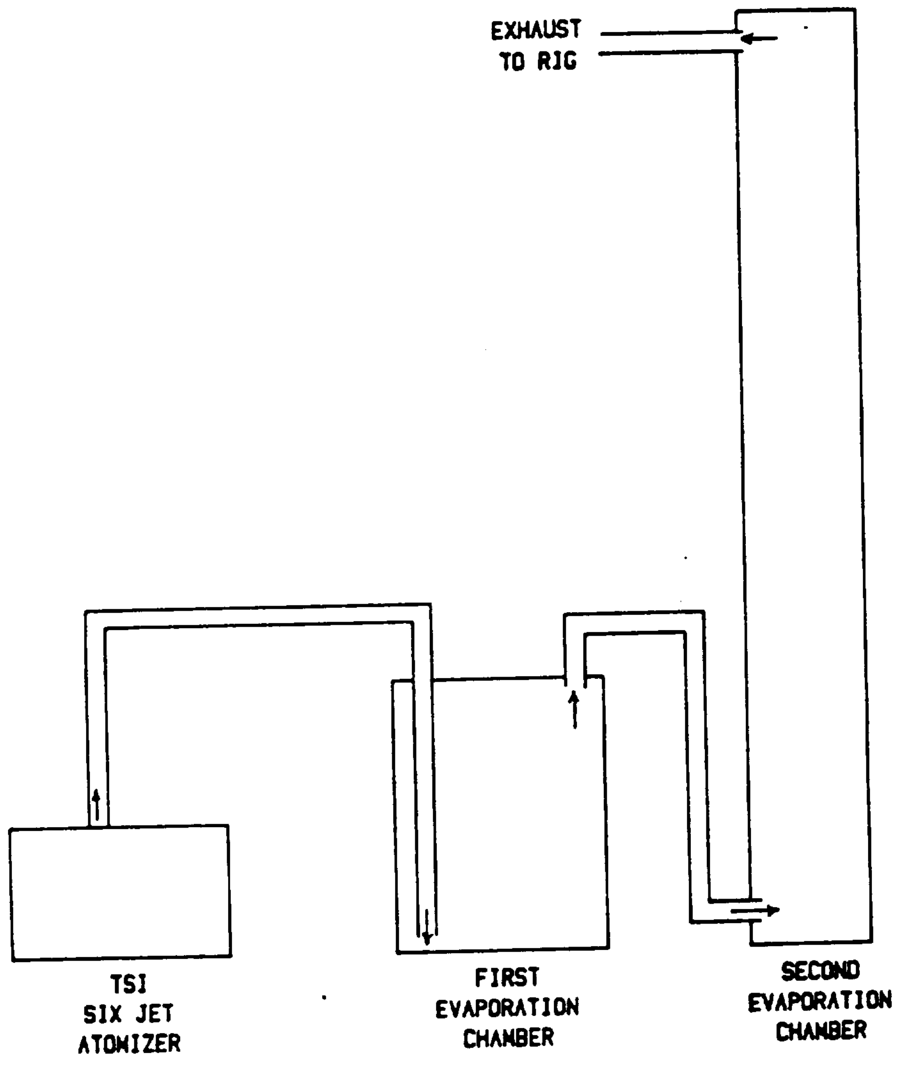

Figure 2.7 Diagram of Particle Generating System

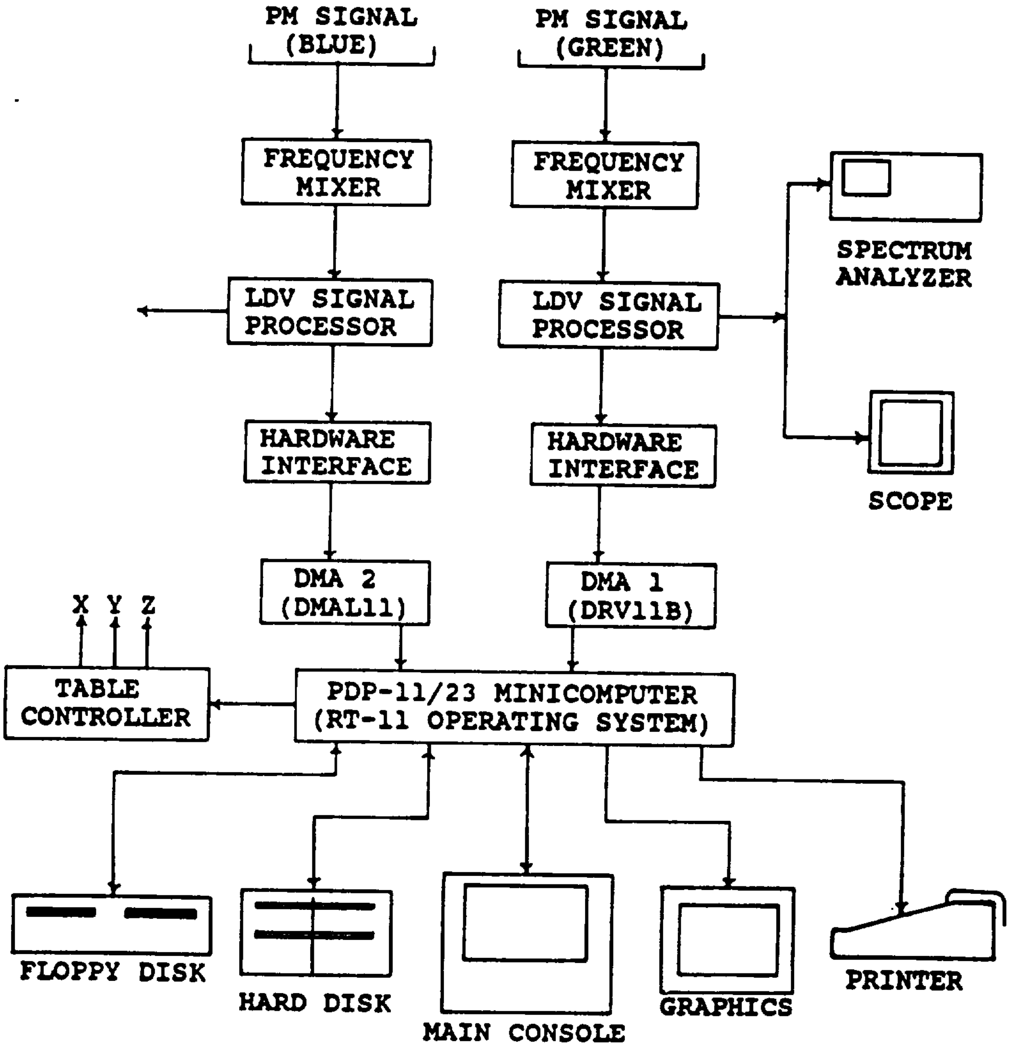

Figure 2.8 Data Acquisition System for LDV Measurements

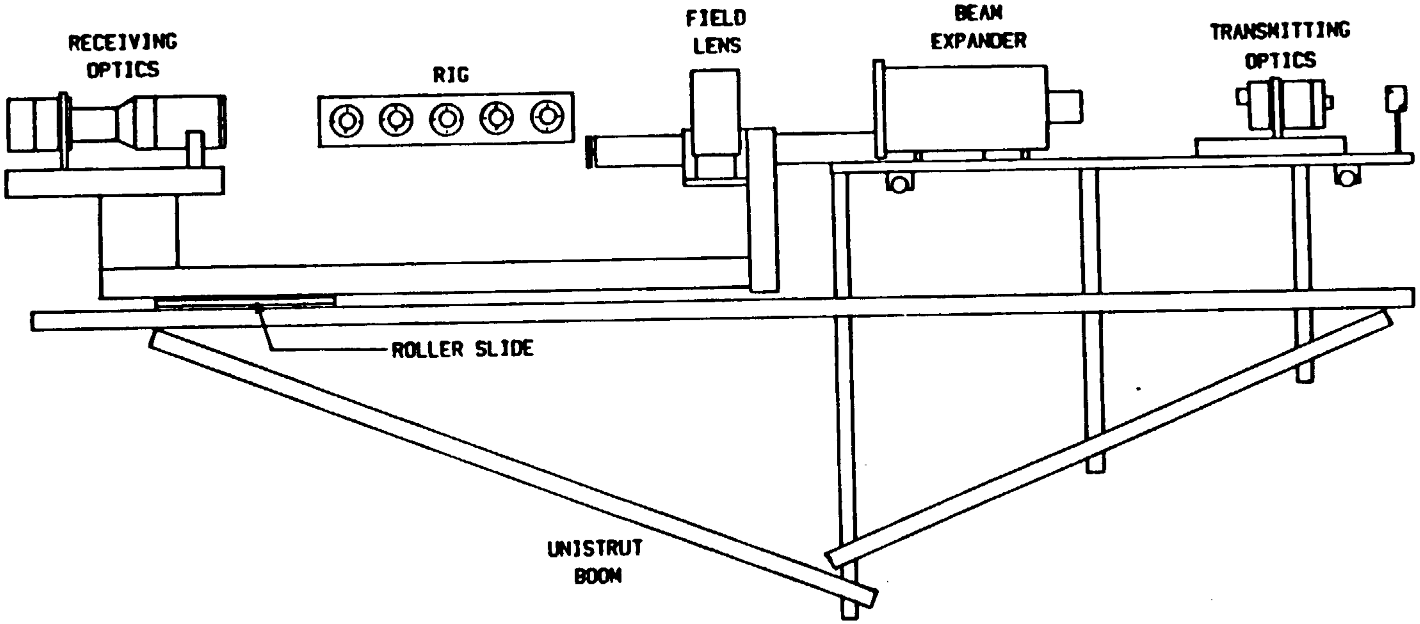

Figure 2.9 Receiving Optics Boom Support

CHAPTER 3

SWIRLER LDV DATA

In order to get the swirler inlet conditions and flow profile due to a single swirler, LDV data was taken in a single swirler rig (shown in figure 3.1). The test section was 7.62 cm (3.00 in) square and extended 10 duct heights downstream. The annulus and swirler was one of those described in chapter 1 for the five swirler rig.

From the LDV data the mean and rms values were calculated.

3.1 INLET CONDITIONS

To establish the swirler inlet flow, a finely detailed scan was taken in front of the swirler at 0.127 cm (0.050 in) downstream of the exit. The spatial grid used is shown in figure 3.2. A 39 x 20 point grid was taken with 0.381 mm (0.015 in) in between each nodal point, for a total of 780 spatial points. For each spatial point the mean and rms were computed from the 3000 samples taken. In all, a total of 9.36 million data samples were taken of the swirler inlet.

Referring to figure 3.2, at each spatial point the laser was able to measure two components of velocity. The two components are the x component (into the plane of the paper) and y component (towards the top of the page). In order to get all 3 components, two scans were taken and the use of symmetry imposed. Scan 1 was able to measure u and v velocity and scan 2 was able to measure u and w components. Thus all 3 components are measured, with the u velocity being measured twice.

Figure 3.3 contains cascade plots of the x component of velocity for scans 1 and 2. In general, the axial velocity is lower at the hub and has maximum values at the outer flow radius. However, there is considerable discrepancy in the u velocity measured by the two scans. Referring to figure 3.4, the maximum axial velocity varies by 40 ft/sec between scans 1 and 2.

It is expected that there would be some spatial averaging between scans 1 and 2. The probe volume has a certain length and width, and for each spatial point the measured velocity is an average over the probe volume. In scan 1 the probe volume dimension is only 0.001 in. along the y axis where for scan 2 the probe volume dimension is 0.015 in. along the y direction. Thus, the spatial resolution in the y direction is considerably finer for scan 1 than scan 2. This would account for a slight variation between the two scans, but not a 40 ft/sec difference.

Plots of v and w velocities are provided in figures 3.5 and 3.6. The v component converges to a relatively constant value near or in front of the hub. This is a strong indication of the back flow being drawn into the swirling exit flow. Also, the w component converges to near zero in front of the hub indicating low swirl in this region.

As expected, at the left side of the plane (low z position) the v velocity is high, while the w velocity is low. With the values changing as z increases. The combination of v and w velocities are plotted in vector form in figure 3.7. Here, the effect of the swirl is clearly evident.

As mentioned earlier, rms values were also measured. Figure 3.8 is a diagram of the laser orientation. The green and blue beams are orthogonal to each other at approximately 45 degree angles to the faceplate. The rms values have been nondimensionalized with the local mean velocity for that particular beam. Thus, figures 3.9 thru 3.12 are plots of the turbulence intensity ratio or rms/|mean| velocities.

Figures 3.9 and 3.10 are plots of intensities for scan 1. The turbulence intensity is lowest in front of the annular hub or at the outer flow radius. At the edge of the inner flow radius the intensities get very large or for the green beam tend to infinity. Here the flow is very near zero and even slight fluctuations make the turbulence intensity very large.

For scan 2 the results are similar (figures 3.11 and 3.12). The turbulence intensities are lowest at the outer flow radius and tend to infinity at the inner flow radius. However, even at its lowest the turbulence intensity is still upward of 20 percent.

3.2 DOWNSTREAM DATA

Mean and rms velocities were also taken at four downstream locations. These locations were at 0.5, 1.0, 1.5, and 2.0 duct heights downstream of the swirler exit. For each downstream location a 26 x 31 point grid was used for a total of 806 spatial points, with a spatial resolution of 1.270 mm (0.050 in). As with the inlet conditions 2 scans were taken and symmetry invoked. The grid and scans taken are shown in figures 3.13 and 3.14. In all, a total of over 38 million data samples were taken downstream of the swirler exit.

The laser orientation for each scan is shown in figure 3.15.

Figures 3.16 through 3.19 are plots of the velocity components for the first downstream location (x=1.5 in). Referring to figure 3.16, the u velocity is greatest along the walls and in the corners. That is, in the center of the flow there is a strong back flow, with the bulk downstream flow along the walls and in the corners. Referring to figure 3.17 there is very good agreement between the two different values of u velocity obtained from the different scans. Looking at the centerline scan for z=1.5 inches. The extent of the back flow region can easily be seen. Only the half inch nearest the wall has a positive u velocity. The rest of the channel is in back flow.

The extent of the swirling flow can be seen quite clearly in figures 3.18 through 3.20. For the centerline scan of w velocity at y=2.75 (figure 3.19) the w component is twice as strong as the u component for the same position. Figure 3.20 is a vector plot of the v and w components. Here the strong swirling flow is clearly evident. Also, there is a slight asymmetry in the flow. That is, the apparent center of the swirl is not at the geometric center of the channel. Furthermore, the effect of the square channel is easily seen in figure 3.52. In this plot the areas of positive u velocity are in black, and those of negative value are shown with a dot pattern. The recirculation region takes the shape of the square duct at the 1.5 inch location.

Figures 3.21 through 3.24 are plots of turbulence intensity for the first downstream location. As with the inlet condition data, when the mean velocity goes towards zero the turbulence intensity goes to infinity. In areas where this is not the situation, the turbulence intensity varies from 35 to 100 percent.

Figures 3.25 through 3.33 are plots for the second downstream location at x=3.0 inches. Referring to figure 3.25, the u velocity for scan 2 shows a strong velocity deficit in the corner. This could possibly be due to a corner vortex. However it is uncertain if this is actually the case. It is only possible to measure two components of velocity at these positions. Thus, a full velocity profile for these positions is unavailable.

Comparing figures 3.26 to 3.17 for the centerline scan, the point of zero crossing has moved in towards the center of the duct. Thus the size of the area of back flow has decreased considerably. Also, the magnitude of the peak velocities has decayed. For the centerline position the maximum velocity near the wall has dropped from 40 ft/sec to 15 ft/sec. Although the strength of the flow along the walls has decreased dramatically the strength of the recirculation flow has only decreased slightly from -25 ft/sec to -20 ft/sec.

Comparing figure 3.19 to 3.28 the w component for the centerline scan has decreased only slightly. Thus, the swirl component has only decreased slightly.

The turbulence intensity for the 1.0 duct height position is similar to that for the 0.5 duct height position. At positions where the individual green and blue velocities approach zero the intensity goes to infinity. Elsewhere, the intensity level remains around 30 to 100 percent.

Figures 3.34 thru 3.42 are plots of velocity and turbulence intensity for x=4.5 inches or 1.5 duct heights downstream from the swirler exit. Referring to figures 3.34 and 3.36. Again there is a sudden change in velocity at the corners.

Figures 3.43 thru 3.51 are plots for x=6.0. The plots at x=4.5 and 6.0 are very similar to those for x=3.0. The only difference is that there is a slight decay in the magnitude of the velocities but the flow profiles remain rather constant. Also the turbulence intensity plots for these three planes are quite similar.

Thus the flow goes through some radical changes in the first duct height (3.0 in.). After this the flow profiles remain rather constant with only slight decay of the magnitude of the velocities. Referring to figure 3.52. These are contour plots of u velocity with areas of negative or back flow showing up as dotted areas. From these plots the size of the recirculation region is clearly visible. At x=1.5 the effect of the square duct can easily be seen in the squared off back flow region. By x=3.0 or 1.0 duct height the area of recirculation has diminished considerably and has become circular in shape. For x=4.5 in. and 6.0 in. the size of the recirculation region diminishes very little if at all. This is also seen in figure 3.53. This figure is a vector plot at the center line or z=1.5 inch position.

In doing some flow visualization, it was later discovered that there are two exit flow regimes. These are shown schematically in figure 3.53. At low mass flow rates the exit flow expands outward at an angle considerably less than 90 degrees, and is not attached to the head plate. At high mass flow rates the exit flow remains attached to the head plate all the way out to the side wall. With moderate flow rates a bistable flow situation is set up. That is, the flow will oscilate between the two regimes.

It is believed that this is the cause of the velocity discrepancy indicated in figure 3.4. Also, evidence of this phenomenon can be seen in figure 3.37. For the v velocity at z=0.3 inches there is a very definite jump in the velocity profile when the exit flow switches from one regime to the other and back again.

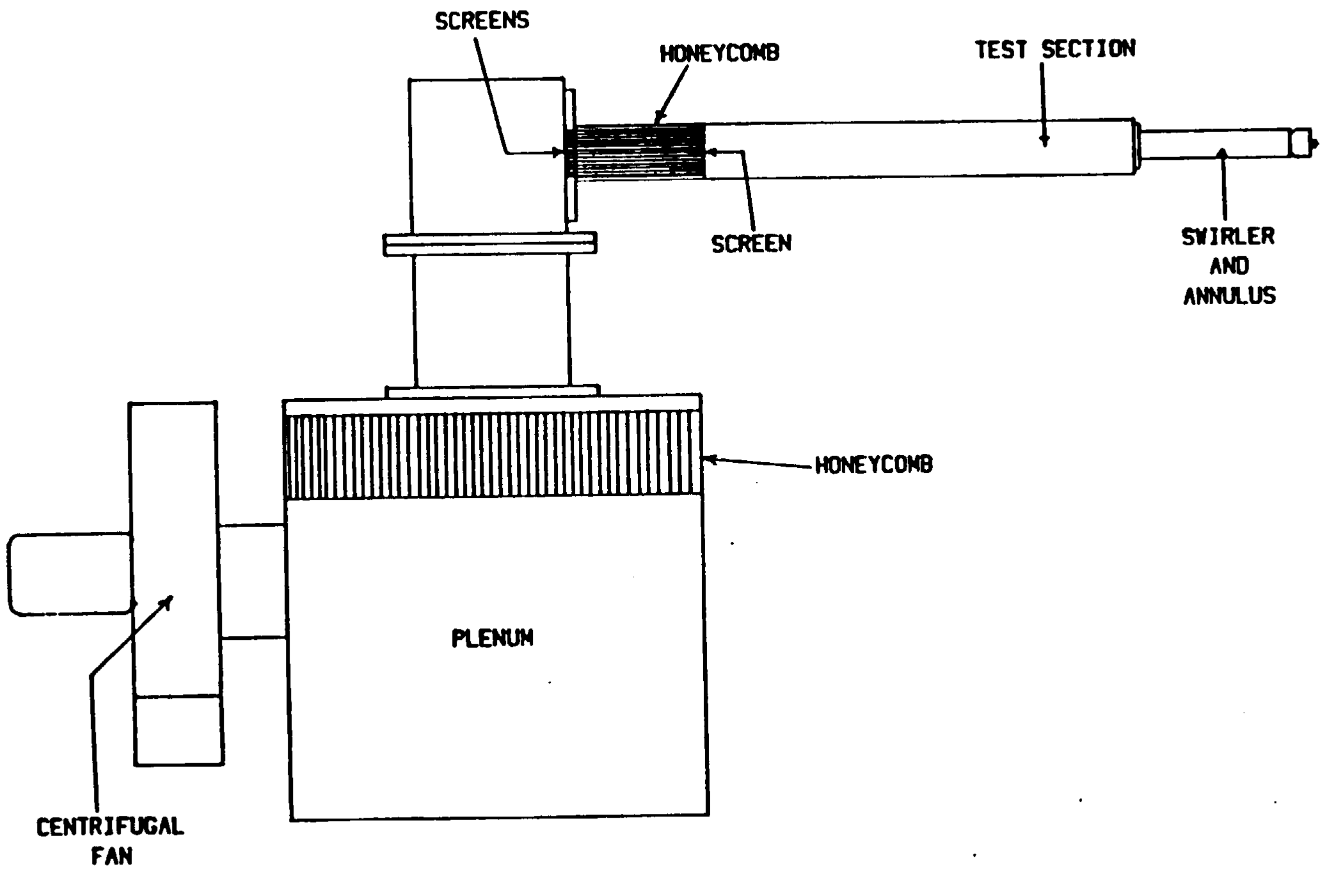

Figure 3.1 Single Swirler Rig for LDV Measurements

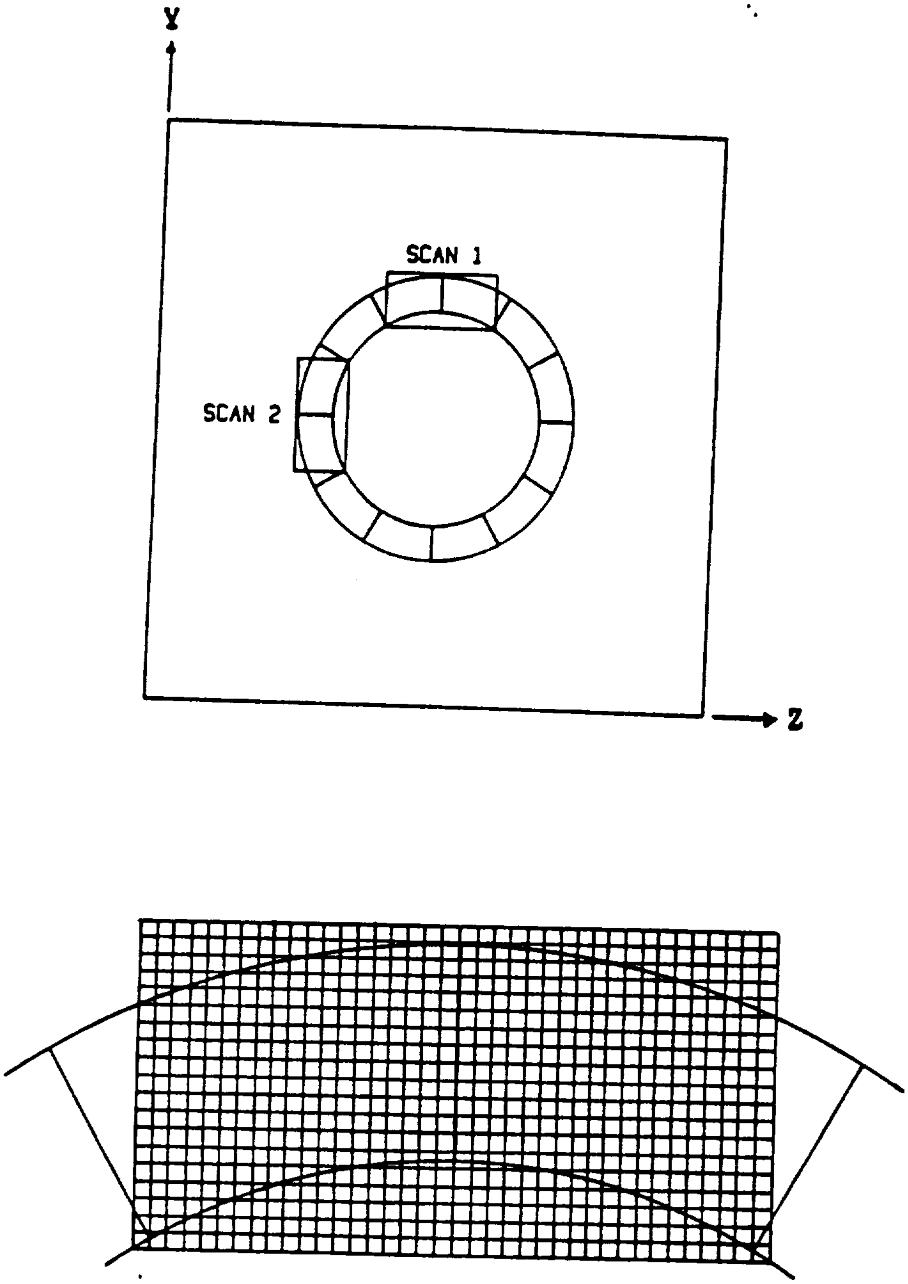

Figure 3.2 Swirler Inlet Data Grid

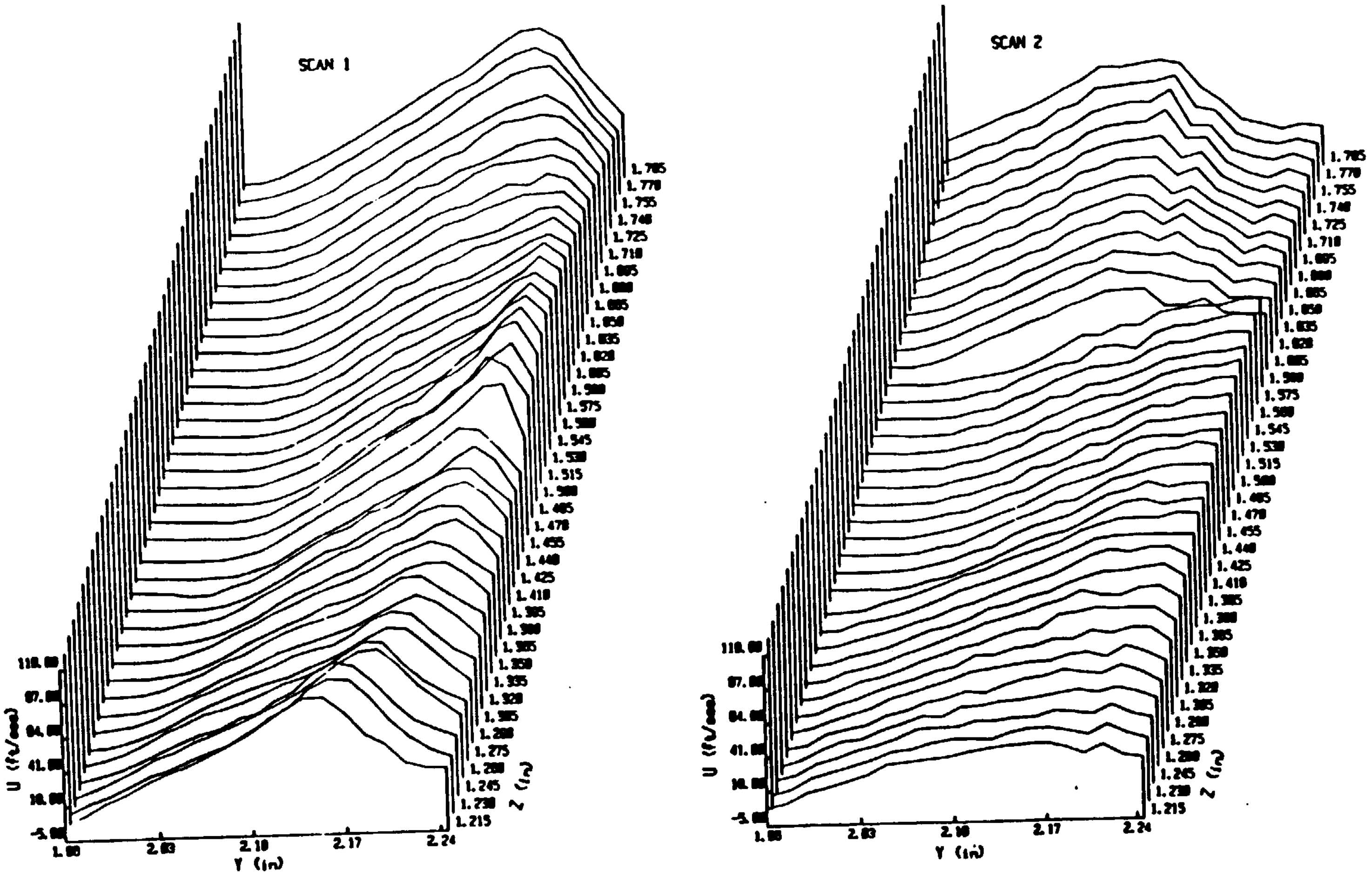

Figure 3.3 Cascade Plots of Swirler Inlet u Velocity
(scans 1 and 2)

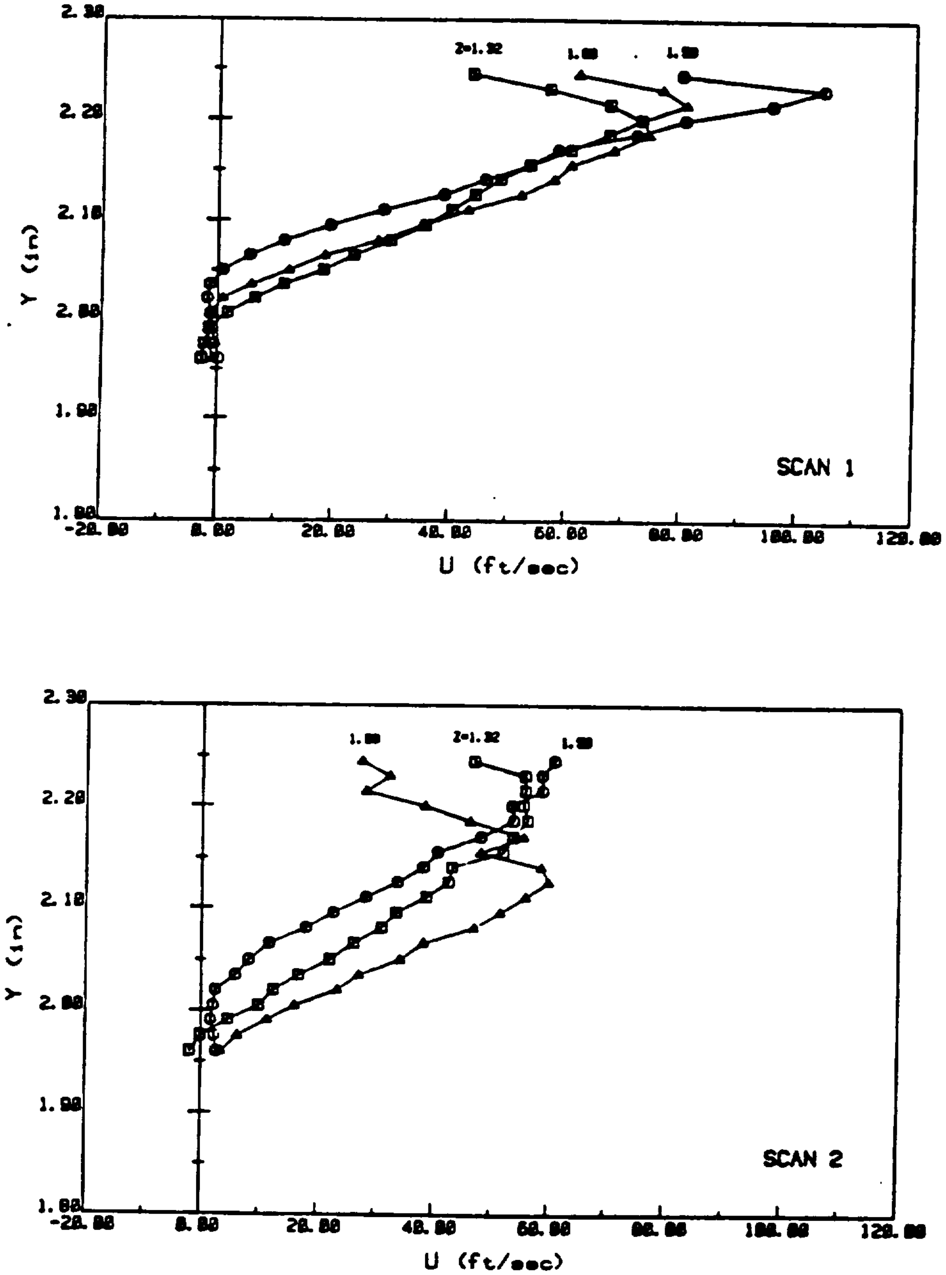

Figure 3.4 Swirler Inlet Plots of u Velocity at Specific z Locations (scans 1 and 2)

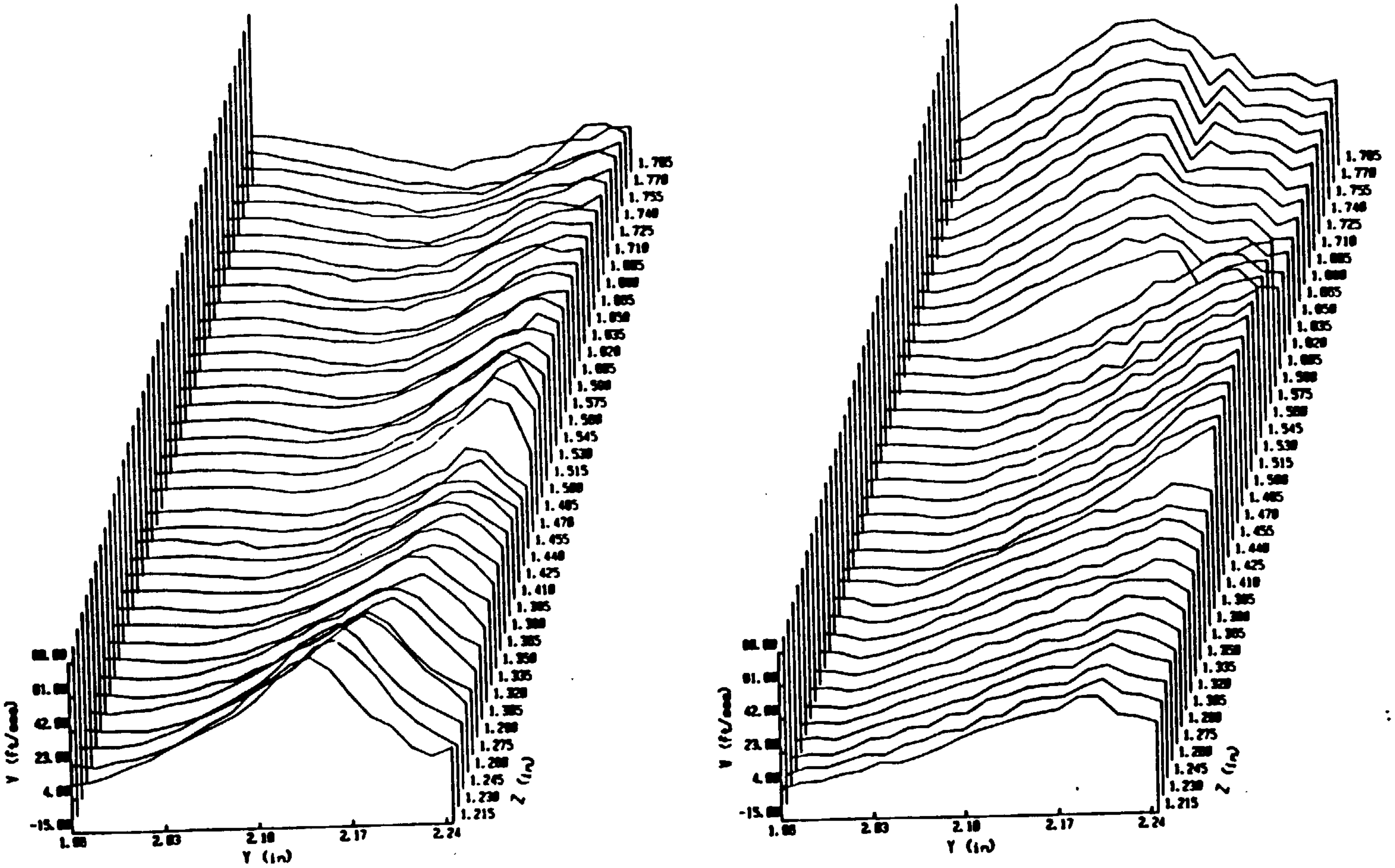

Figure 3.5 Cascade Plots of Swirler Inlet v and w Velocities

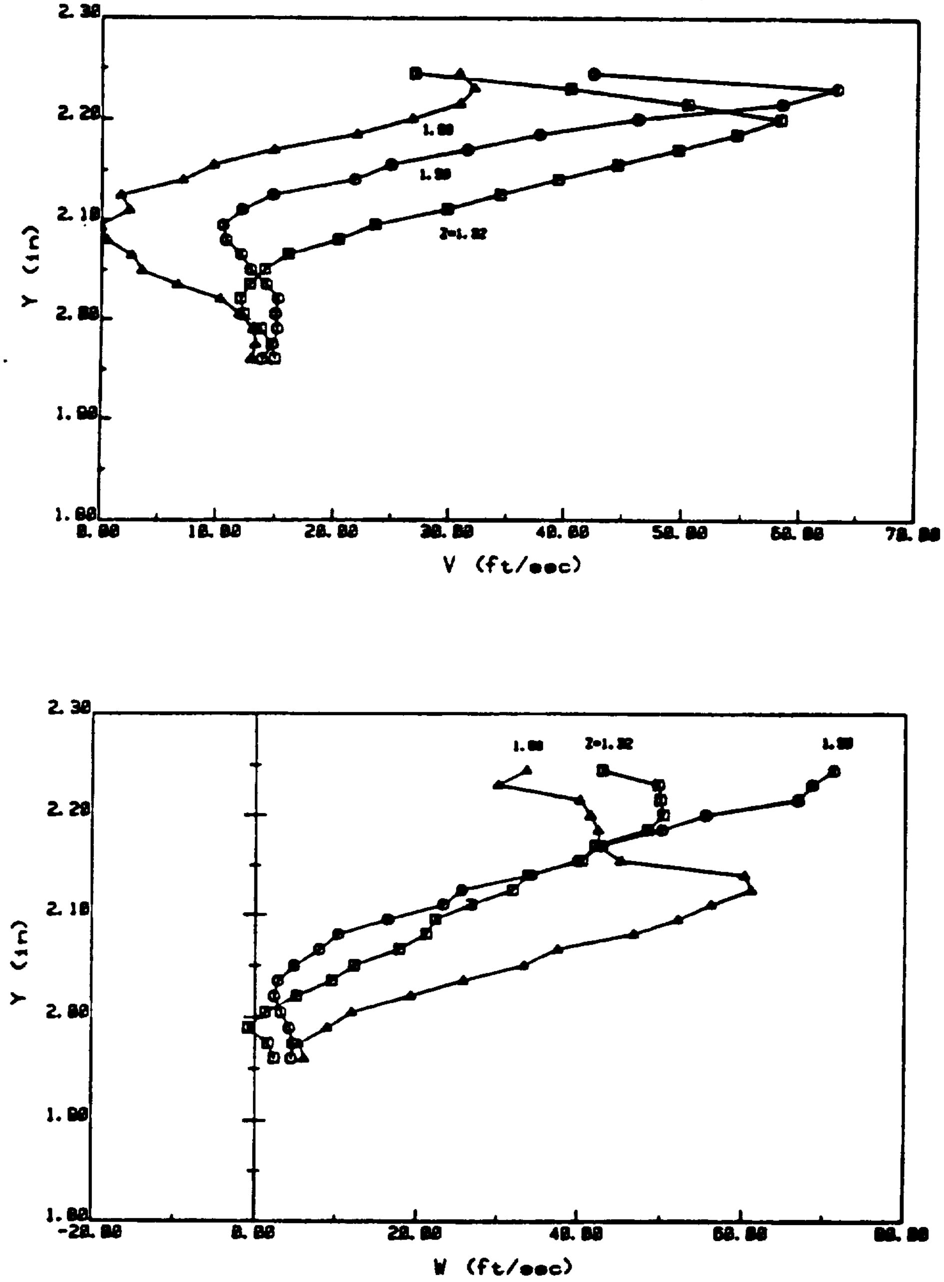

Figure 3.6 Swirler Inlet Plots of v and w Velocities at Specific z Locations

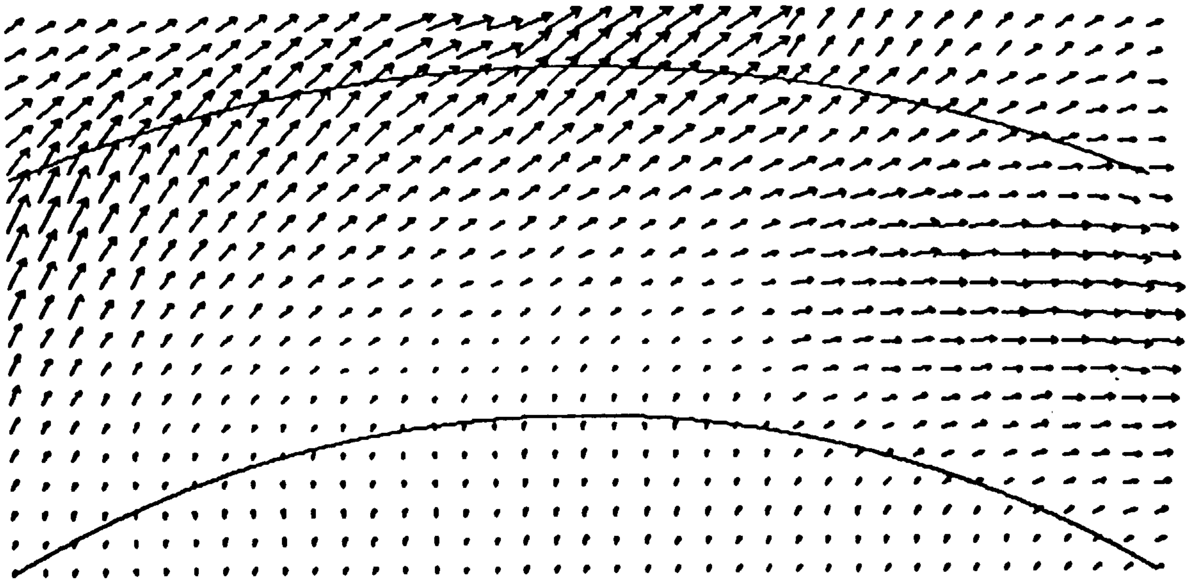

Figure 3.7 Vector Plot of Swirler Inlet v and w Velocities

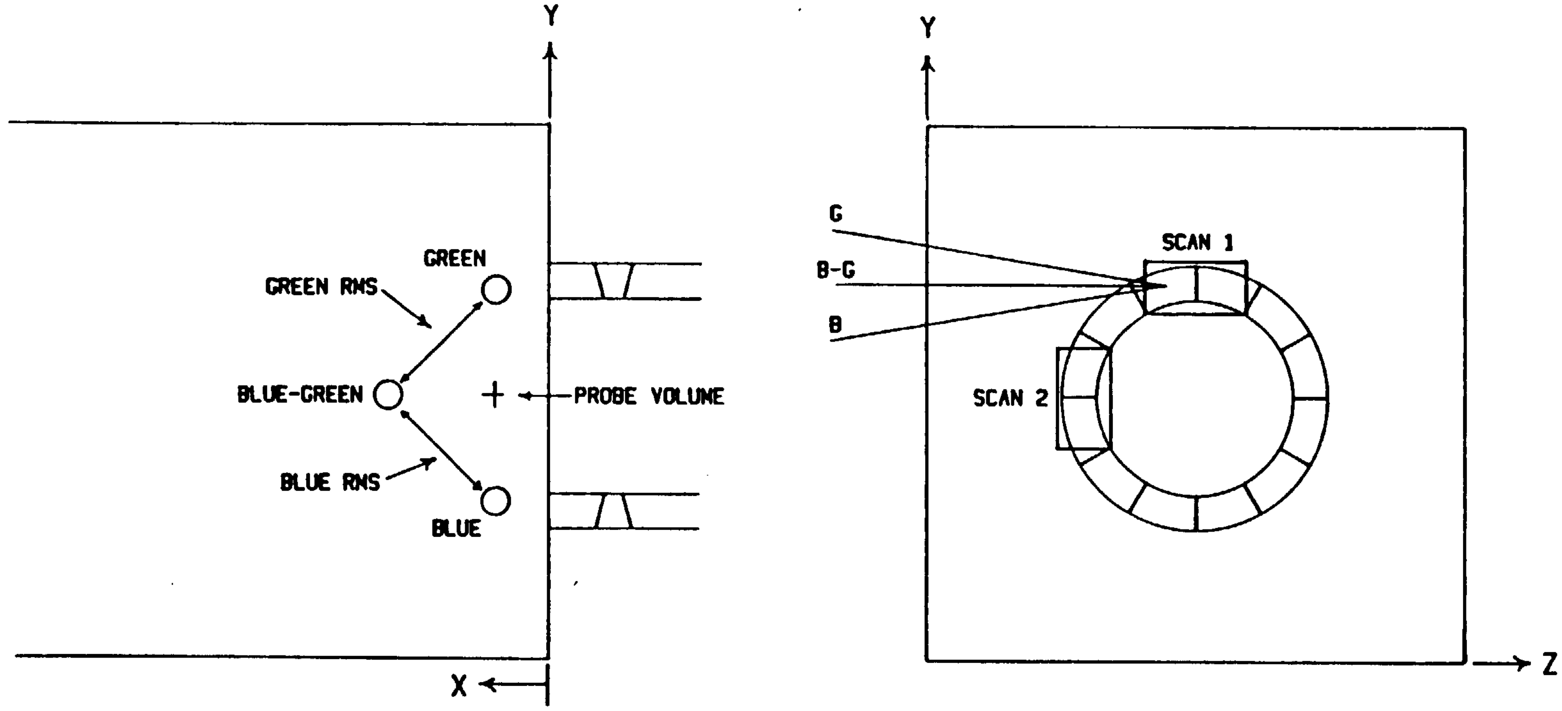

Figure 3.8 Swirler Inlet Laser Orientation

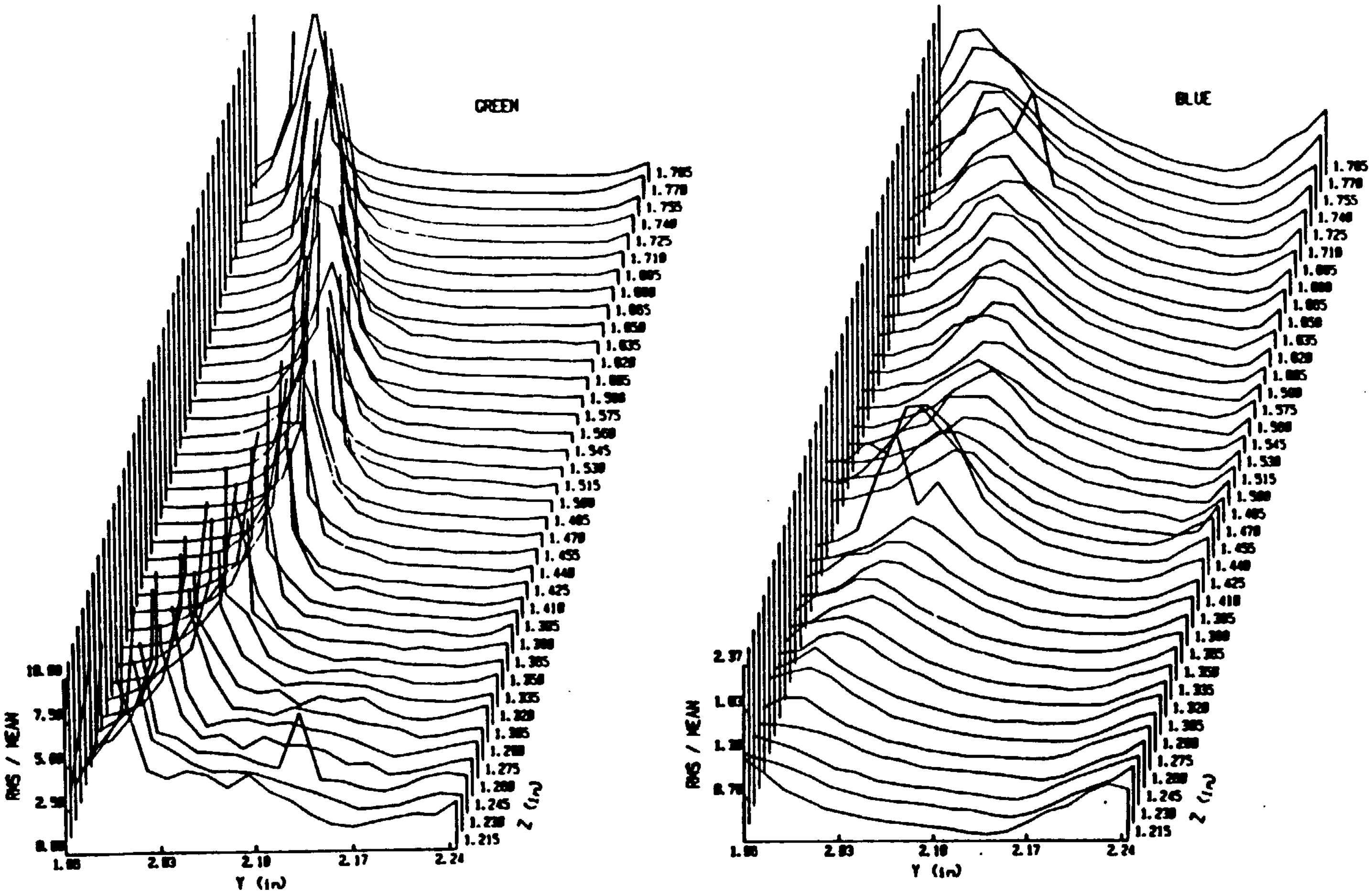

Figure 3.9 Cascade Plots of Turbulence Intensity for Swirler Inlet (scan 1)

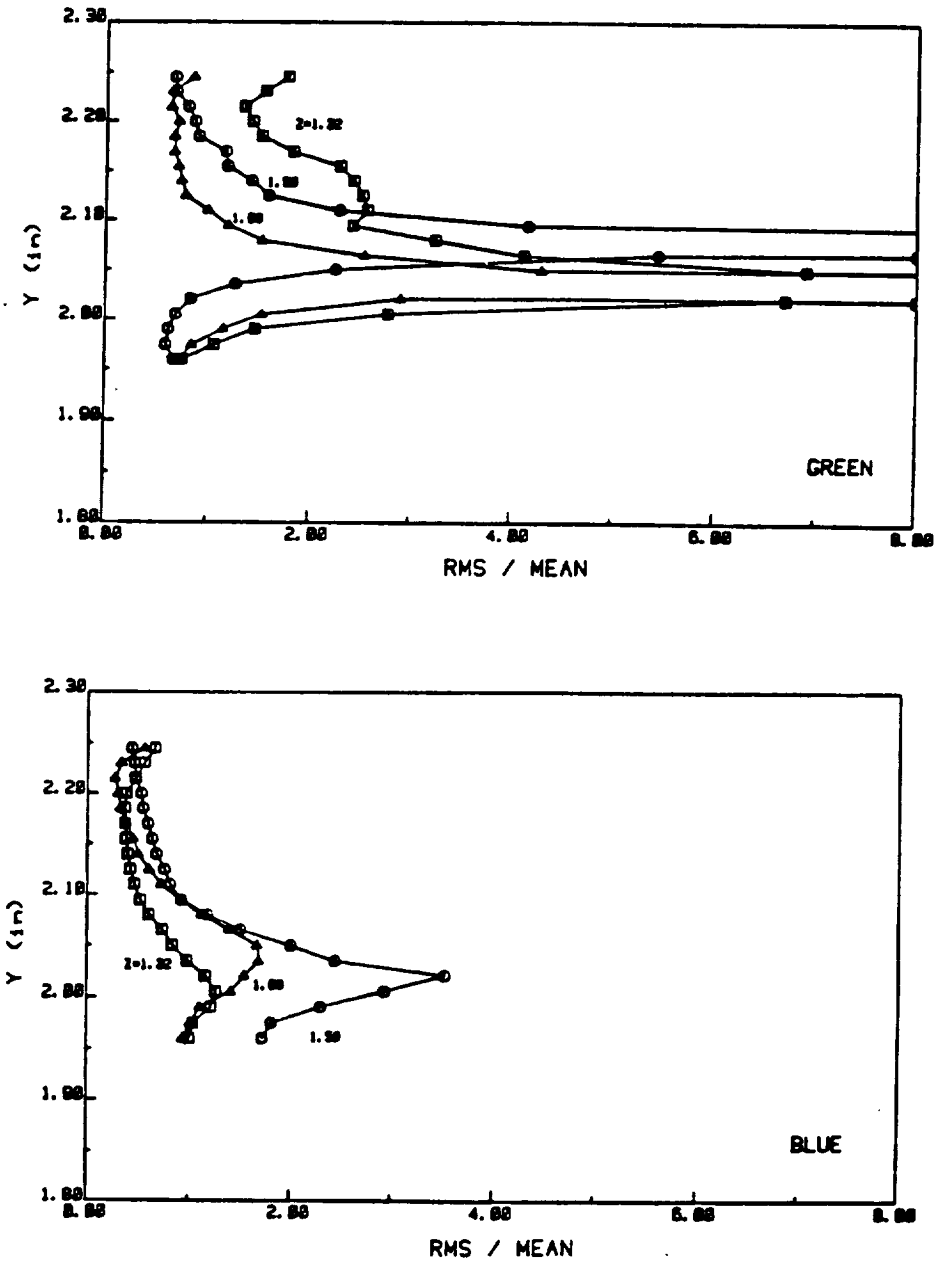

Figure 3.10 Swirler Inlet Plots of Turbulence Intensity at Specific z Locations (scan 1)

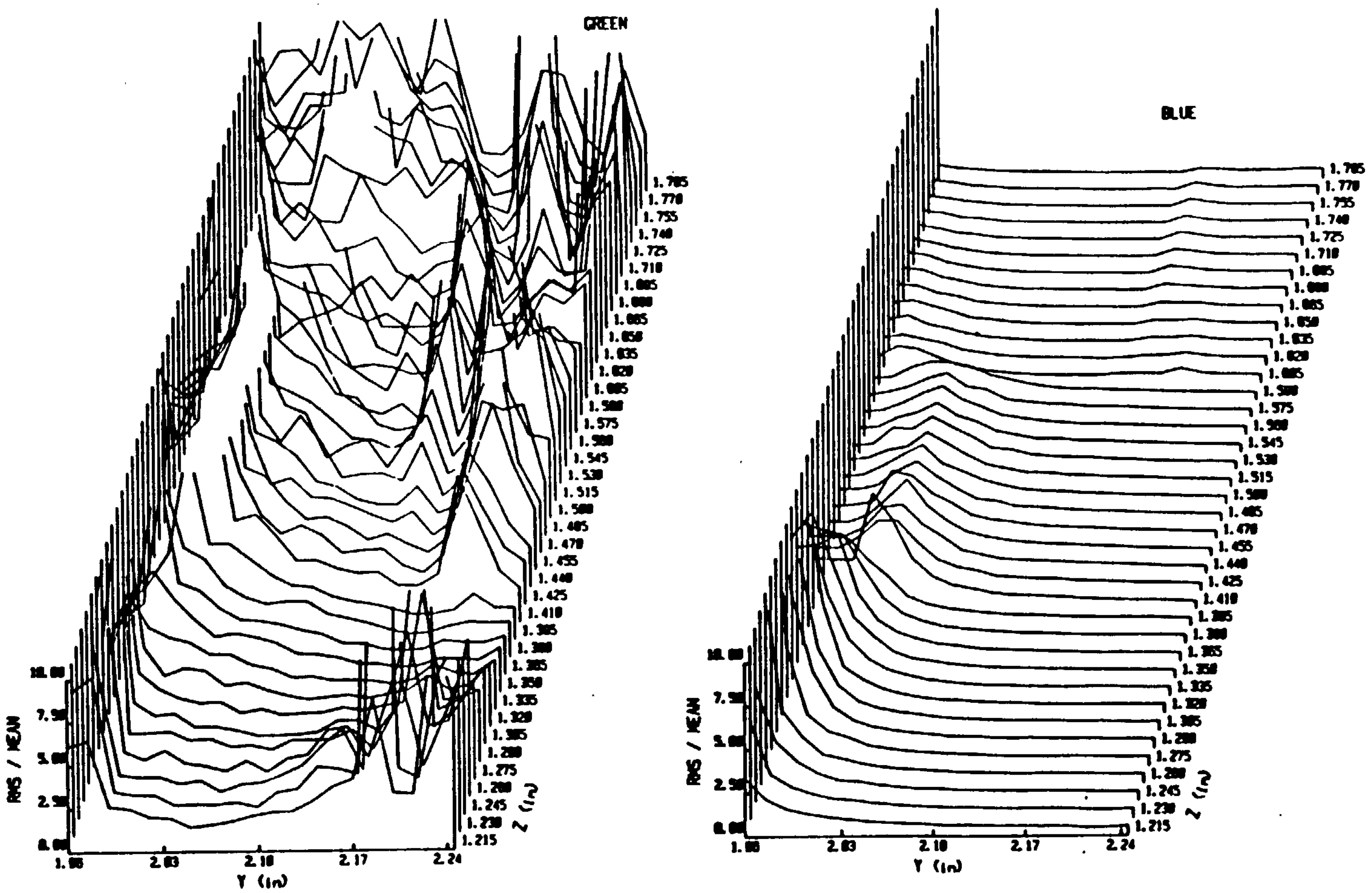

Figure 3.11 Cascade Plots of Turbulence Intensity for Swirler Inlet (scan 2)

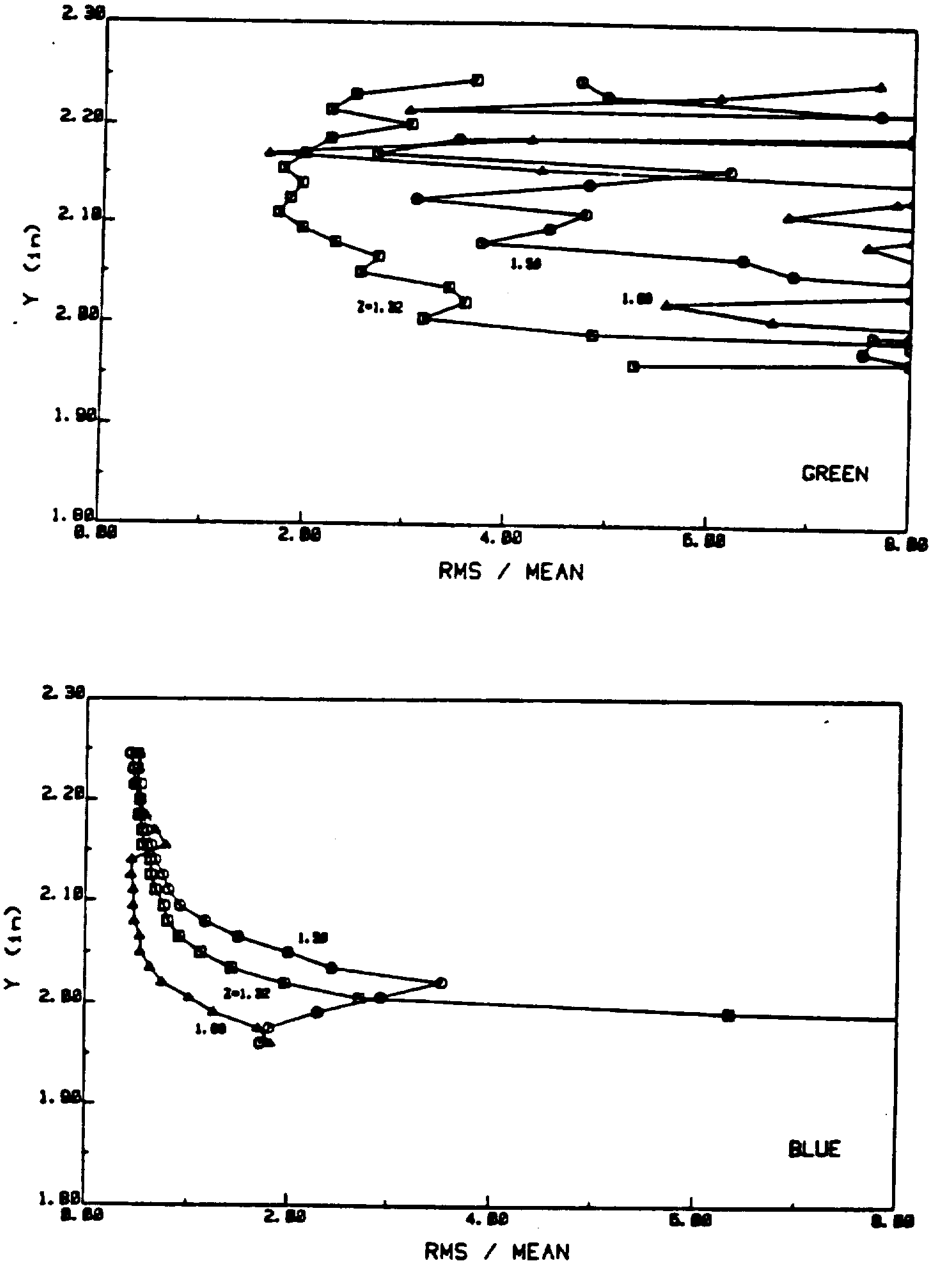

Figure 3.12 Swirler Inlet Plots of Turbulence Intensity at Specific z Locations (scan 2)

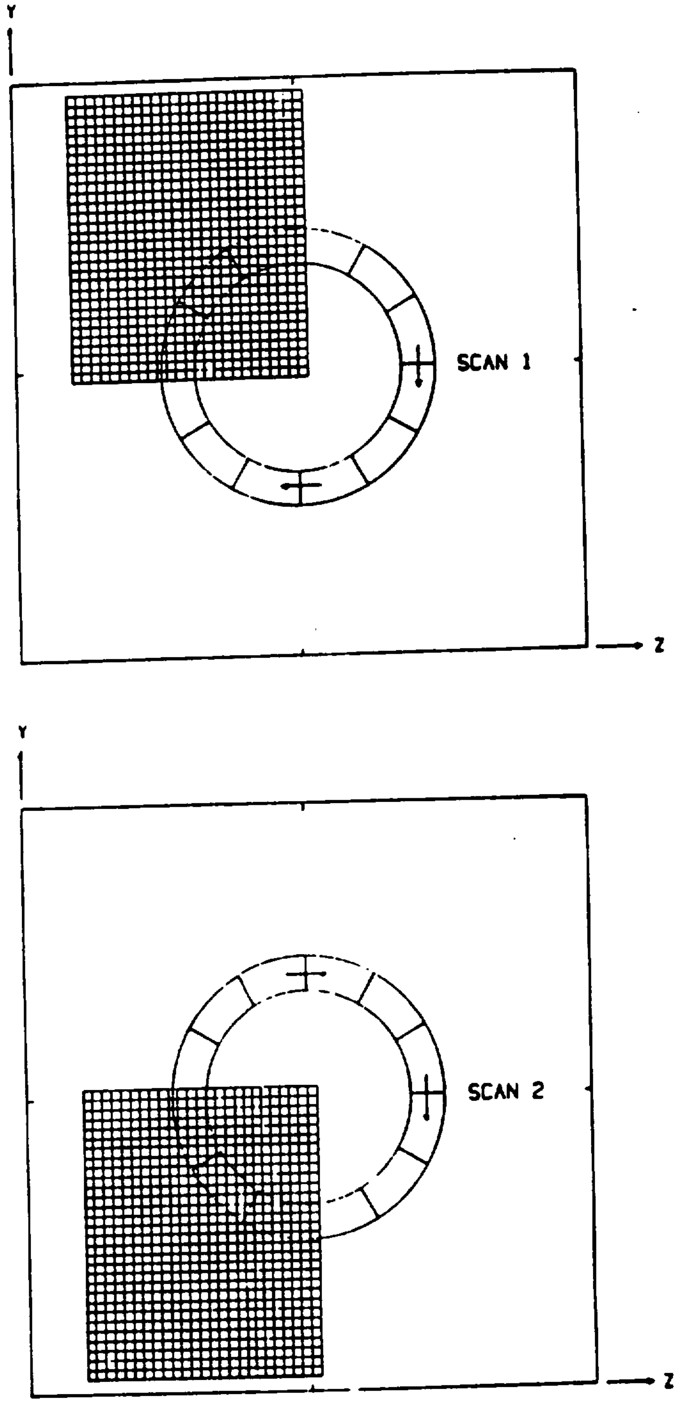

Figure 3.13 Downstream Data Grid (scans 1 and 2)

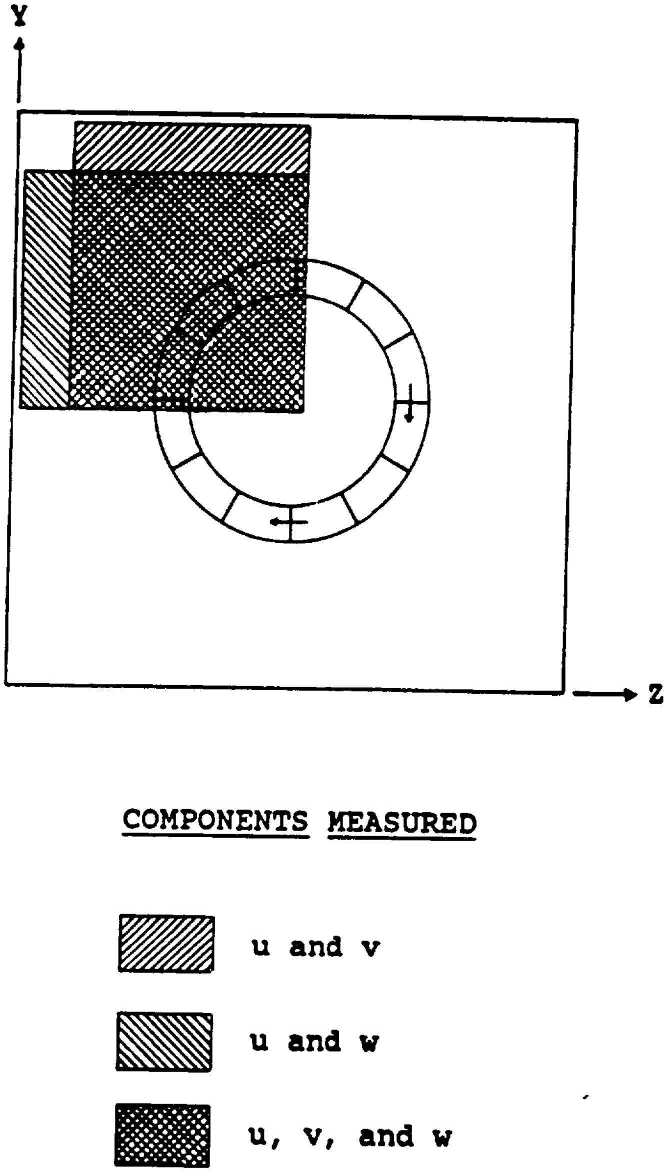

Figure 3.14 Combined Data Grid

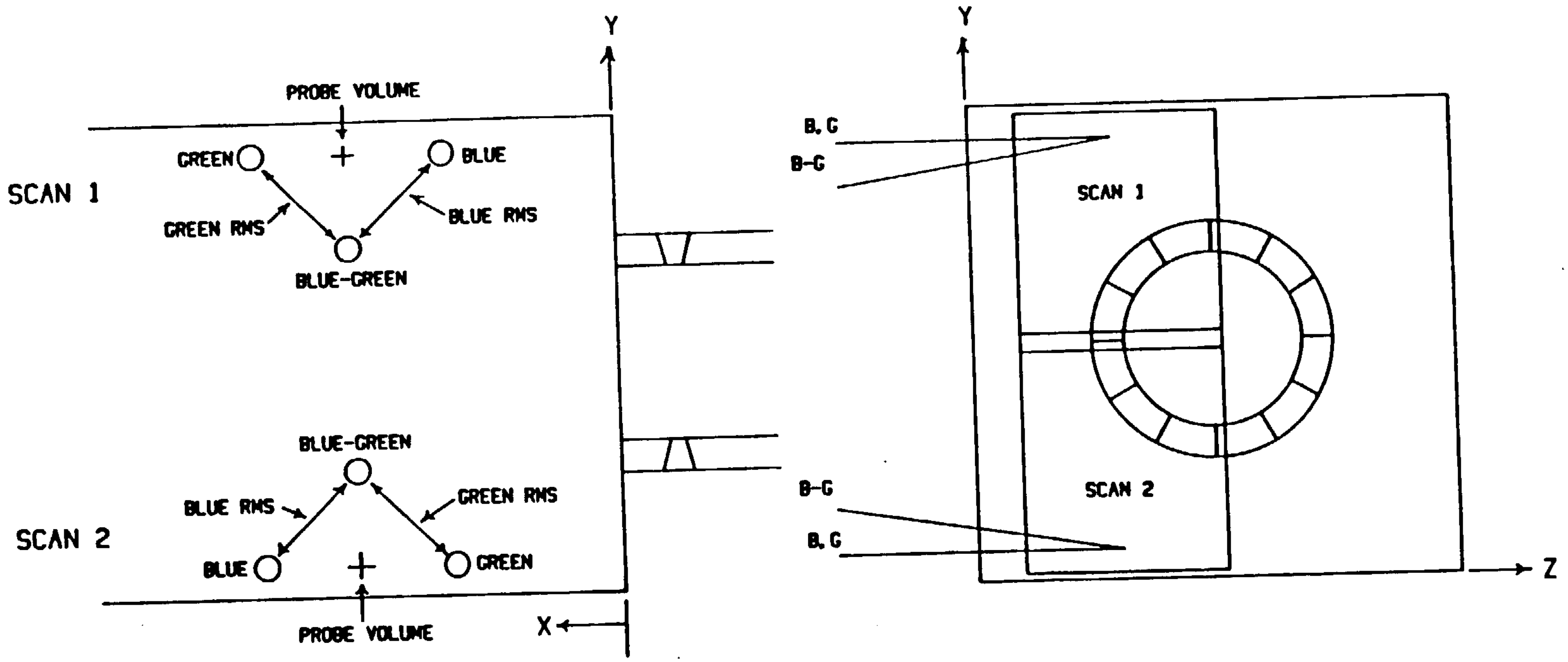

Figure 3.15 Laser Orientation for Downstream Data

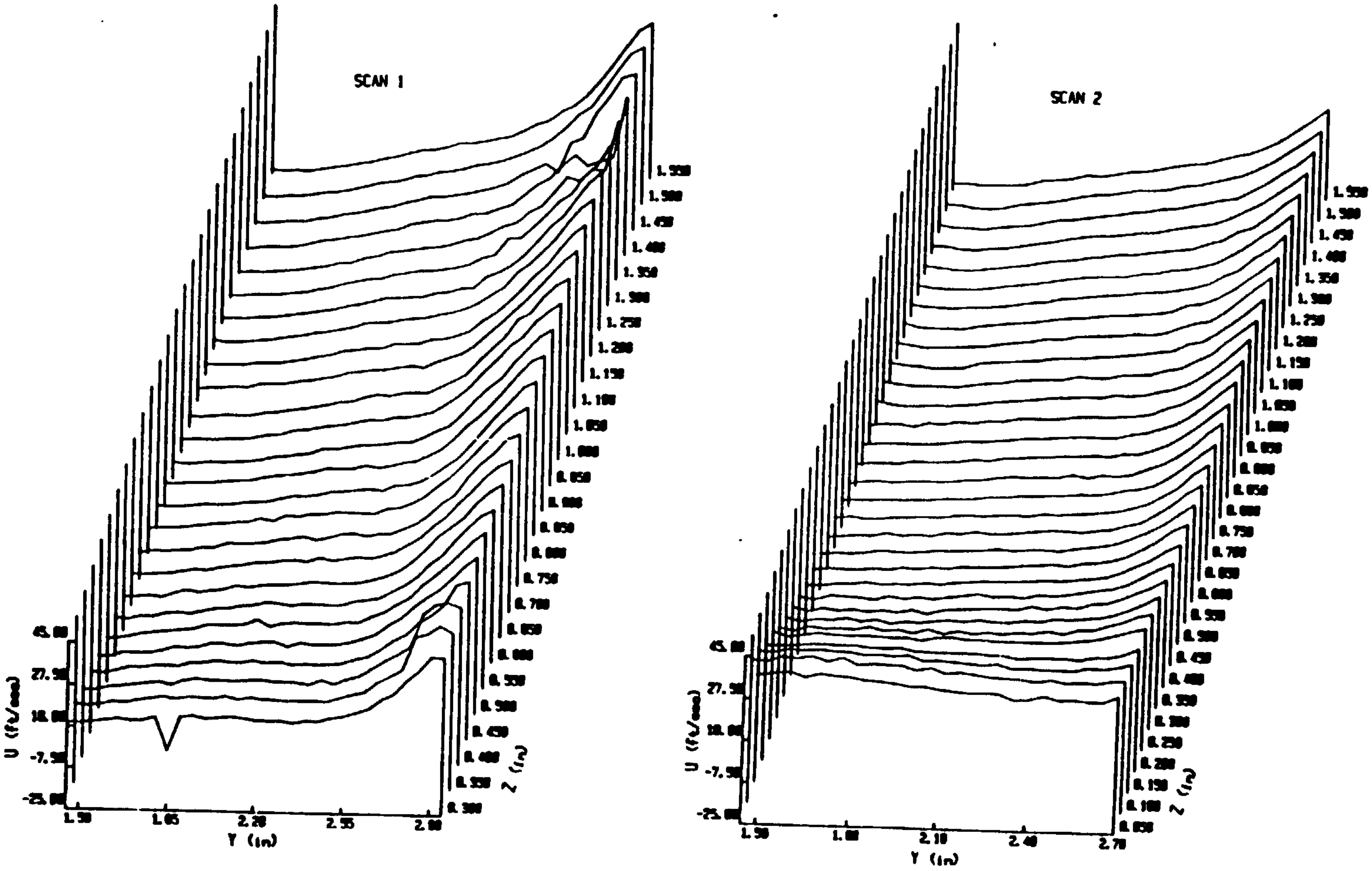

Figure 3.16 Cascade Plots of u Velocity at x=1.5 inches
(scans 1 and 2)

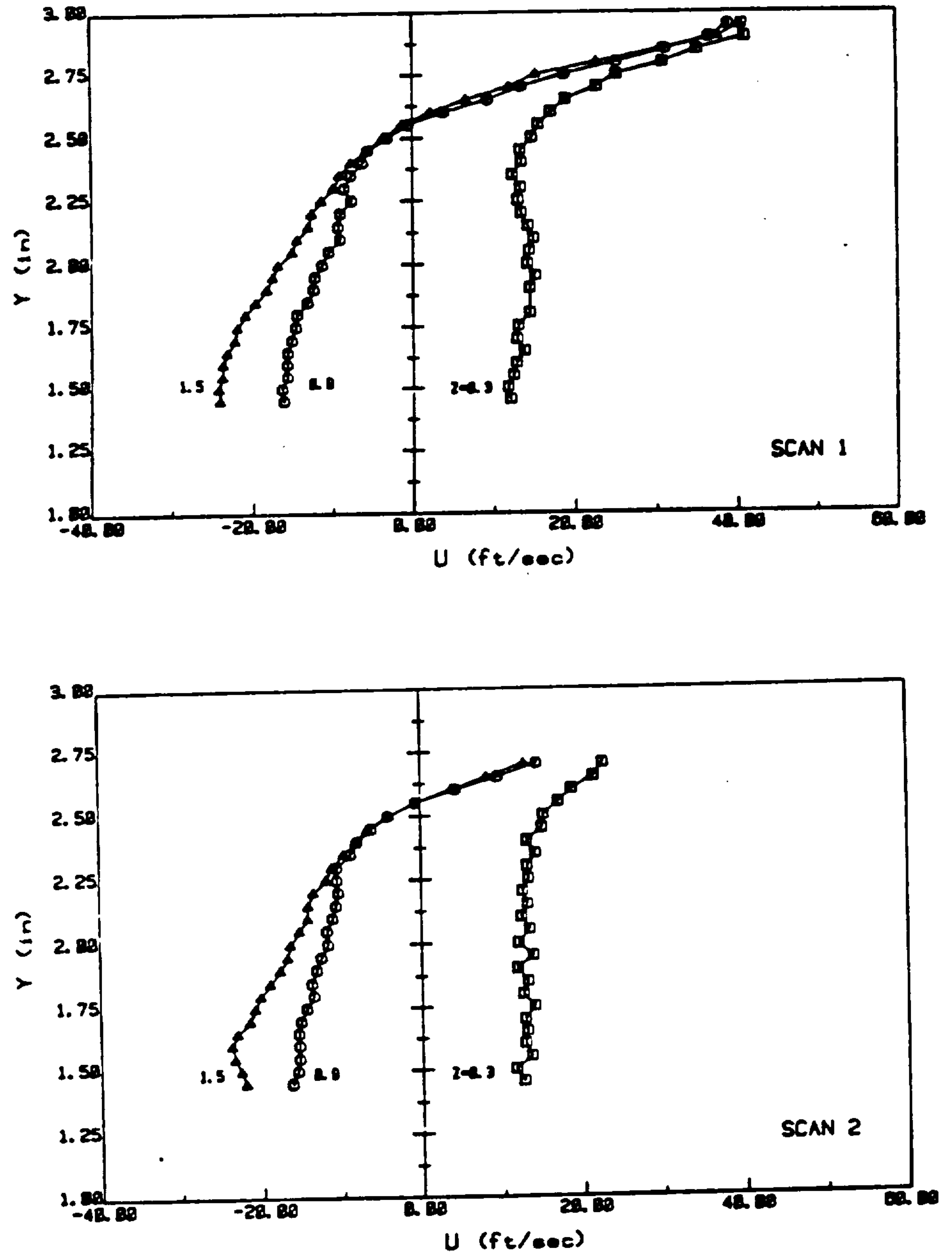

Figure 3.17 Plots of u Velocity at x=1.5 inches
(scans 1 and 2)

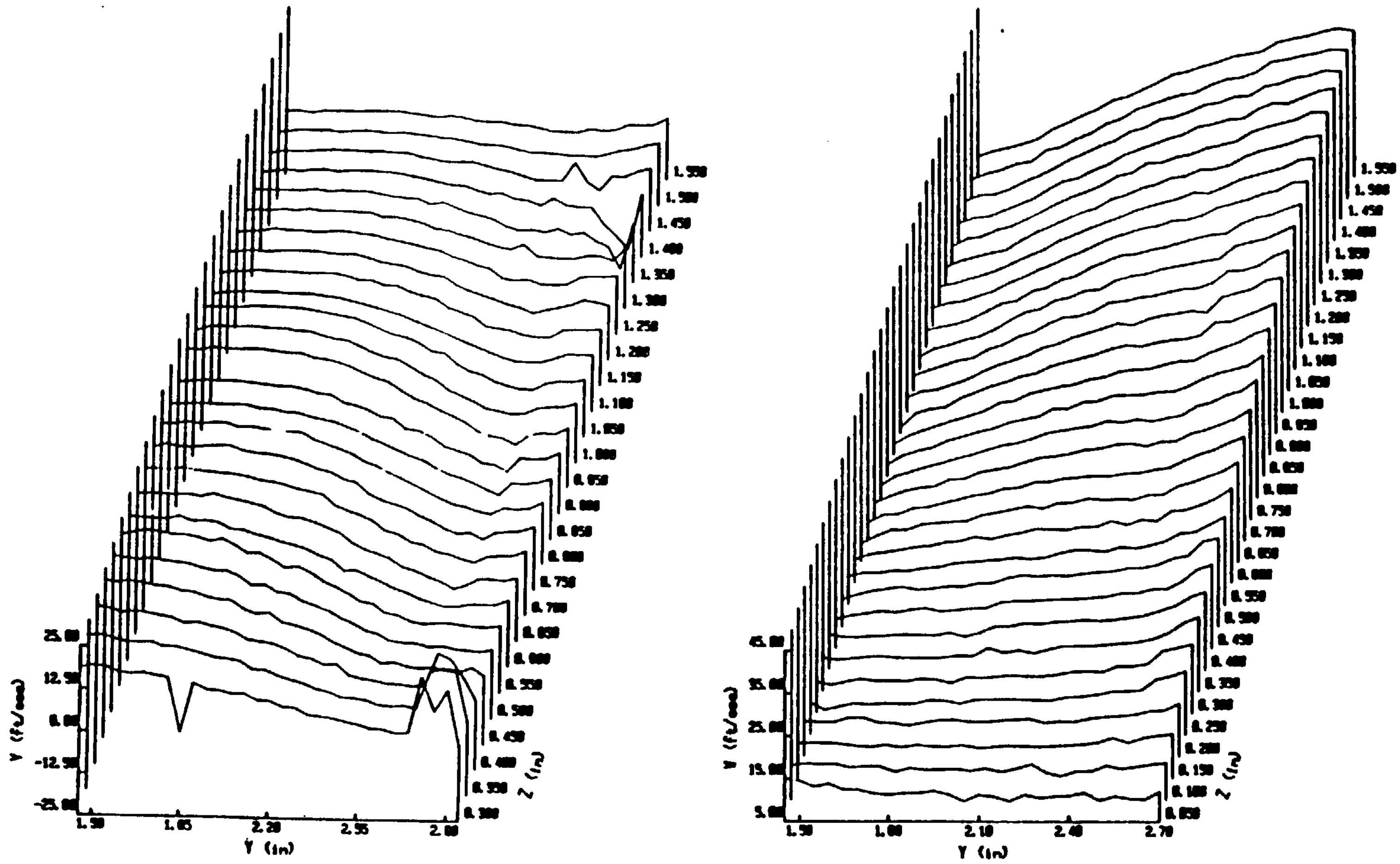

Figure 3.18 Cascade Plots of v and w Velocities at x=1.5 inches

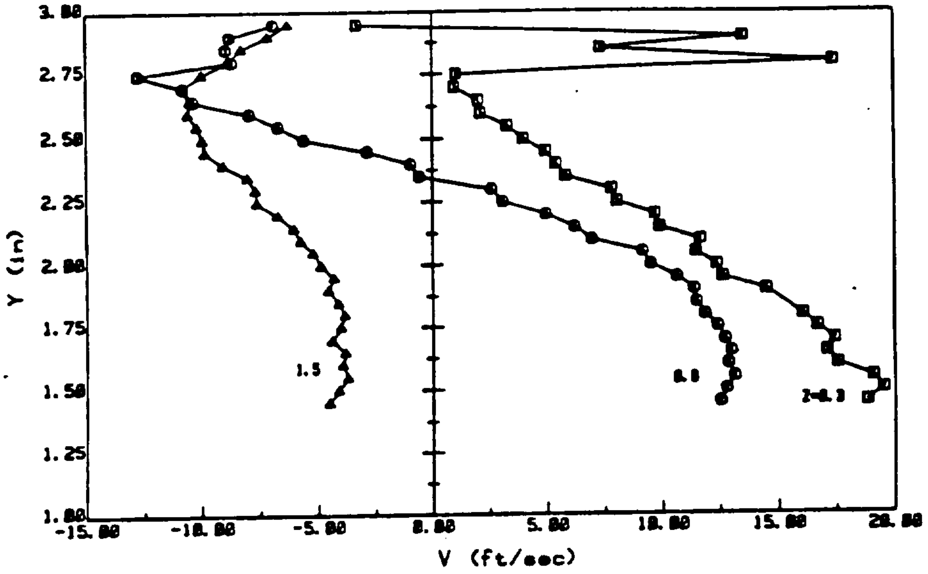

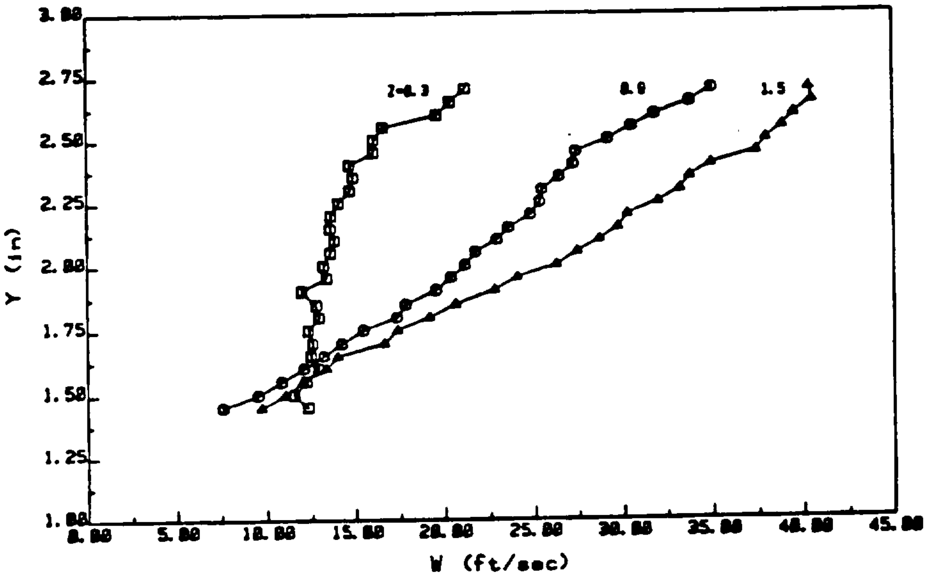

Figure 3.19 Plots of v and w Velocities at x=1.5 inches

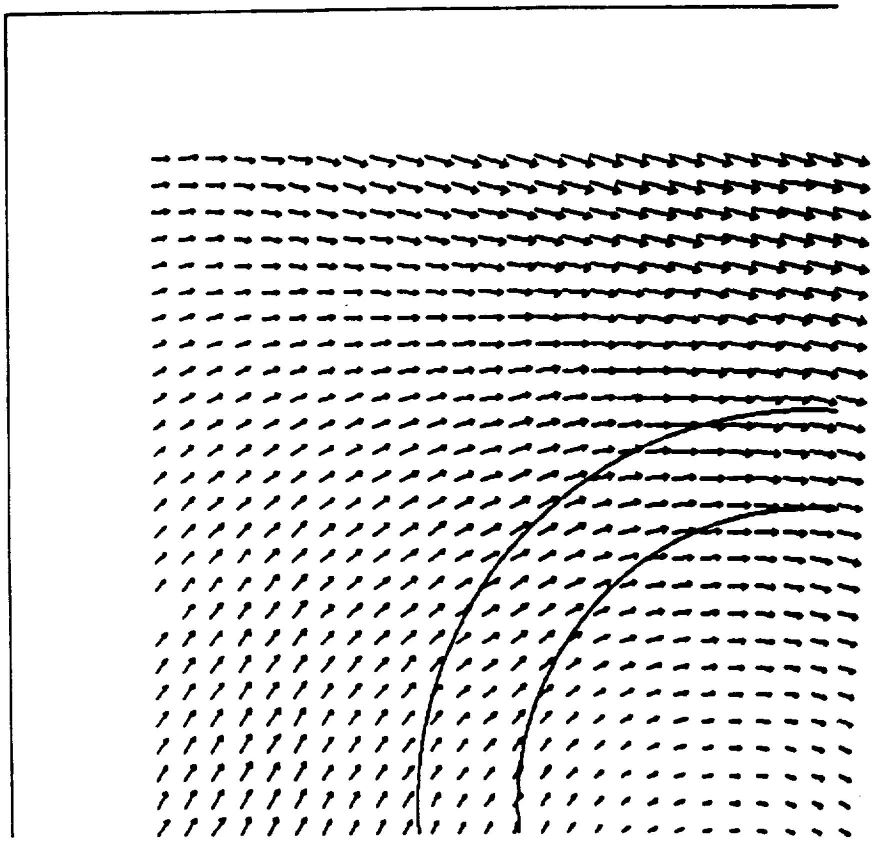

Figure 3.20 Vector Plot of v and w Velocities at x=1.5 inches

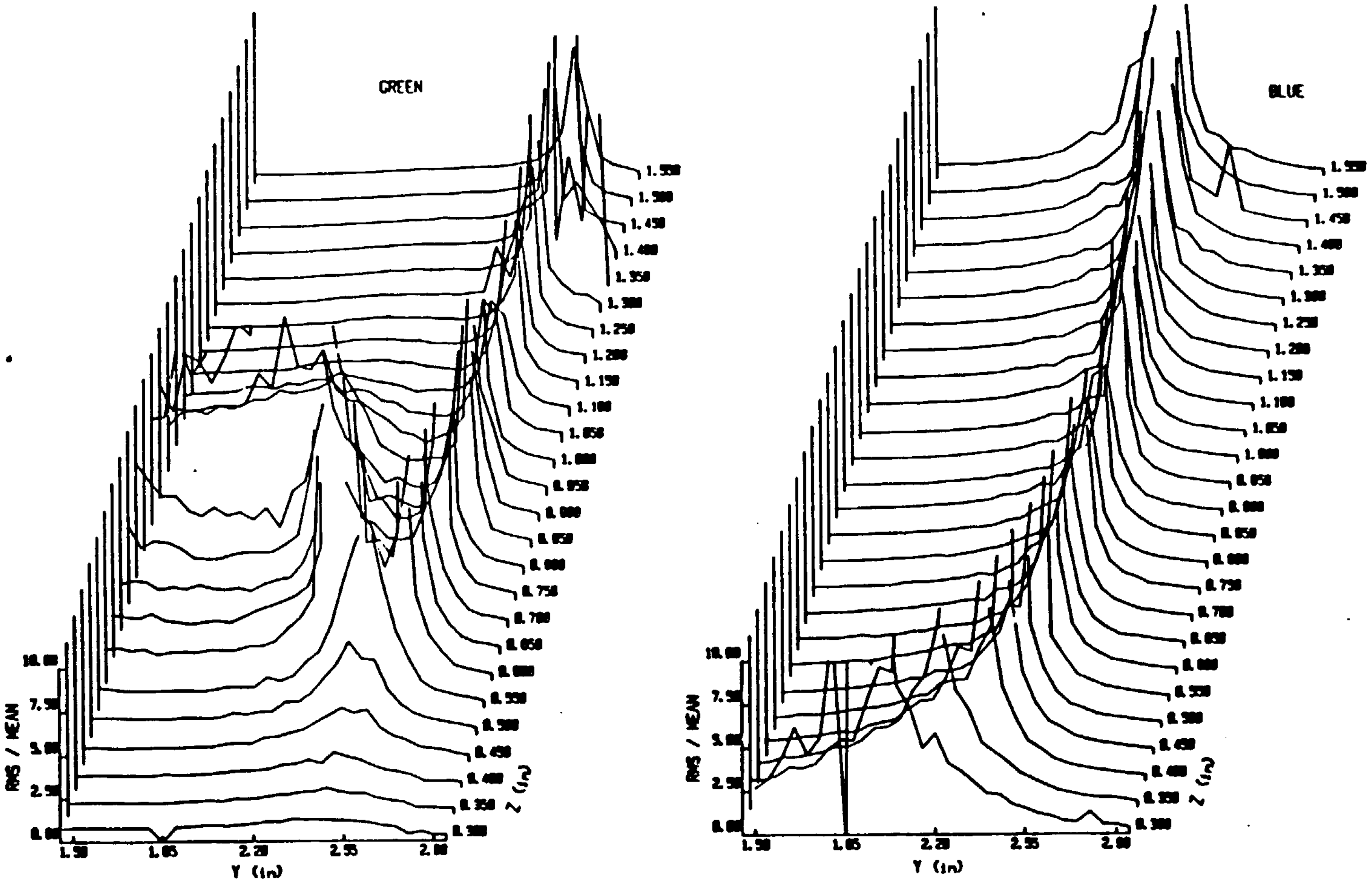

Figure 3.21 Cascade Plots of Turbulence Intensity at x=1.5 inches (scan 1)

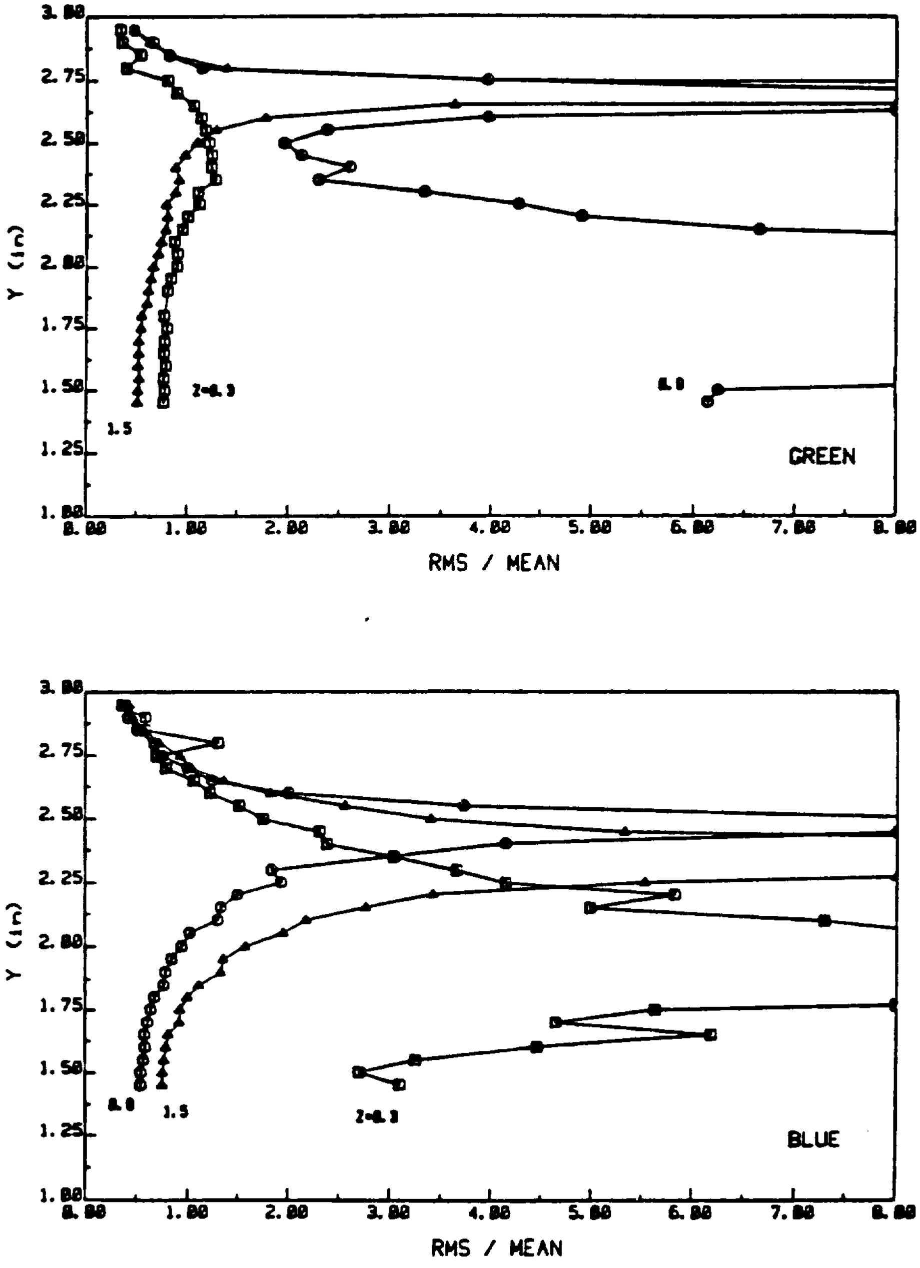

Figure 3.22 Plots of Turbulence Intensity at x=1.5 inches (scan 1)

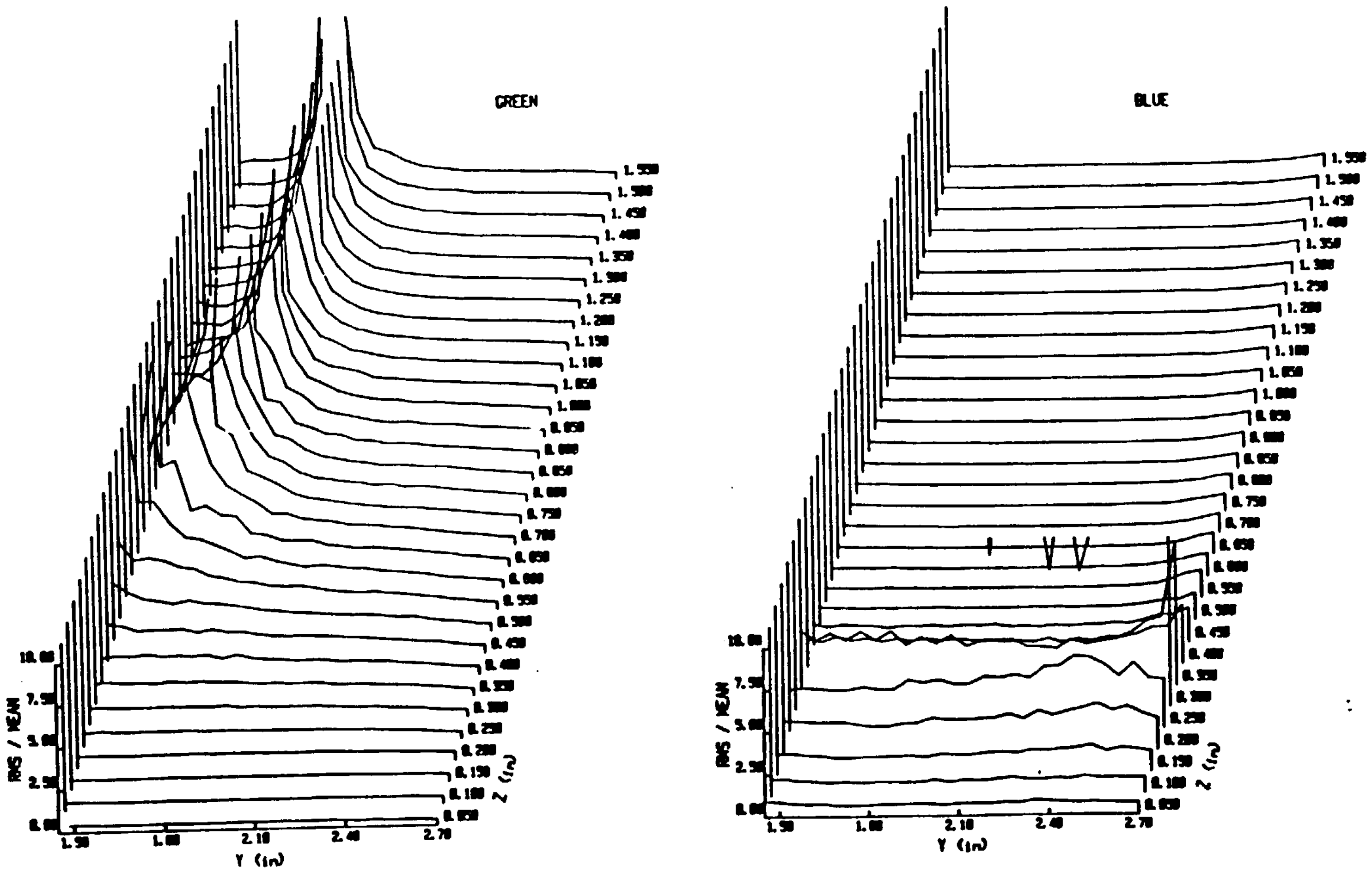

Figure 3.23 Cascade Plots of Turbulence Intensity at x=1.5 inches (scan 2)

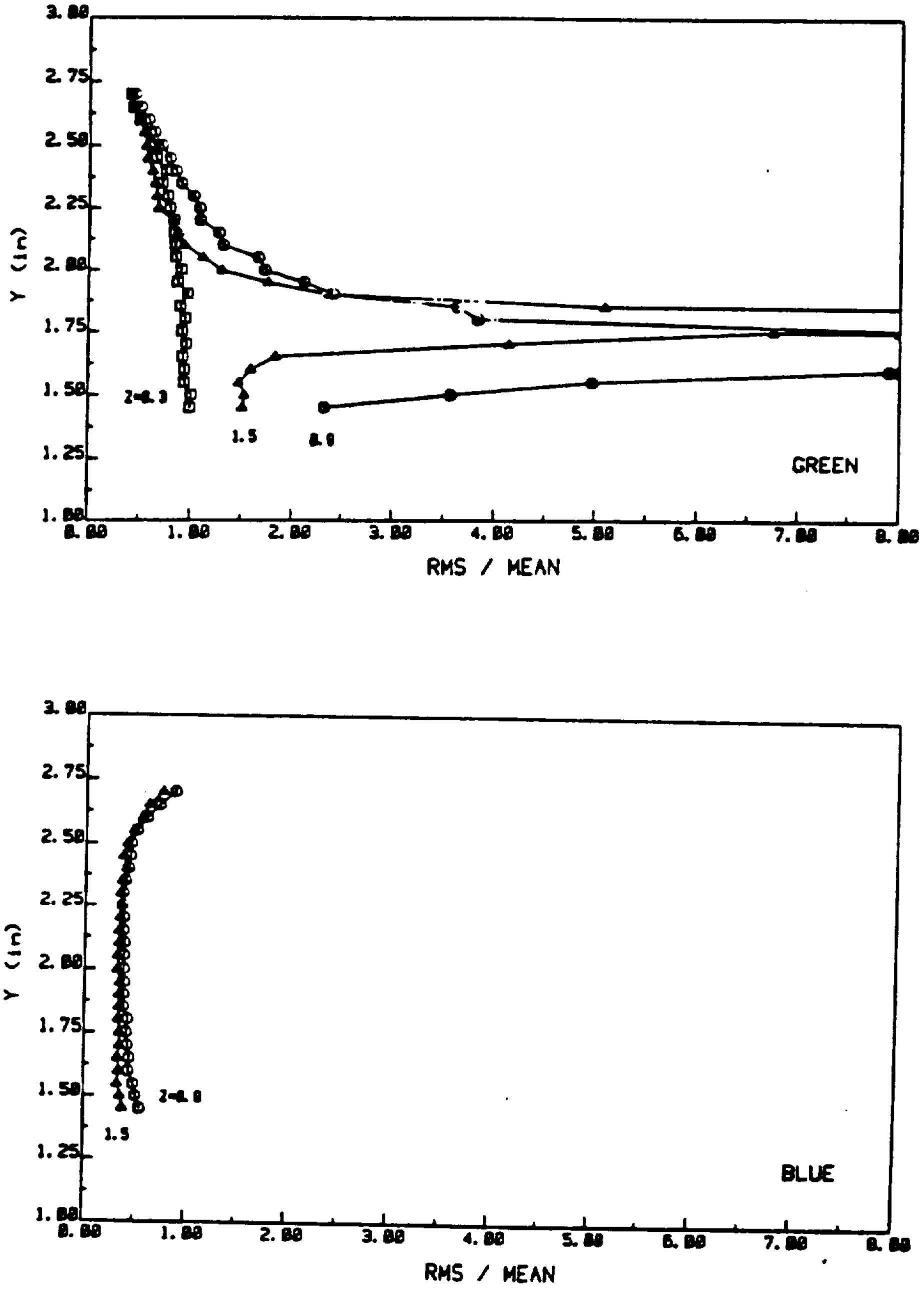

Figure 3.24 Plots of Turbulence Intensity at x=1.5 inches (scan 2)

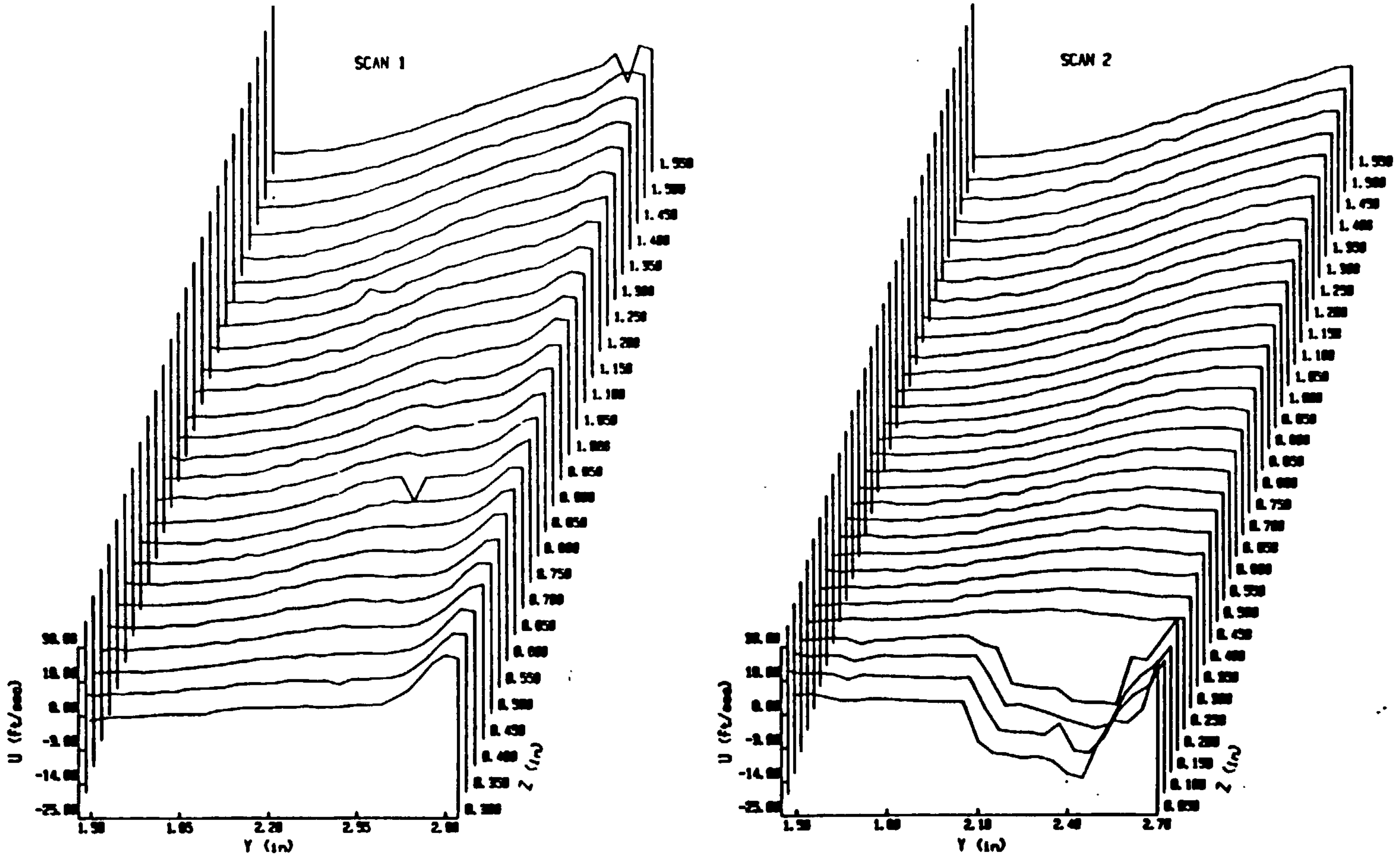

Figure 3.25 Cascade Plots of u Velocity at x=3.0 inches
(scans 1 and 2)

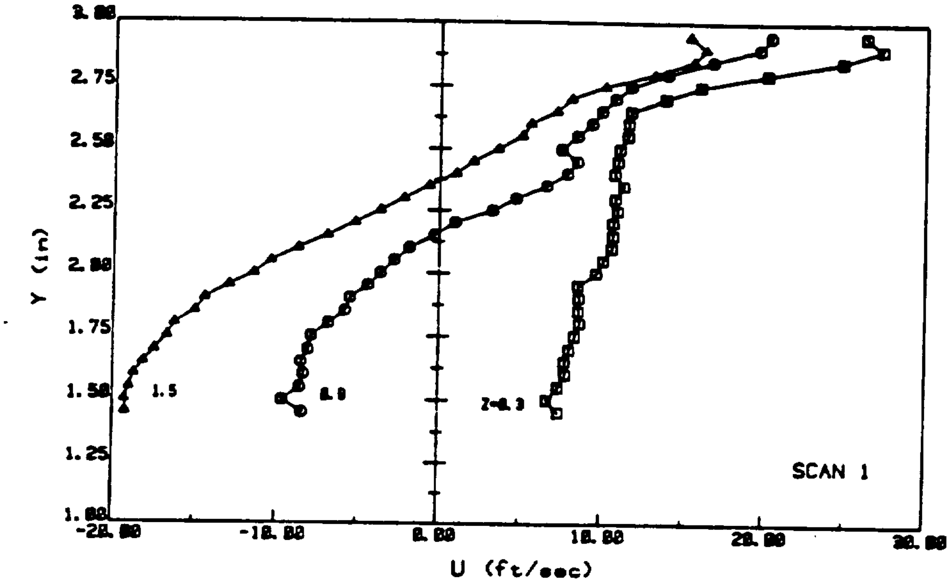

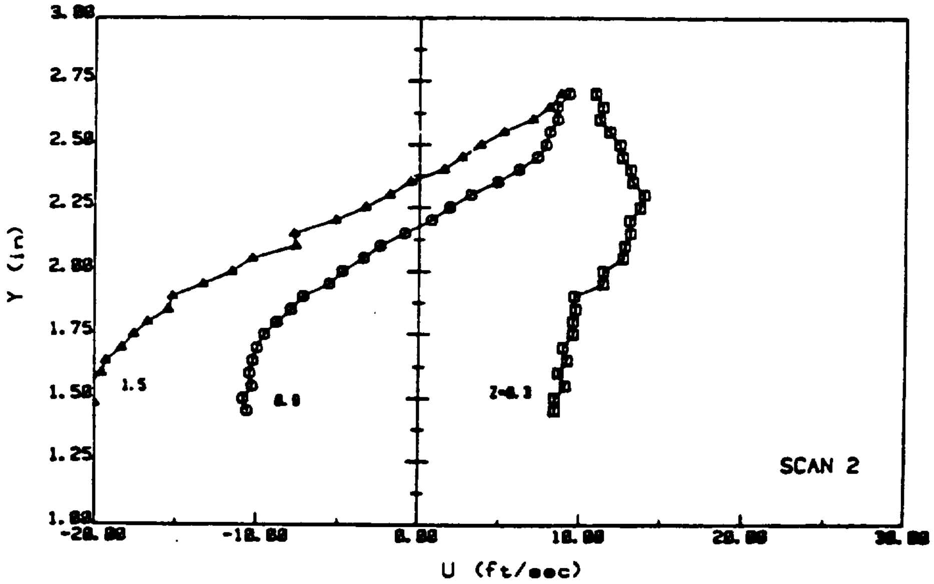

Figure 3.26 Plots of u Velocity at x=3.0 inches (scans 1 and 2)

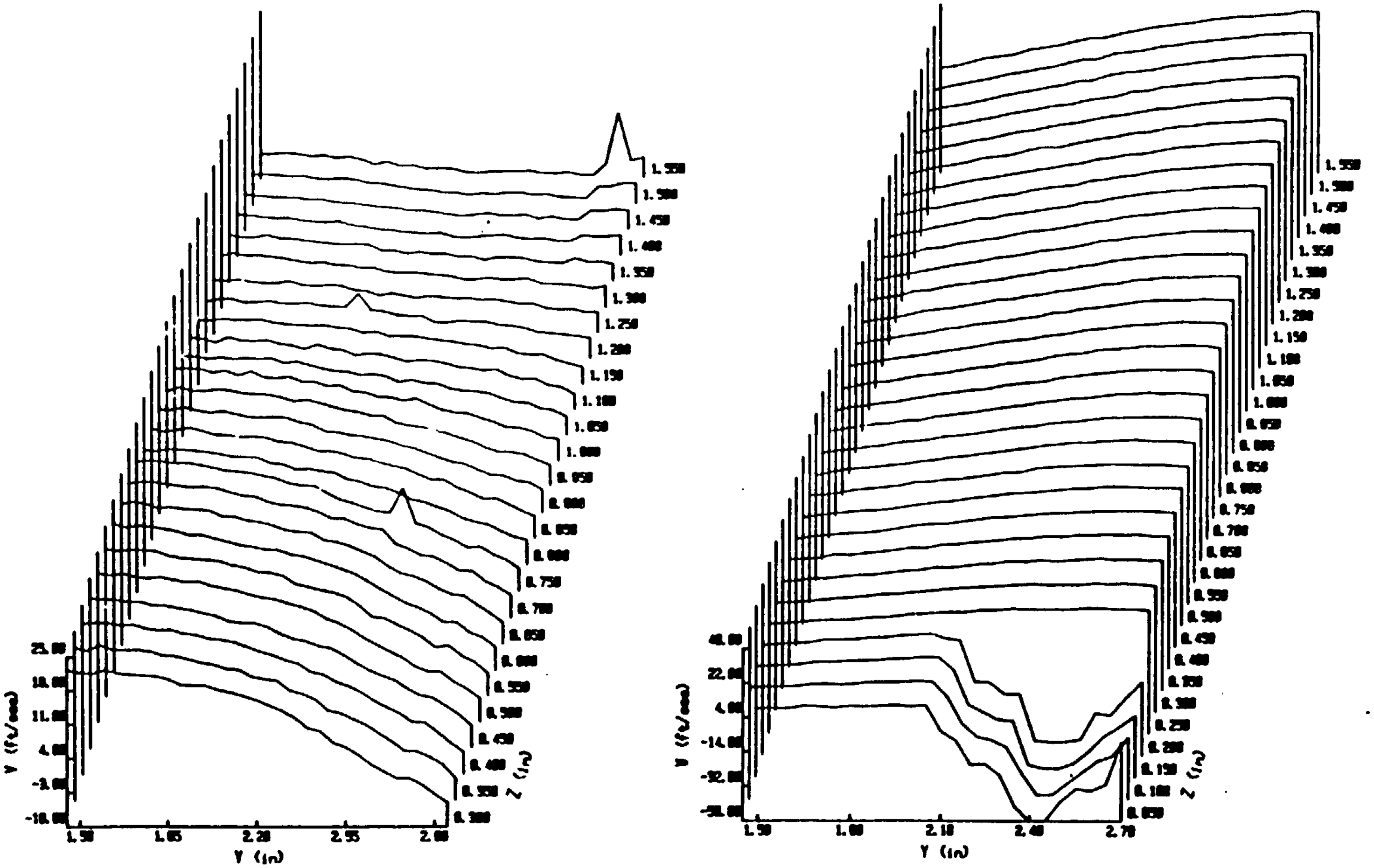

Figure 3.27 Cascade Plots of v and w Velocities at x=3.0 inches

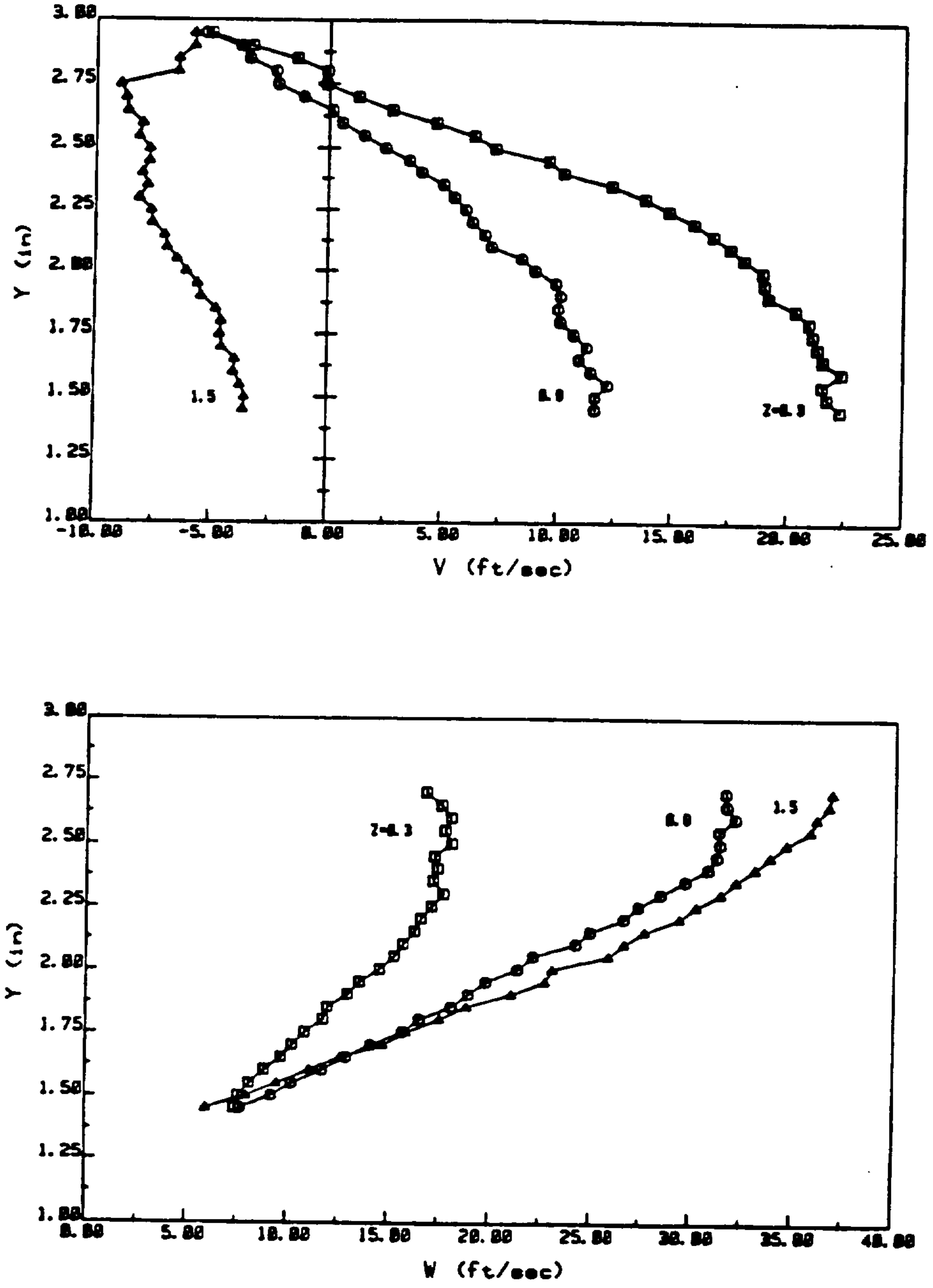

Figure 3.28 Plots of v and w Velocities at x=3.0 inches

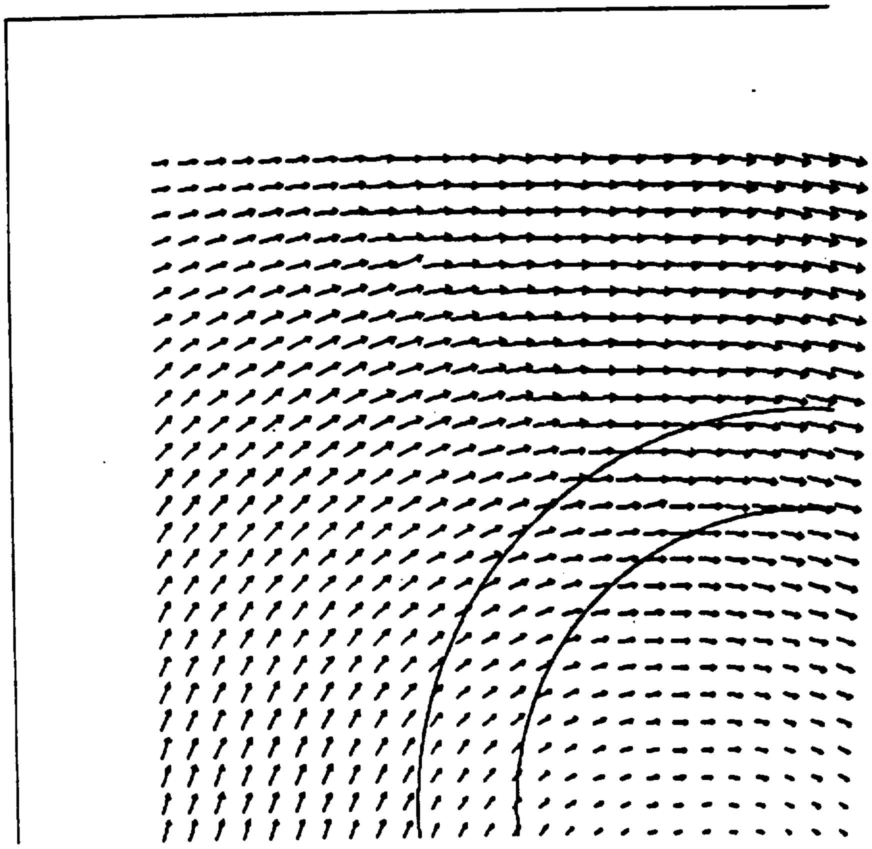

Figure 3.29 Vector Plot of v and w Velocities at x=3.0 inches

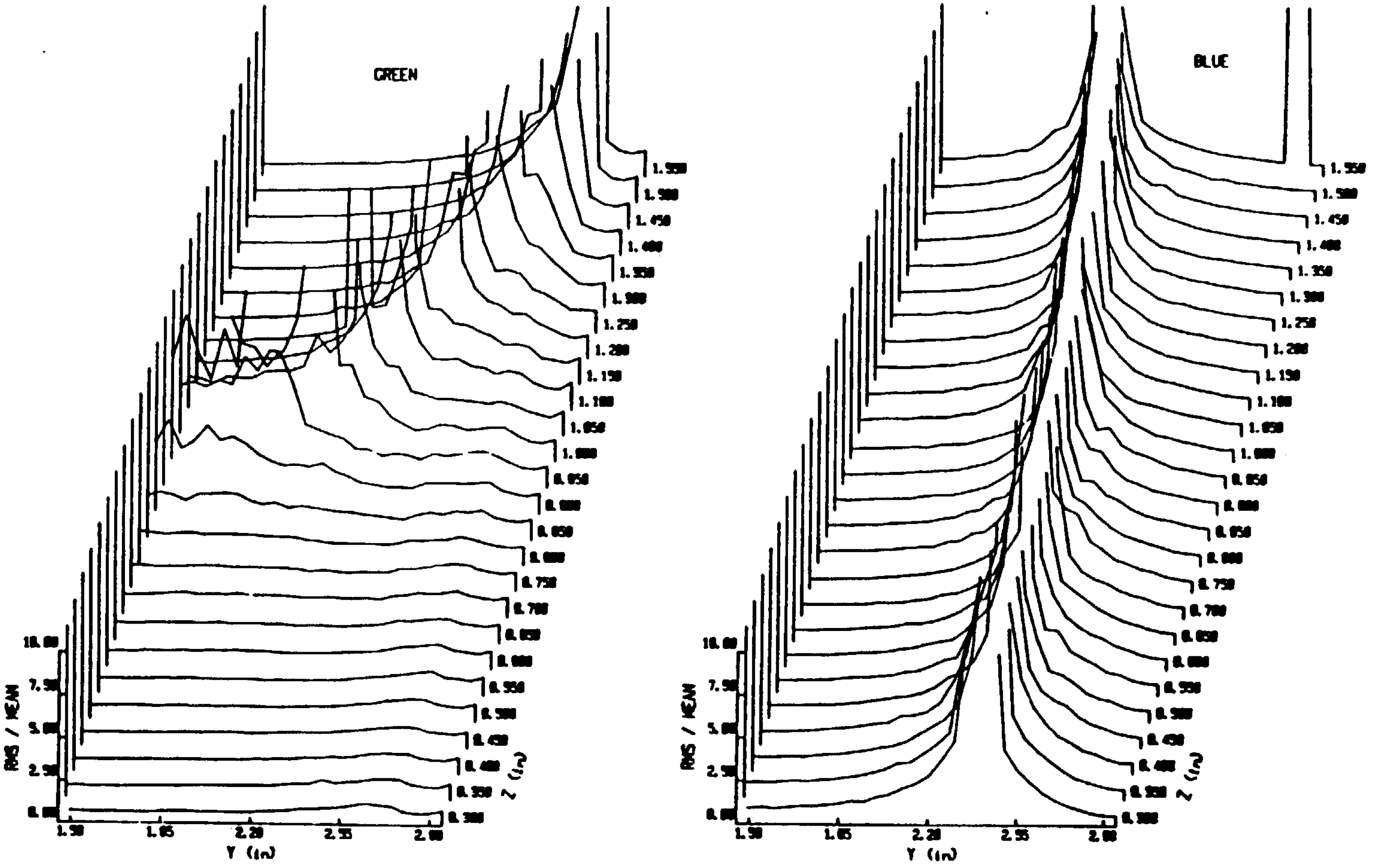

Figure 3.30 Cascade Plots of Turbulence Intensity at x=3.0 inches (scan 1)

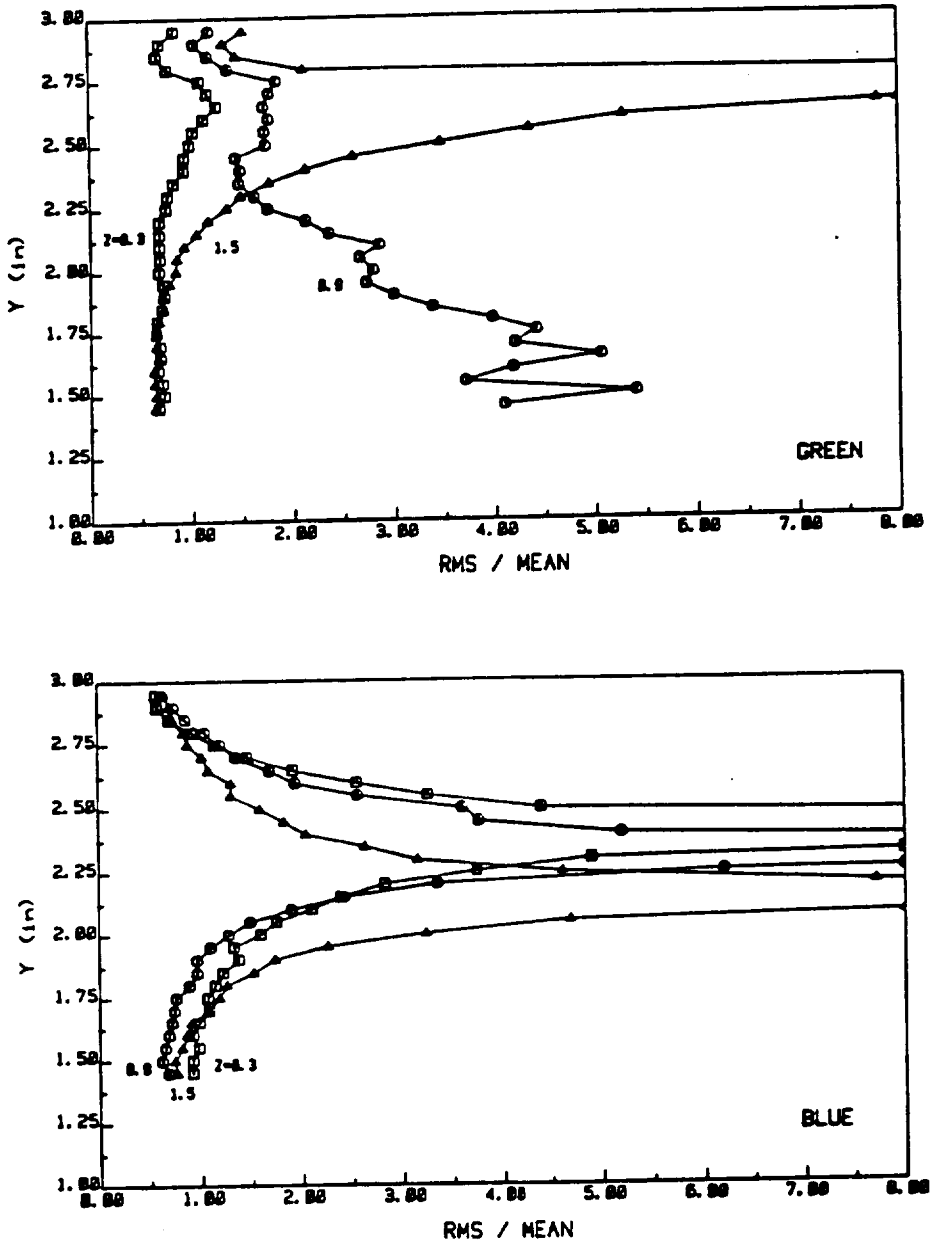

Figure 3.31 Plots of Turbulence Intensity at x=3.0 inches (scan 1)

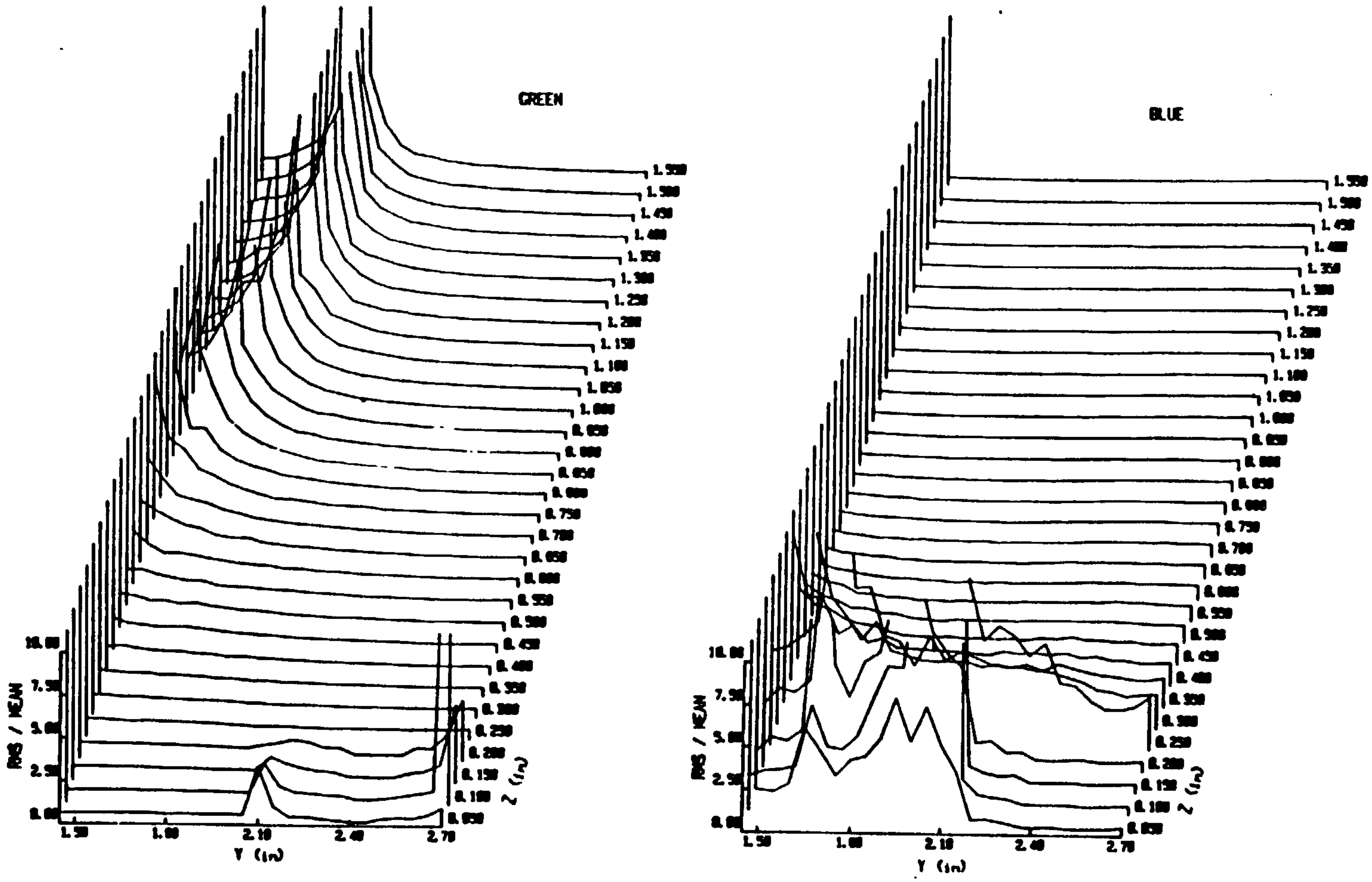

Figure 3.32 Cascade Plots of Turbulence Intensity at x=3.0 inches (scan 2)

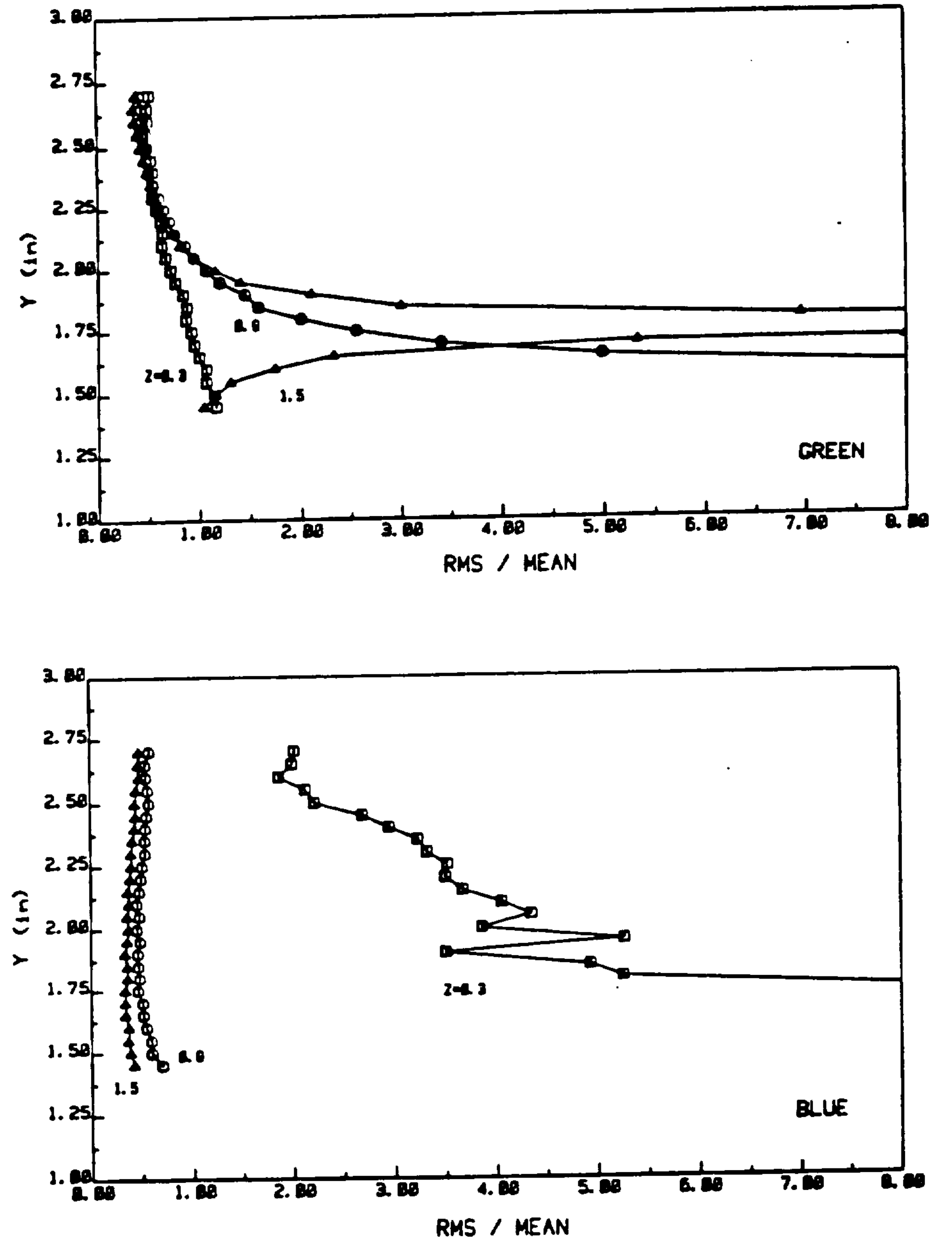

Figure 3.33 Plots of Turbulence Intensity at x=3.0 inches (scan 2)

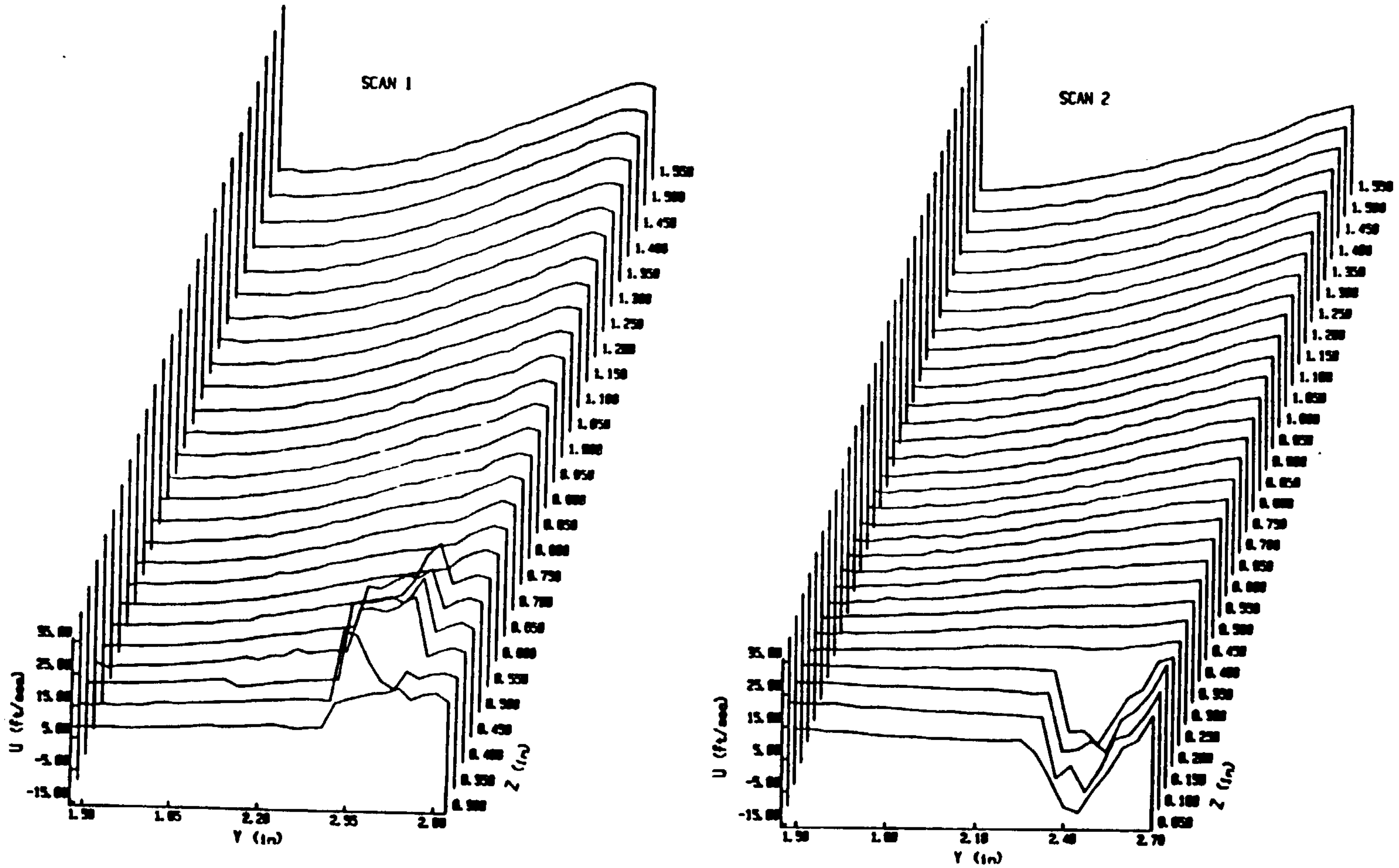

Figure 3.34 Cascade Plots of u Velocity at x=4.5 inches (scans 1 and 2)

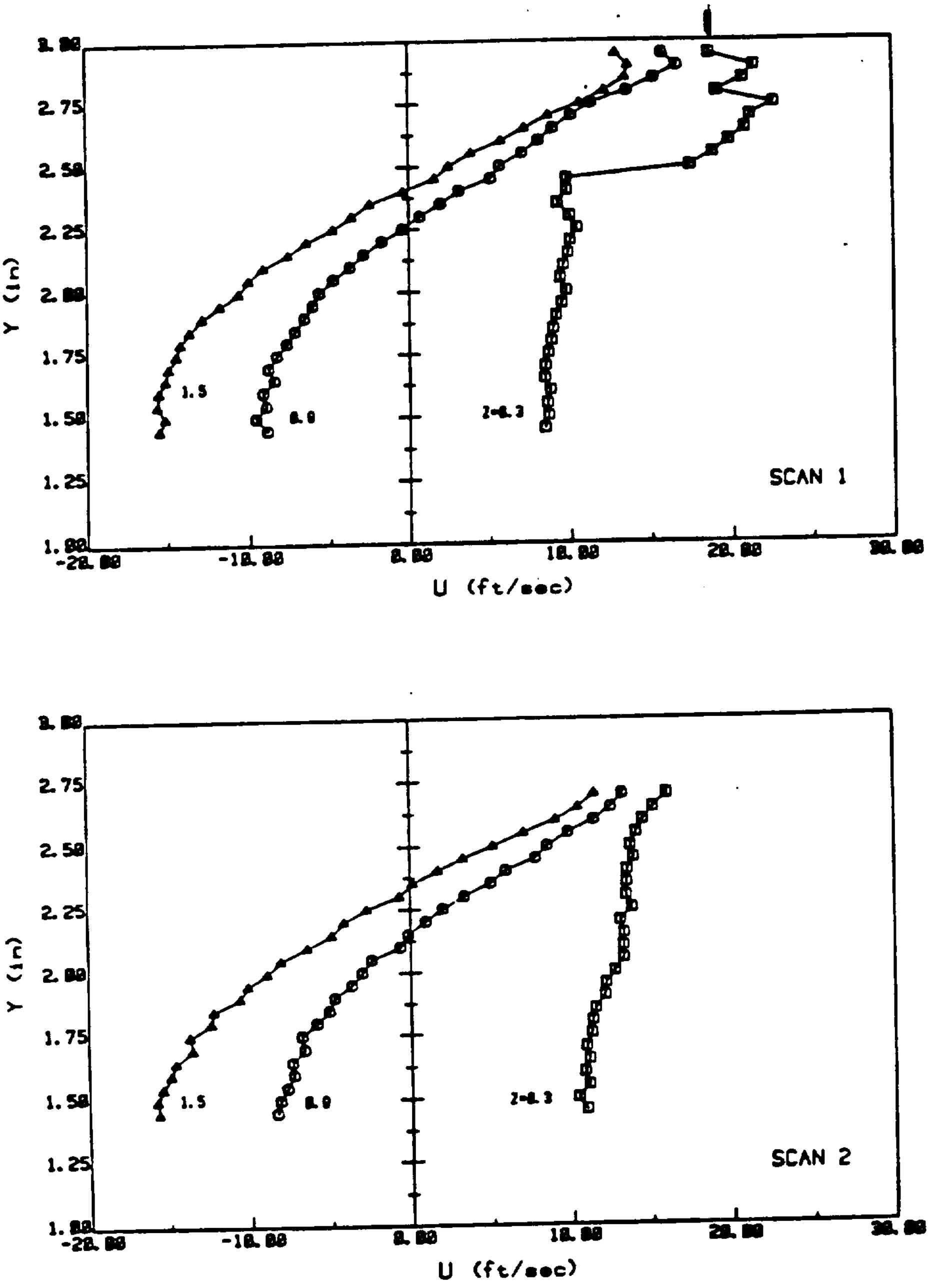

Figure 3.35 Plots of u Velocity at x=4.5 inches (scans 1 and 2)

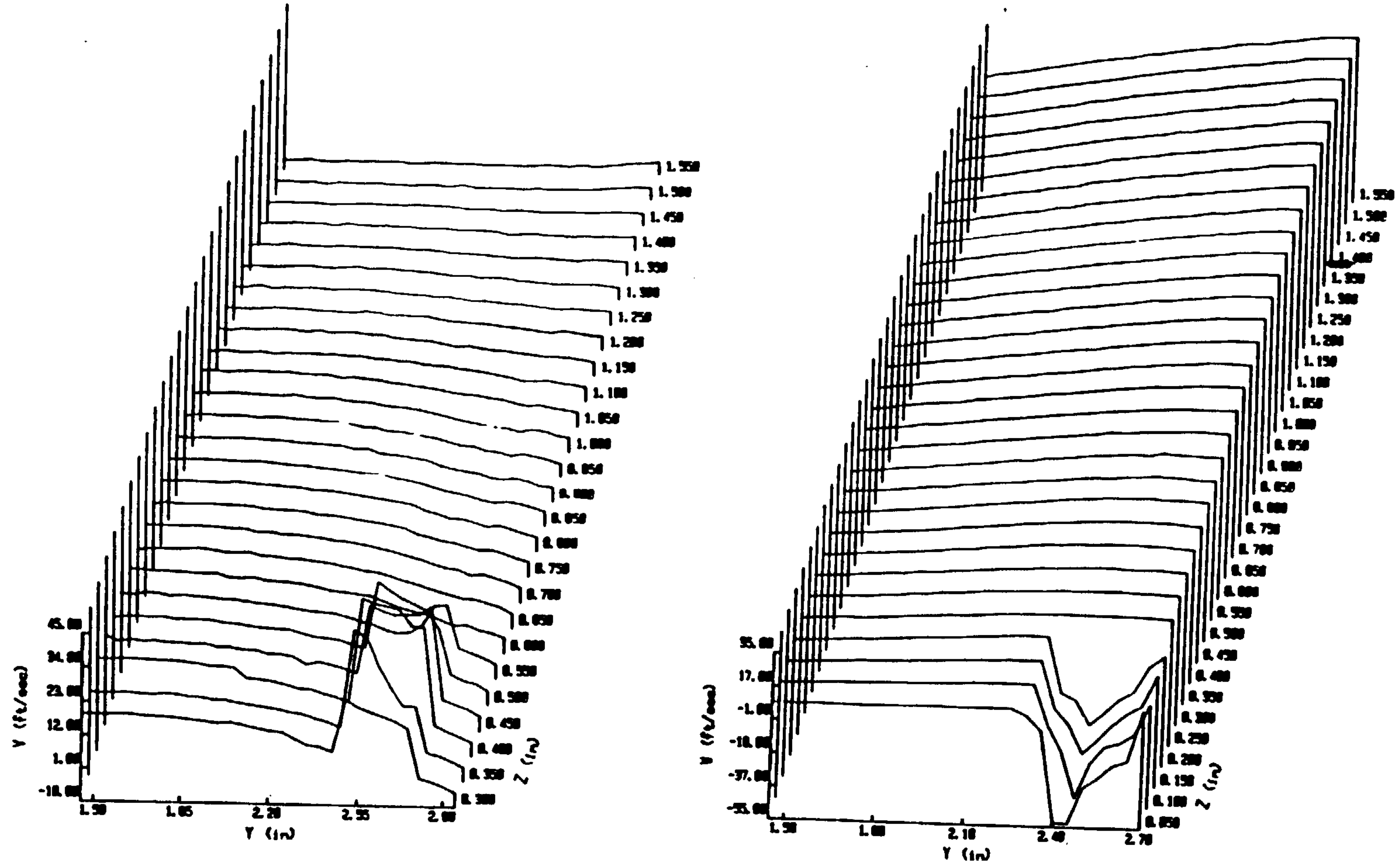

Figure 3.36 Cascade Plots of v and w Velocities at x=4.5 inches

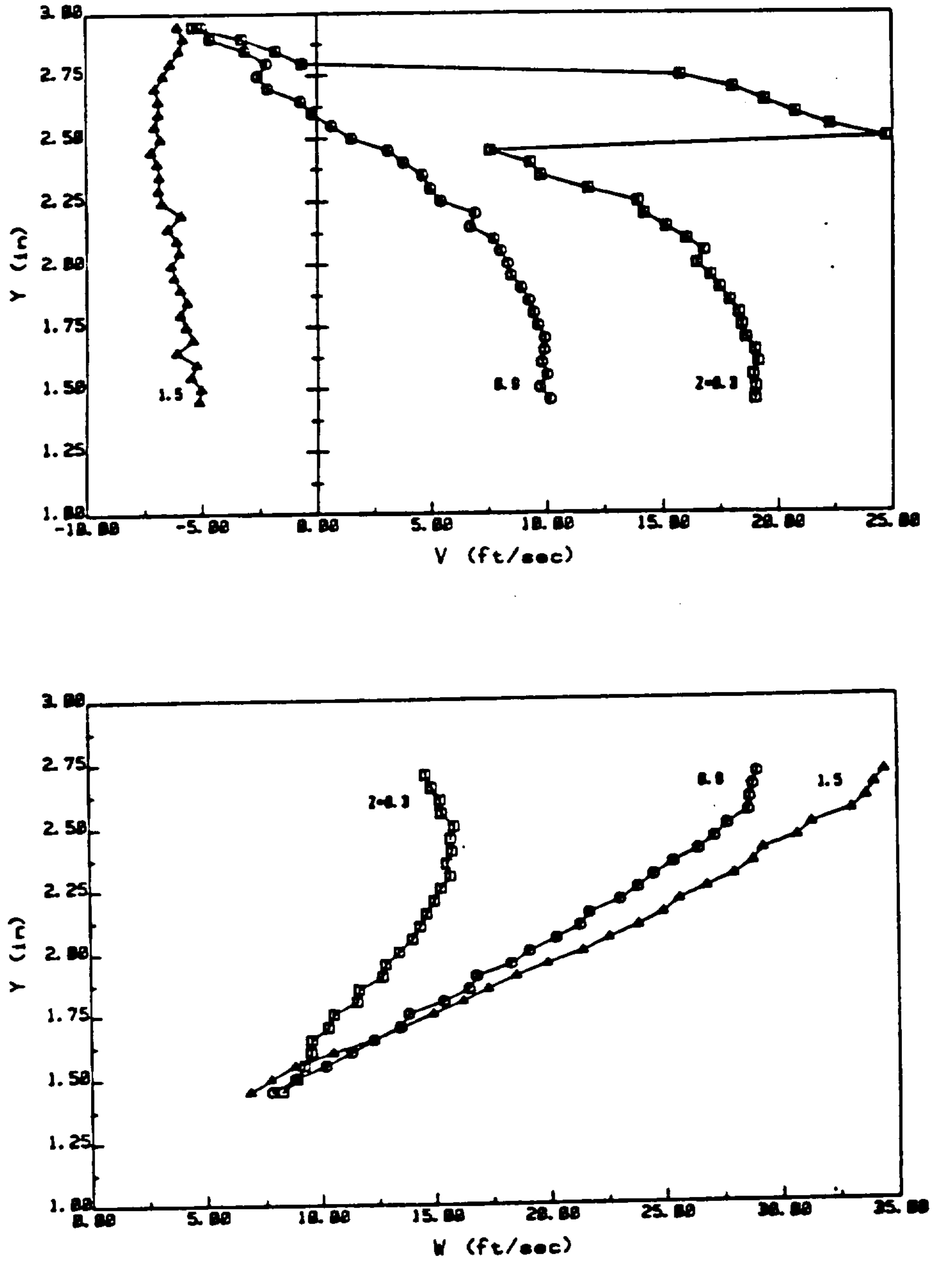

Figure 3.37 Plots of v and w Velocities at x=4.5 inches

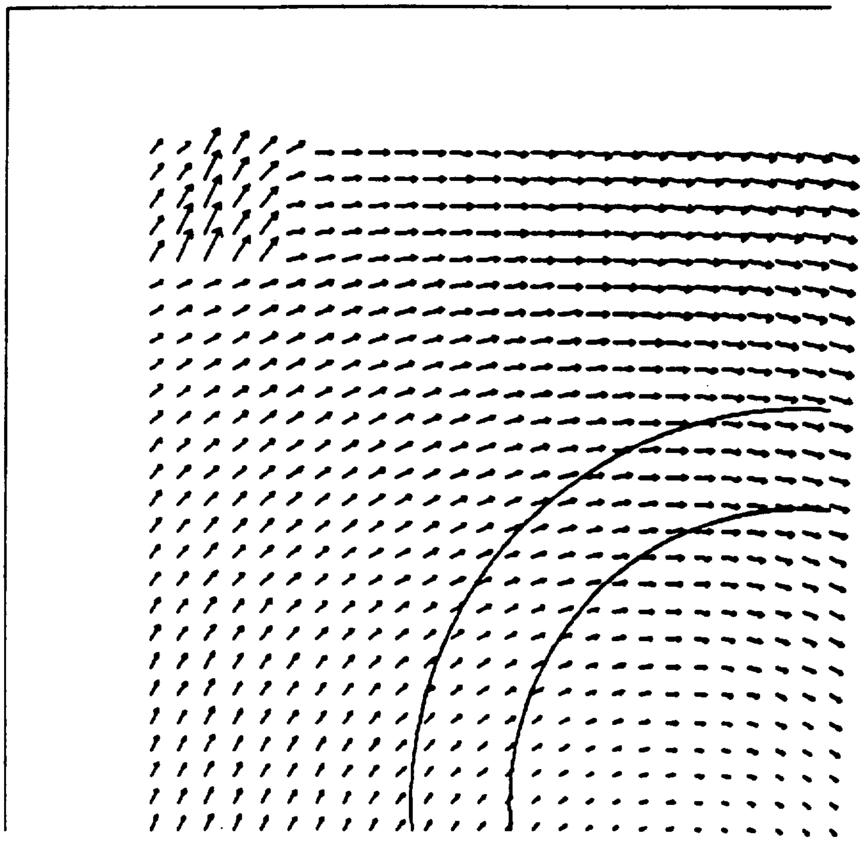

Figure 3.38 Vector Plot of v and w Velocities at x=4.5 inches

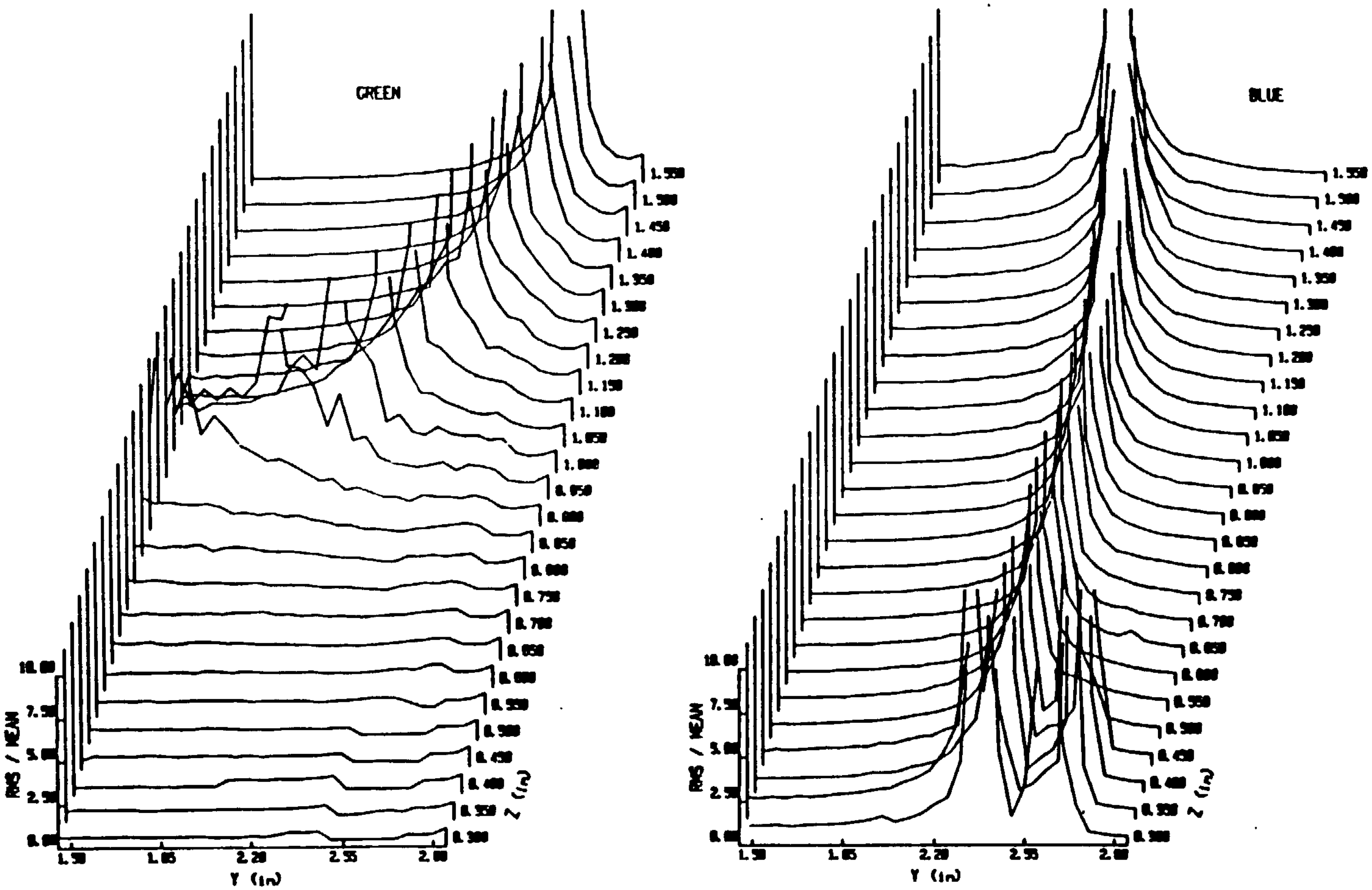

Figure 3.39 Cascade Plots of Turbulence Intensity at x=4.5 inches (scan 1)

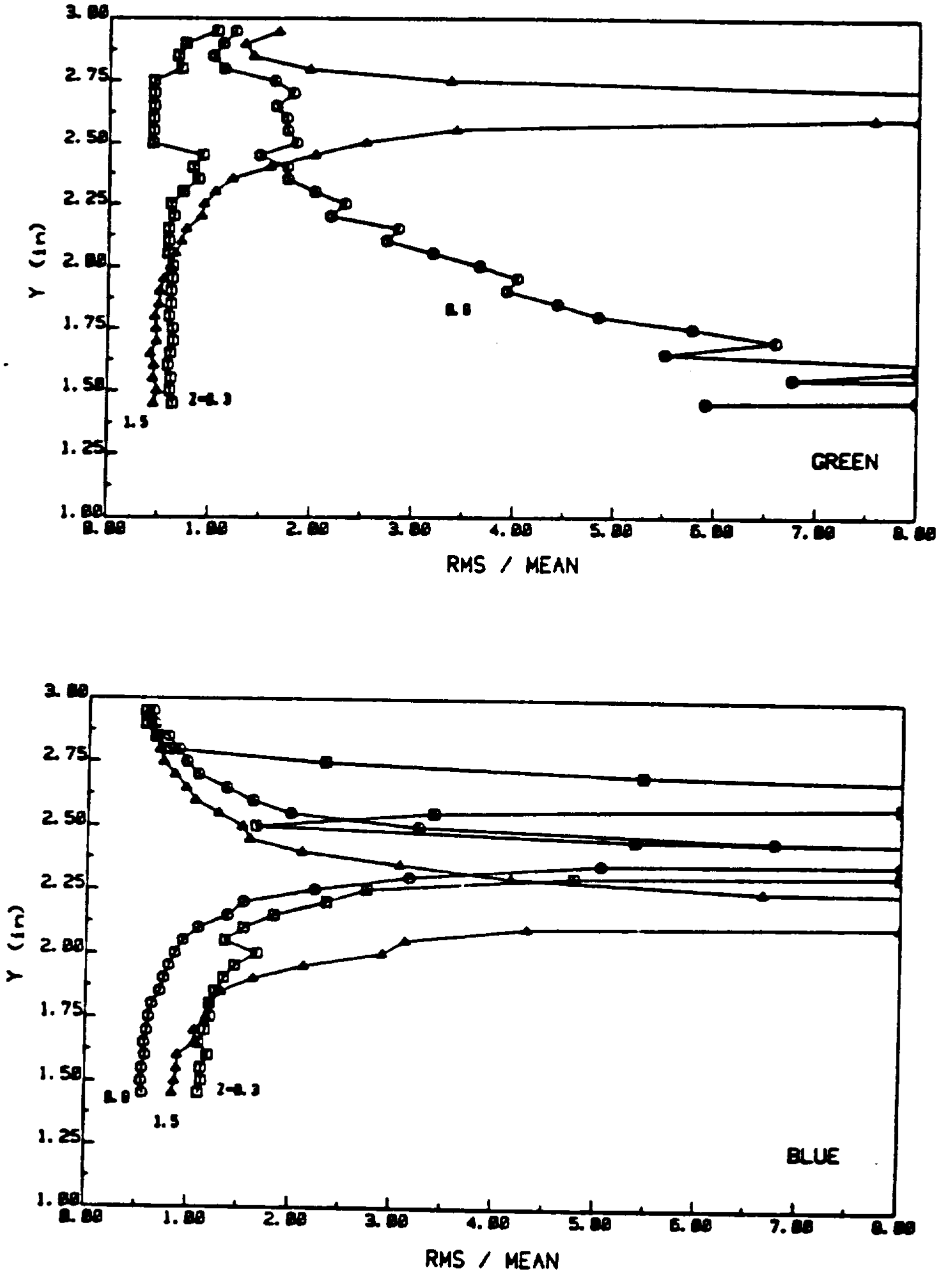

Figure 3.40 Plots of Turbulence Intensity at x=4.5 inches (scan 1)

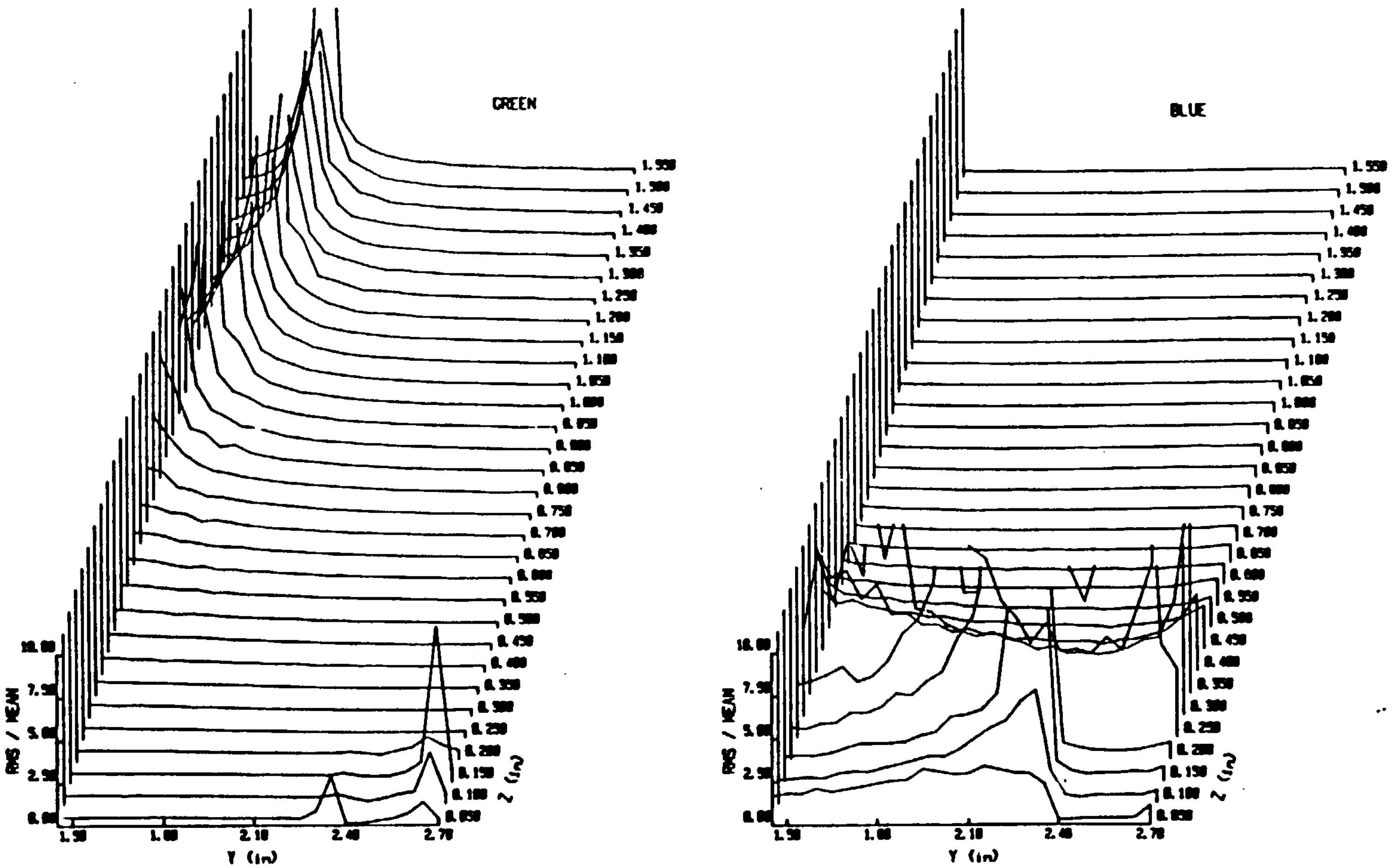

Figure 3.41 Cascade Plots of Turbulence Intensity at x=4.5 inches (scan 2)

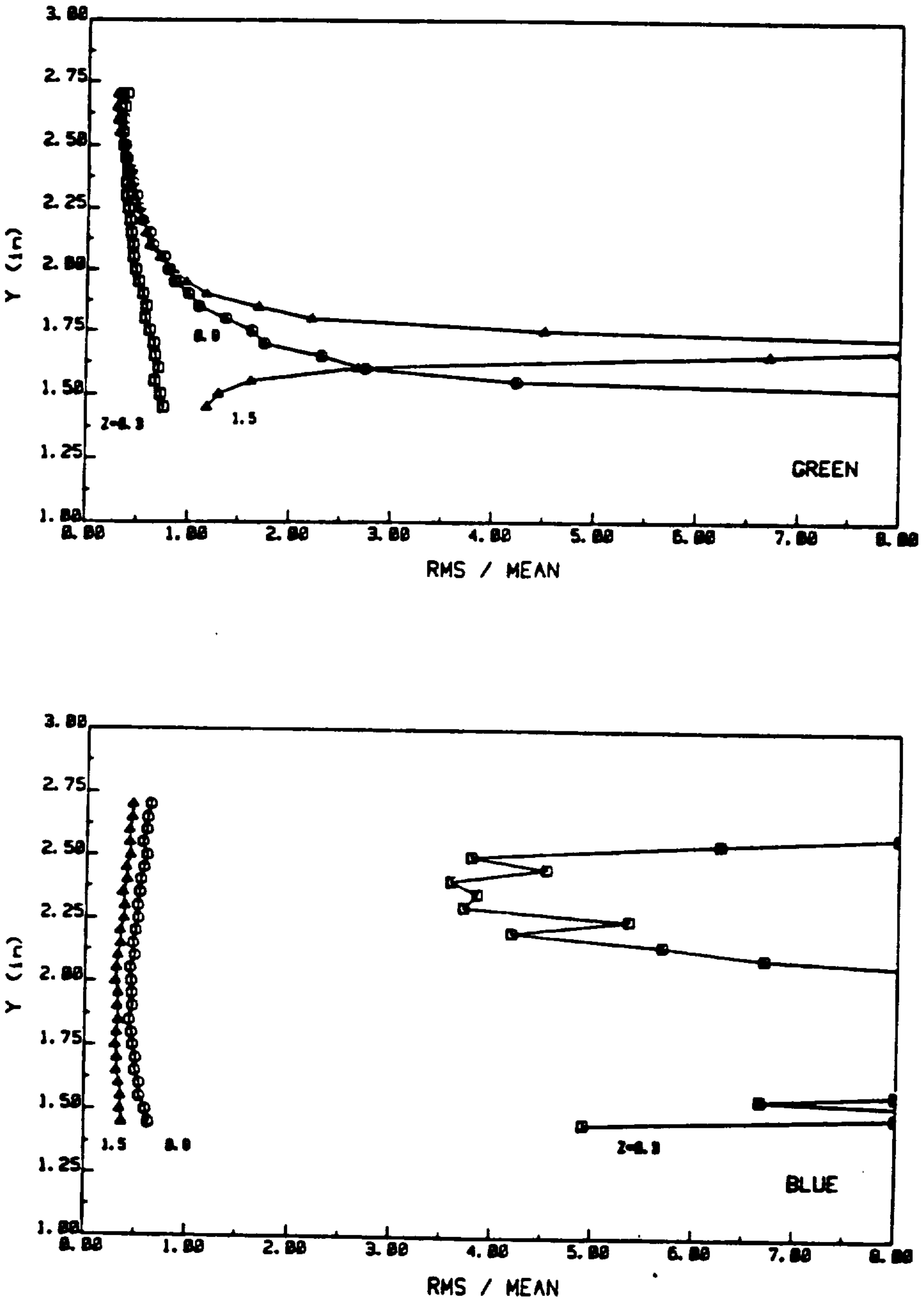

Figure 3.42 Plots of Turbulence Intensity at x=4.5 inches (scan 2)

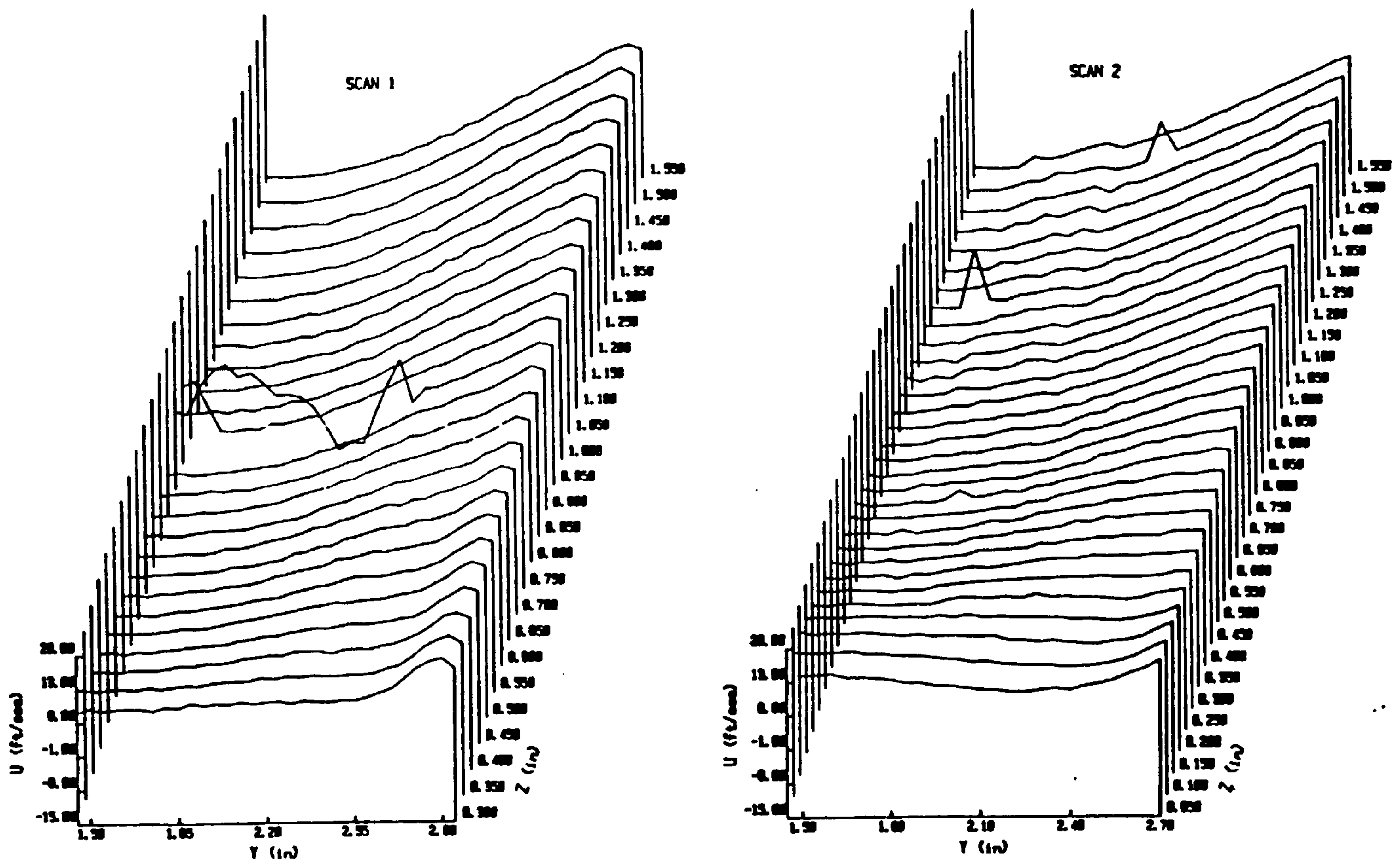

Figure 3.43 Cascade Plots of u Velocity at x=6.0 inches
(scans 1 and 2)

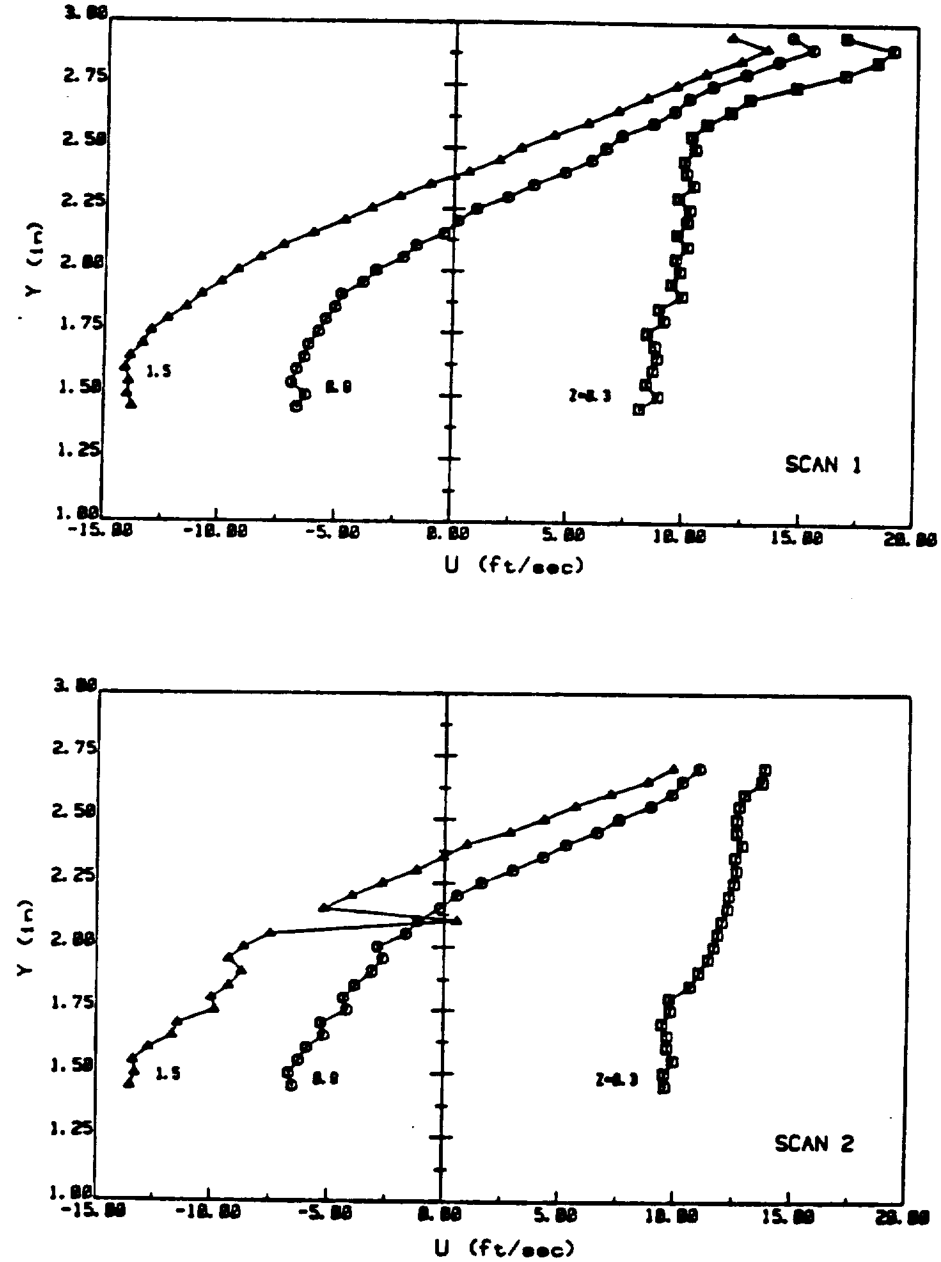

Figure 3.44 Plots of u Velocity at x=6.0 inches
(scans 1 and 2)

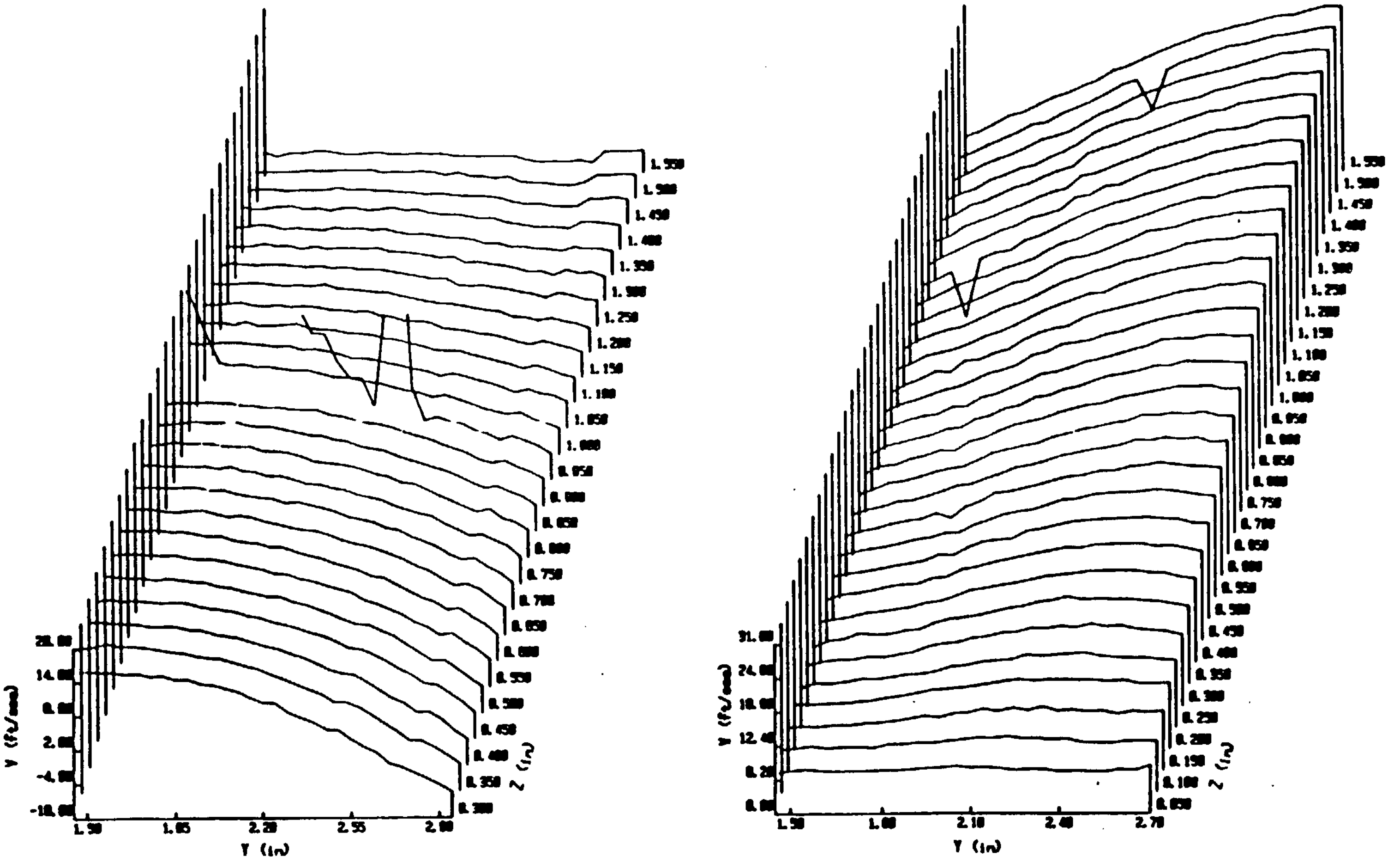

Figure 3.45 Cascade Plots of v and w Velocities at x=6.0 inches

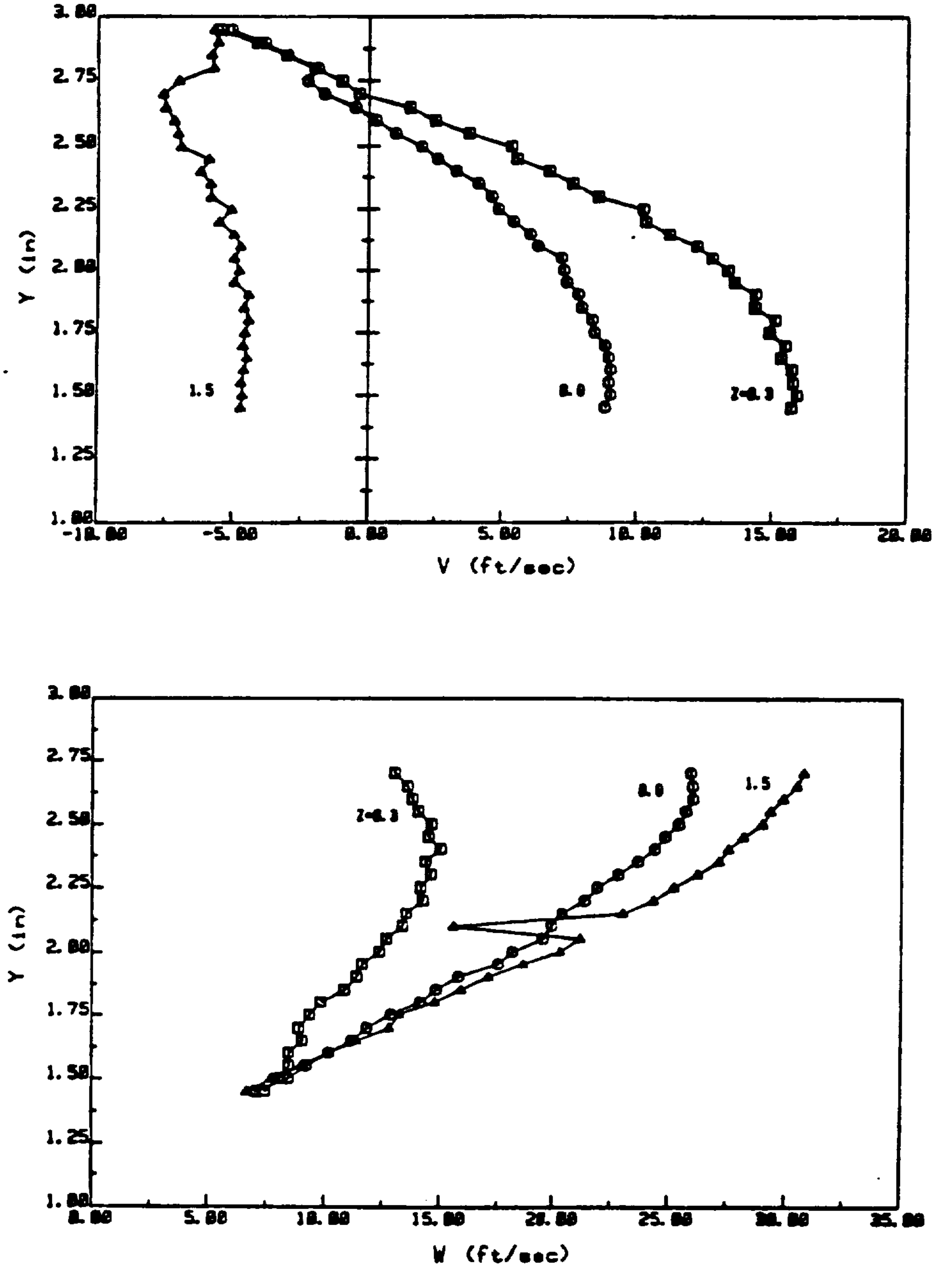

Figure 3.46 Plots of v and w Velocities at x=6.0 inches

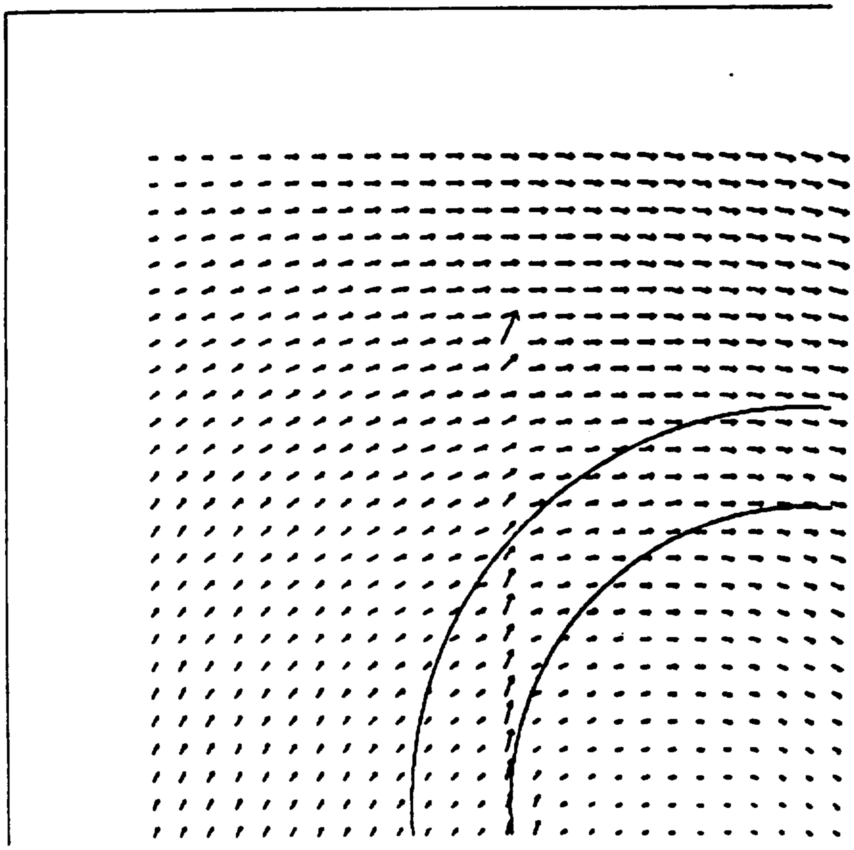

Figure 3.47 Vector Plot of v and w Velocities at x=6.0 inches

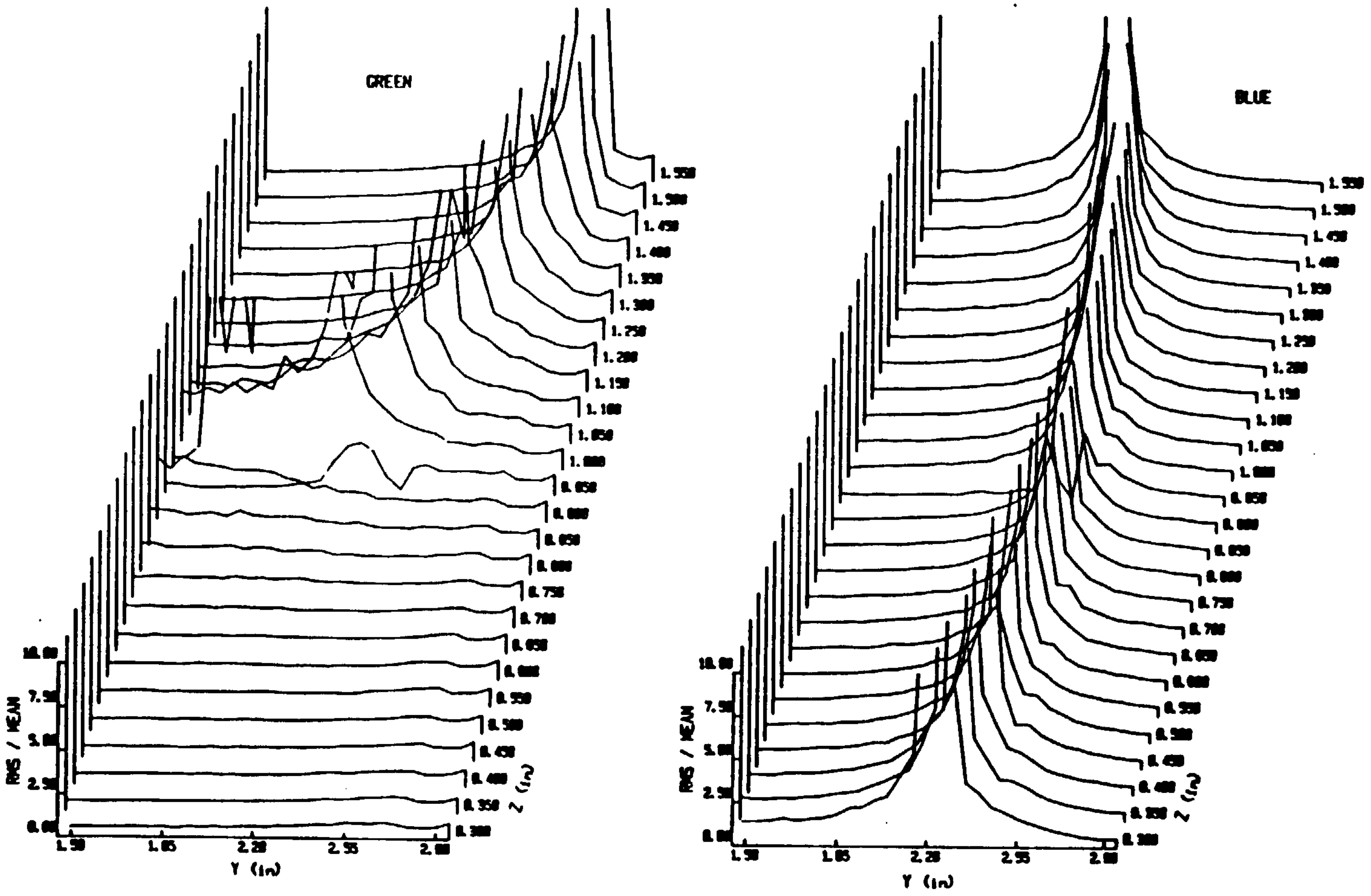

Figure 3.48 Cascade Plots of Turbulence Intensity at x=6.0 inches (scan 1)

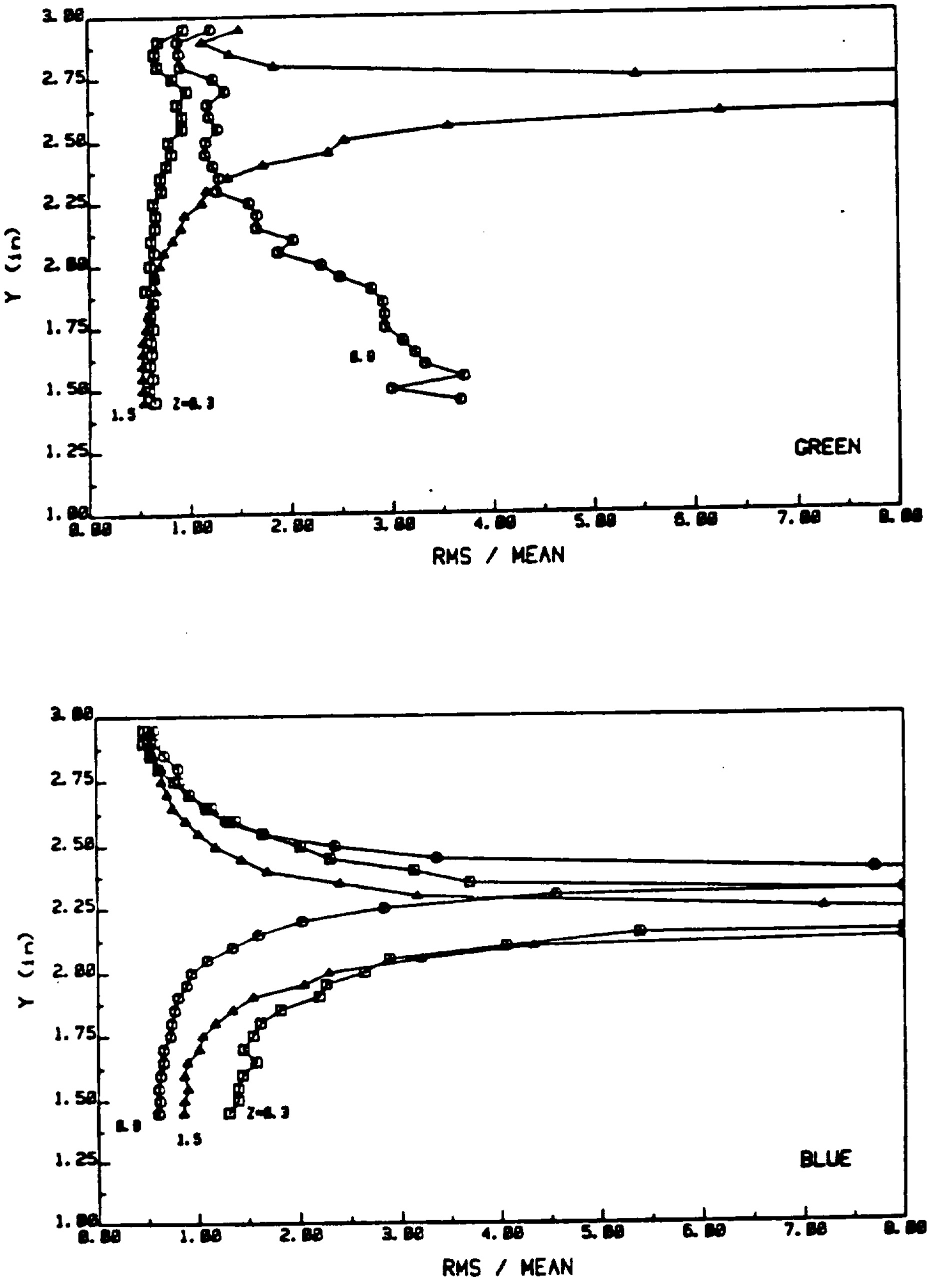

Figure 3.49 Plots of Turbulence Intensity at x=6.0 inches (scan 1)

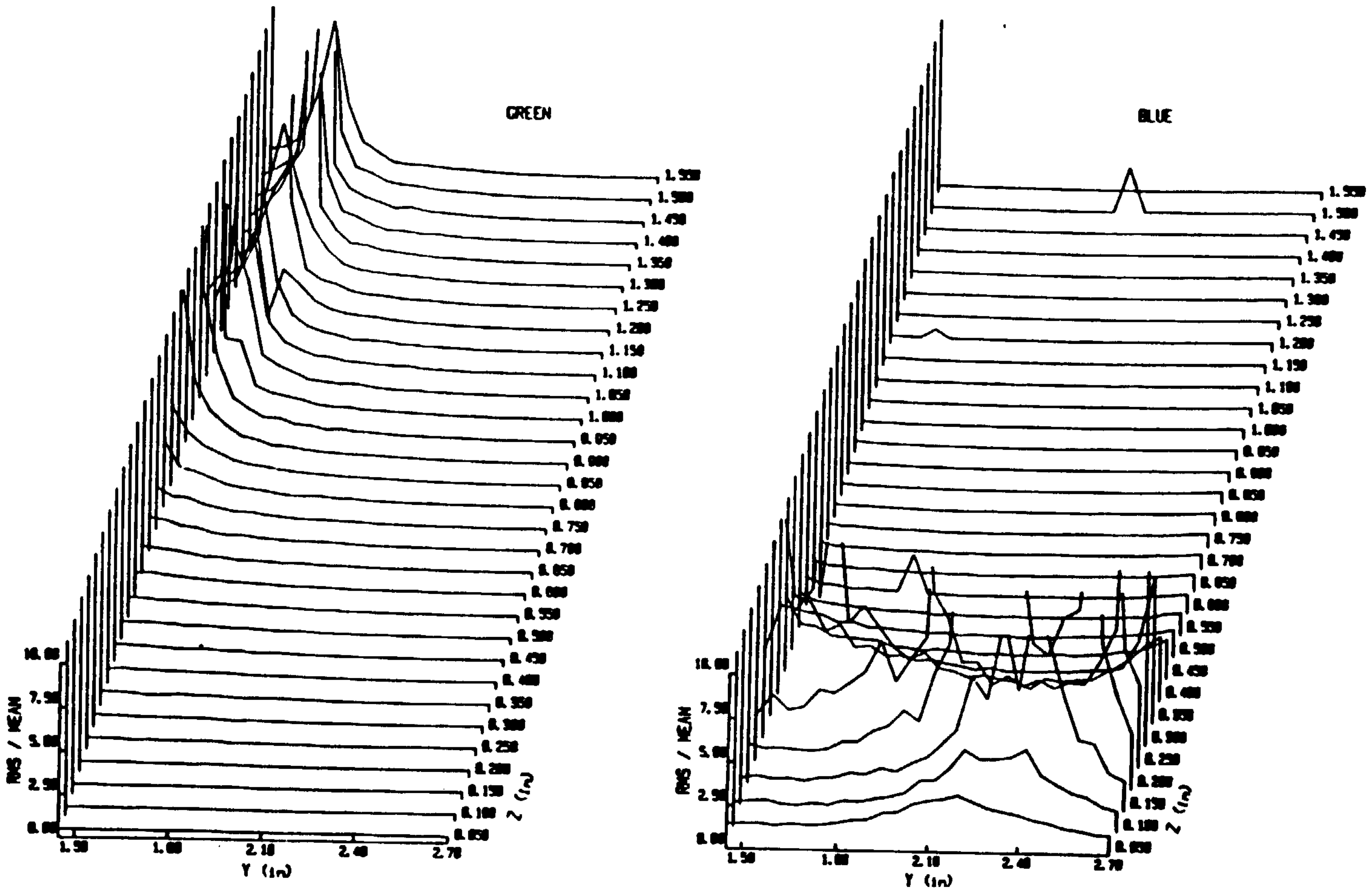

Figure 3.50 Cascade Plots of Turbulence Intensity at x=6.0 inches (scan 2)

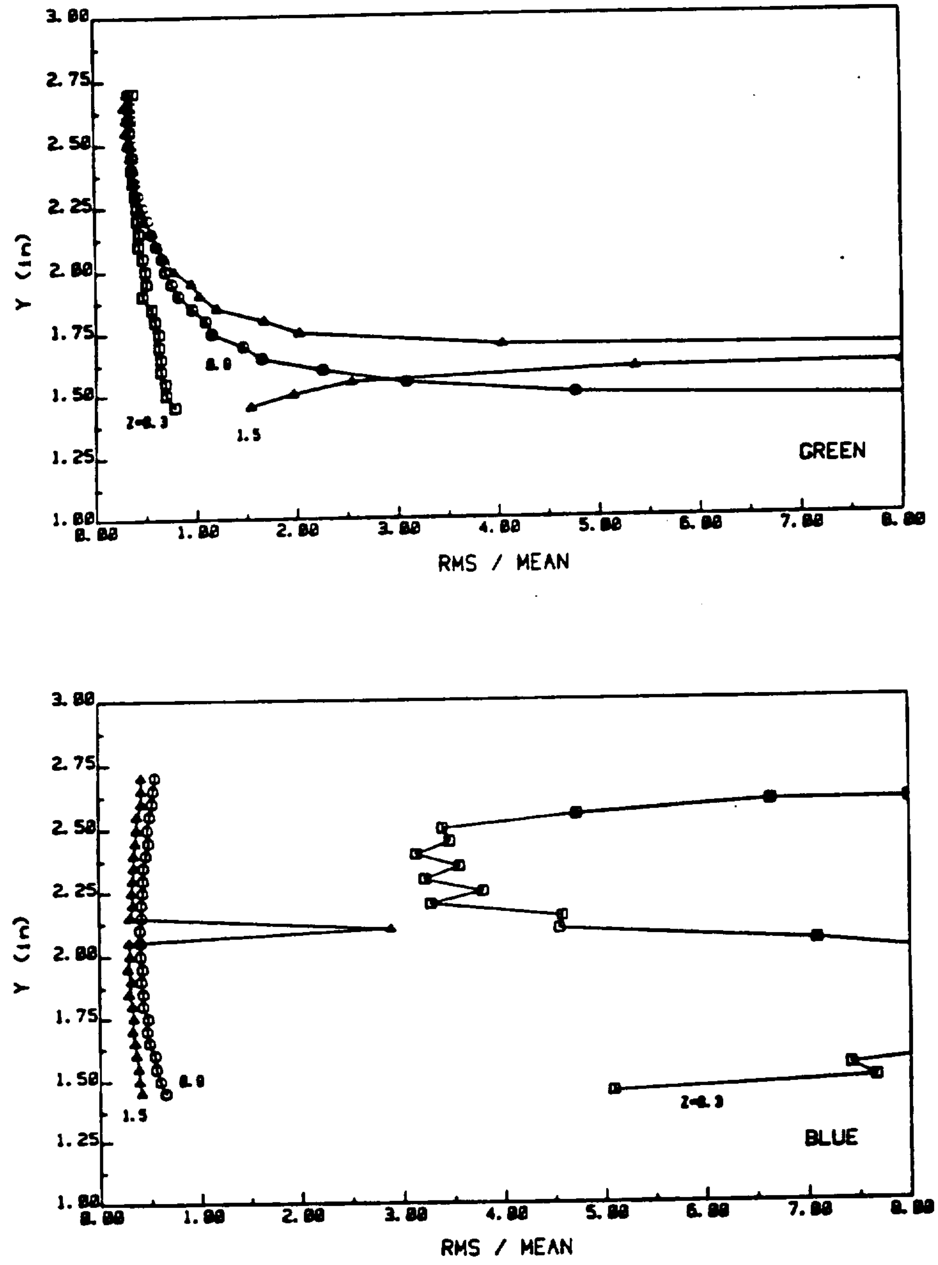

Figure 3.51 Plots of Turbulence Intensity at x=6.0 inches (scan 2)

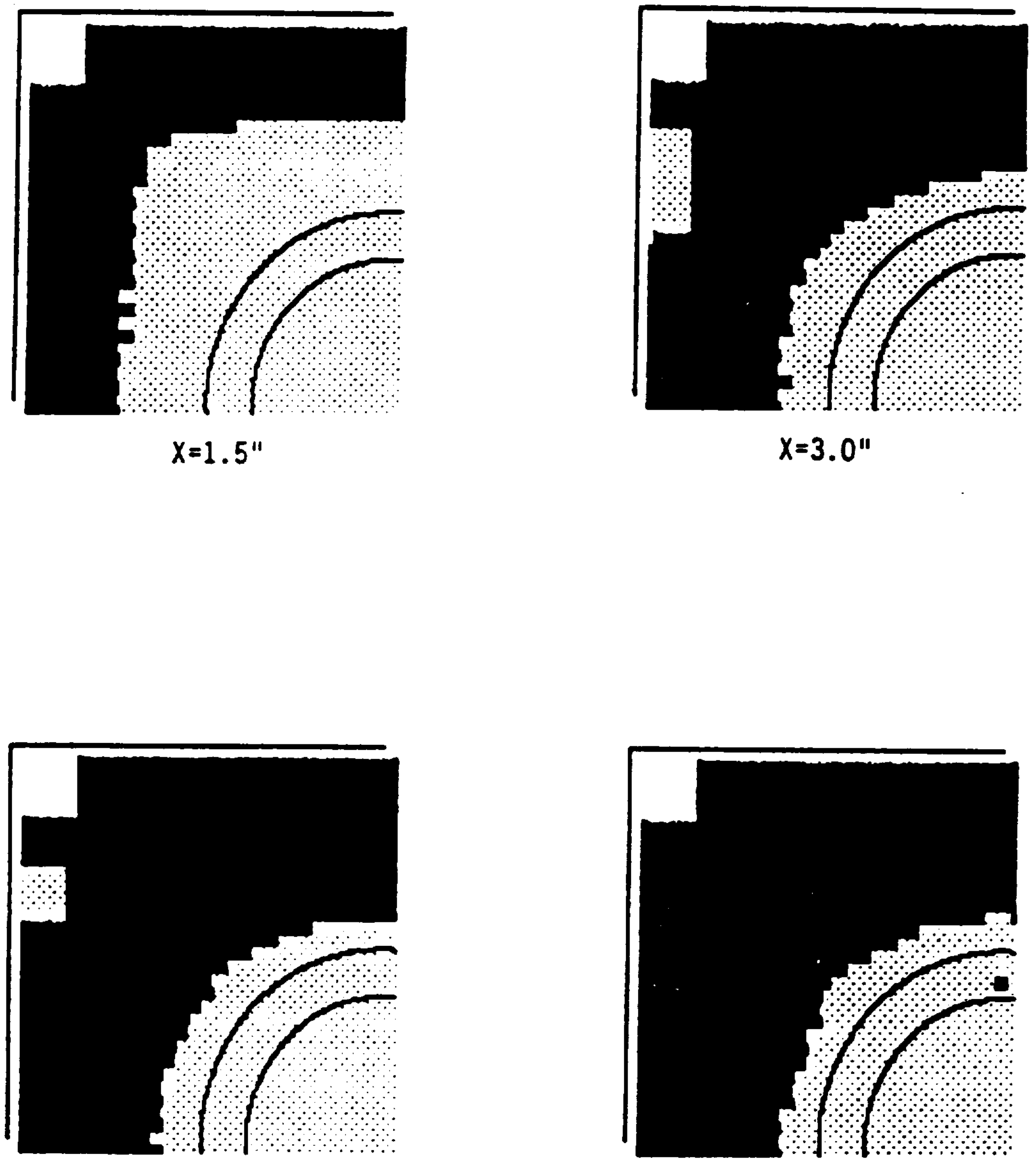

X=1.5"

X=3.0"

X=4.5"

X=6.0"

Figure 3.52 Contour Plots of u Velocity Indicating Regions of Reverse Flow

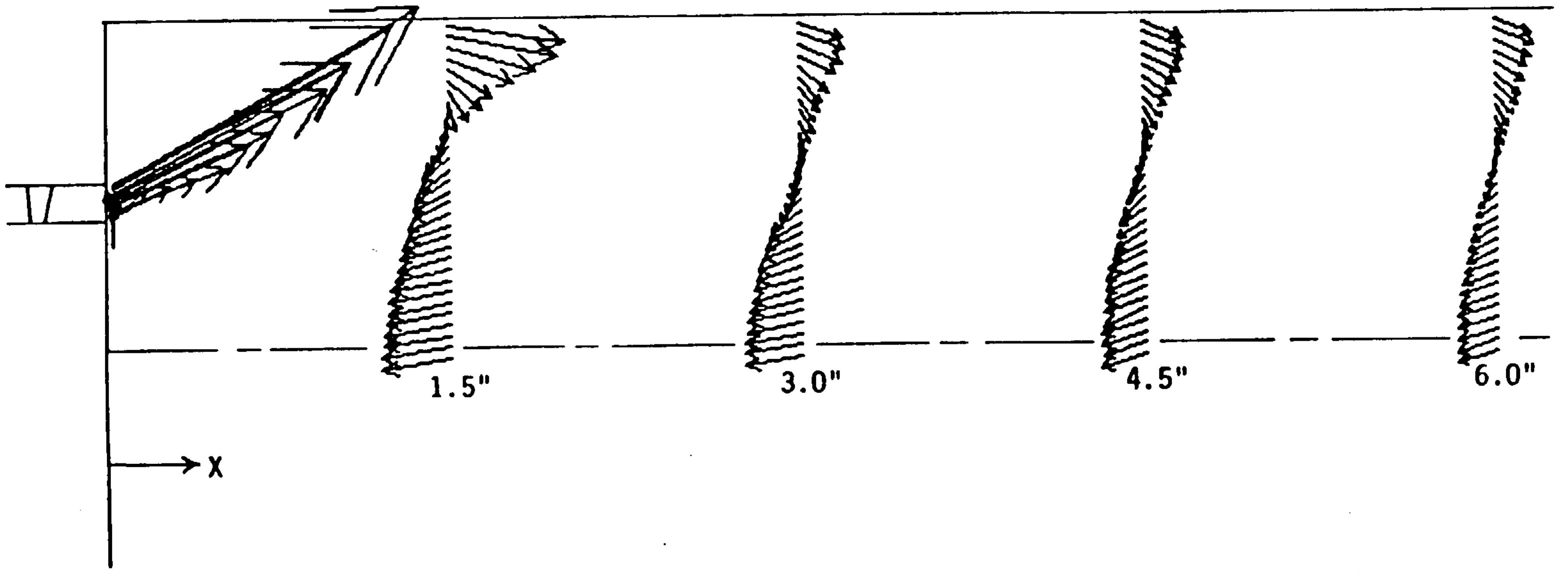

Figure 3.53 Vector Plot at z=1.5 inches

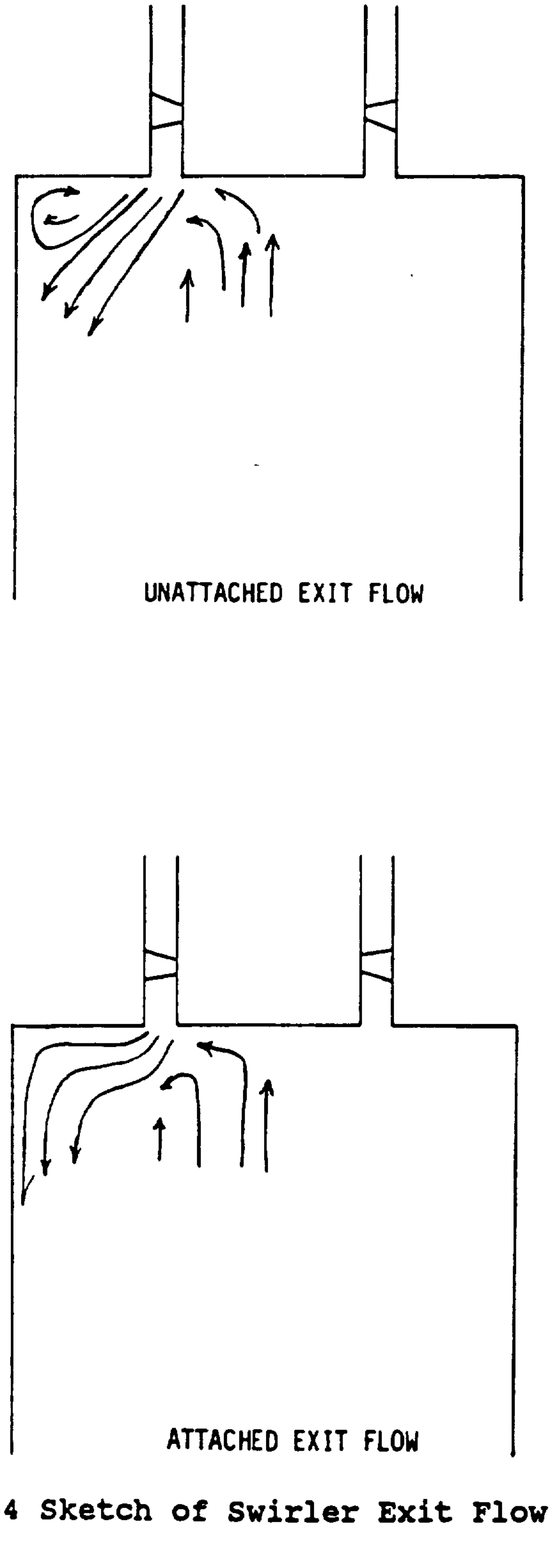

Figure 3.54 Sketch of Swirler Exit Flow Regimes

CHAPTER 4

SUMMARY AND CONCLUSIONS

This thesis comprises the development and setup of a rig and laser doppler velocimeter system to take nonintrusive velocity measurements in the mixing region of an annular combustor simulator. Also, detailed LDV measurements were taken of a single swirler in a square duct.

In the design of the annular pipe it was observed that at a high swirl number with the swirl generator flush with the exit plane the flow would expand at a right angle to the swirl axis. This was also observed by Gore and Ranz [4]. They had reported that this flow did not exist when the flow generator was recessed in to the duct. For this reason the swirler was recessed into the annulus 1/4 of an inch.

Setup of a two component LDV system for this flow has proved to be a formidable task. There are several aspects of the LDV system that need particular attention for use in this type of flow.

The use of a Bragg cell is a must for accurate measurements of turbulent reversing flows. Also, care must be taken to assure balance of power is achieved in the transmitted beams. Imbalance of power promotes poor signal quality.

In developing the optics, care was taken to provide a small measuring volume for the ability to make very detailed measurements. This was achieved by use of a large beam expansion ratio and short focal length field lens. The advantages are seen in the ability to take detailed measurements of the swirler exit.

The use of plexiglass walls was found to be inadequate for making LDV measurements in this particular arrangement. The plexiglass varies too much in thickness and makes measurements improbable when the probe volume is repositioned in the flow.

Due to the high swirling nature of the flow it was necessary to develop a special seed particle for this application. This particle consists of a submicron droplet of fog juice. This use of an exceptionally small particle provides for low scattered light intensities. In which case, the use of forward scatter is a necessity.

Nonintrusive LDV measurements were made in a single swirler rig. These measurements were made at both the swirler exit and at several downstream locations. In all, a total of over 45 million data samples were taken. The results of which were presented in cascade, vector, and 2-d plots.

There has been some research done in the past on swirling free jets [3,5]. However, very little is known about the effect of swirling flows in an enclosed duct, especially, one with a square cross-section. As such, there is nothing with which to compare the data that was taken.

The data taken at the swirler exit did indicate that due to the high rotational flow and the centrifugal forces of this flow that the velocities at outer flow radius were greater than those at the inner flow radius. Also, the fluctuations due to the swirler vanes was clearly evident.

For the downstream data the flow profiles change considerably in the first duct height. After this the flow profile remains essentially unchanged with only viscous effects evident in velocity decay.

From this research some general conclusions can be reached.

1] The operation of the rig has come close to the designed values.

2] Although, the laser doppler velocimeter is a very good tool for taking nonintrusive velocity measurements, very special care must be taken to get good measurements in a very violent flow with tight geometrical restrictions, as opposed to a wide open wind tunnel with few restrictions.

3] LDV measurements in a swirling enclosed flow indicate that for the first duct height the flow is governed by the swirling and sudden expansion. After approximately 1 duct height a flow pattern is established and remains constant in shape with only a decay in magnitude due to viscous damping.

4.1 FURTHER RESEARCH

This paper has reported the mere beginnings of an ongoing project at Purdue University. There is much work yet to be done.

The rig is currently in a state of operation with a working LDV system. Detailed velocity measurements are still to be taken. The author has only laid the ground work necessary to make this possible. Velocity measurements are to be taken for those configurations mentioned in Chapter 1.

Also, detailed flow visualization is to be done in a water rig similar to the air rig. This is also to be done for all of the configurations mentioned in Chapter 1.

Currently work is being conducted to develop a method for taking concentration measurements in the air rig. These measurements are to incorporate the marker nephelometry technique for concentration measurements. For this, the marker is to be injected in to the flow via holes in the center of the swirlers along the swirl axis simulating fuel injection.

LIST OF REFERENCES

LIST OF REFERENCES

[1] Beer, J.M., Chigier, N.A., "Combustion Aerodynamics", Robert E. Krieger Publishing, 1983.

[2] Goldstein, Richard J., "Fluid Mechanics Measurements", Hemisphere Publishing, 1983.

[3] Gore, R.W., Ranz, W.E., "Back Flows in Rotating Fluids Moving Axially Through Expanding Cross Sections", Am. Inst. Chem. Engrs. J., 1964, 10, No. 1, pp. 83-8.

[4] Gupta, A.K., Lilley, D.G., Syred, N., "swirl Flows", Abucus Press, 1984.

[5] Mathur, and Maccallum, "Swirling Air Jets From Vane Swirlers. Part 1: Free Jets", Journal of the Institute of Fuel, May, 1967.

[6] Mongia, H.C., Patankar, S.V., Murthy, S.N.B., Sullivan, J.P., Samuelsen, G.S., "Aerothermal Modeling Program - Phase II", Paper Presented at Turbine Engine Hot Section Technology Conference", NASA Conference Publication 2405, October 1985.

[7] Schlichting, H., "Boundary-Layer Theory", McGraw-Hill, 1979.

[8] Sundar, R.M., "An Experimental Investigation of Propeller Wakes Using a Laser Doppler Velocimeter", Ph.d Thesis, Purdue University, May 1985.

APPENDIX

APPENDIX

CALIBRATION OF ANNULAR PIPE AND PRIMARY JET

To calibrate the primary jet and swirler several setups were used. The first was a setup to determine the flow profile. Figure A.1 is a drawing of this setup. A high pressure air supply and plenum were used to blow air through on of the primary jets. At the exit a total pressure probe was scanned across. A stepper motor driven traverse was used to move the probe and a dial gage was used to measure position. From this, the pipe flow profile was determined.

The measured profile is shown in figure A.2. This profile fits well the one sixth turbulent profile presented by Schlichting [7]. Thus for the rest of the measurements a one sixth turbulent profile is assumed.

The setup used for the mass flow calibration of the primary jet is shown in figure A.3. This is the same rig used for the LDV measurements. The only difference is that the head plate for the swirler is replaced with one to hold the primary jet. Also, a total pressure probe is mounted on the jet centerline over the second pressure tap. Thus, the jet centerline pitot pressure is measured. Figure A.4 is the plot of centerline pitot pressure against the pressure drop across the primary jet pressure taps.

From Bernoulli's equation:

$$\Delta P_{Pitot} = \frac{1}{2} \rho V^2 \tag{A.1}$$

solving for V

$$V = \sqrt{\frac{2 \Delta P_{Pitot}}{\rho}} \tag{A.2}$$

Assuming a 1/6 profile the mean jet velocity is 0.791% of the jet centerline velocity [7].

$$\bar{V} = .791 \sqrt{\frac{2 \Delta P_{Pitot}}{\rho}} \tag{A.3}$$

rearranging (A.3)

$$(.791)^2 \Delta P_{Pitot} = \frac{1}{2} \rho \bar{V}^2 \tag{A.4}$$

The relationship between the mean jet velocity and the static pressure drop across taps 1 and 2 is given by:

$$\Delta P_{12} = K \frac{1}{2} \rho \bar{V}^2 \tag{A.5}$$

Where K is the loss coefficient between the pressure taps. Using equations (A.4) and (A.5):

$$(.791)^2 \Delta P_{Pitot} = \frac{1}{2} \rho \bar{V}^2 = \frac{\Delta P_{12}}{K} \tag{A.6}$$

solving for K

$$K = \frac{\Delta P_{12}}{(.791)^2 \Delta P_{pitot}} \qquad (A.7)$$

$\Delta P_{12} / \Delta P_{pitot}$ is the inverse slope of the plot in figure A.4. A least squares routine was used to calculate the slope. For this plot the slope was calculated to be 3.113 and a loss coefficient of 0.513. With K determined, equation (A.5) is used to generate the plot of figure 1.13.

With this setup it is easy to measure the losses in the other portions of the primary jet by switching pressure tap hook ups. Figures A.5, A.7, and A.9 are sketches of the other pressure transducer configurations. The corresponding data plots are provided in figures A.6, A.8, and A.10.

A similar process was also done on the annular pipe. Figure A.11 is a diagram of the setup used for the annular pipe mass flow calibration. Figure A.12 is a plot of the measured data. The remaining data plots for the annulus are provided in figures A.13 through A.15. These plots are for the same setups as figures A.6, A.8, and A.10, except that these are for the annular pipe instead of the primary jet.

Finally, the same tests were run on the annular pipe with the swirler installed. However, since the pitot probe could not be inserted through the swirler vanes, the required pressure drops are measured against annular pipe pressure drop. That is, the pressure difference between taps 1 and 2. This is easily referenced to centerline pitot pressure through figure A.12 which is a plot of centerline pitot pressure versus annular pipe pressure drop. This data is shown in figures A.16 through A.19.

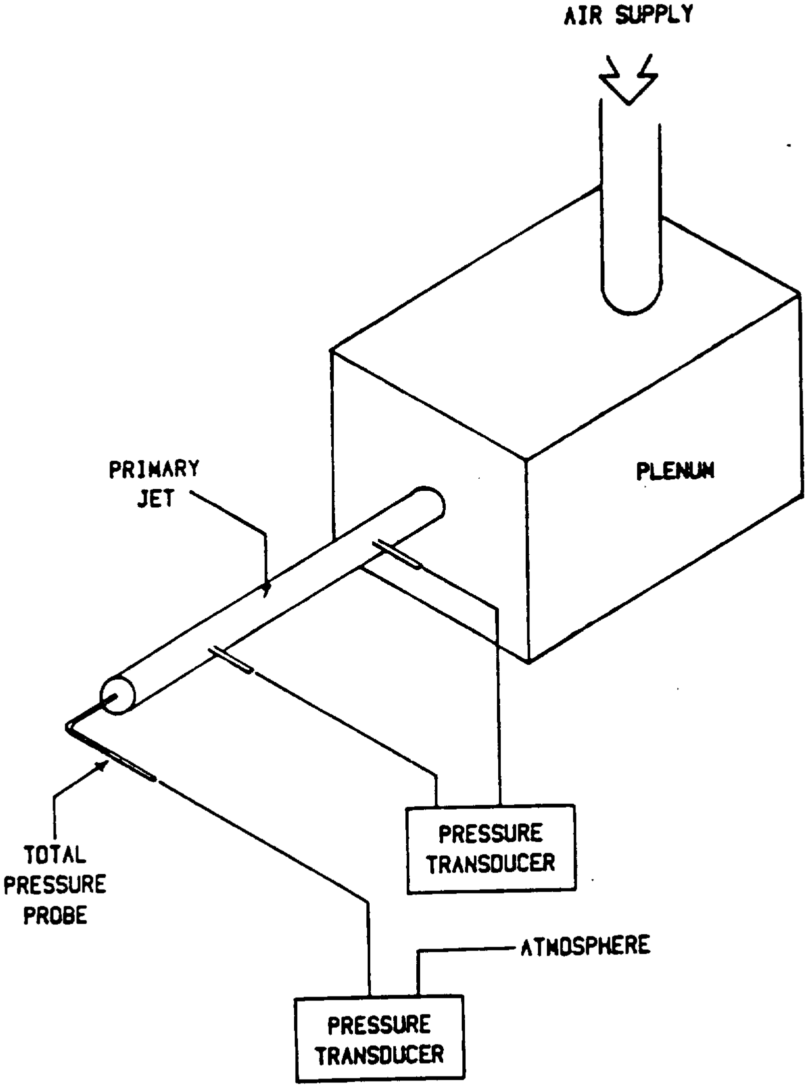

Figure A.1 Setup for Measurement of Flow Profile

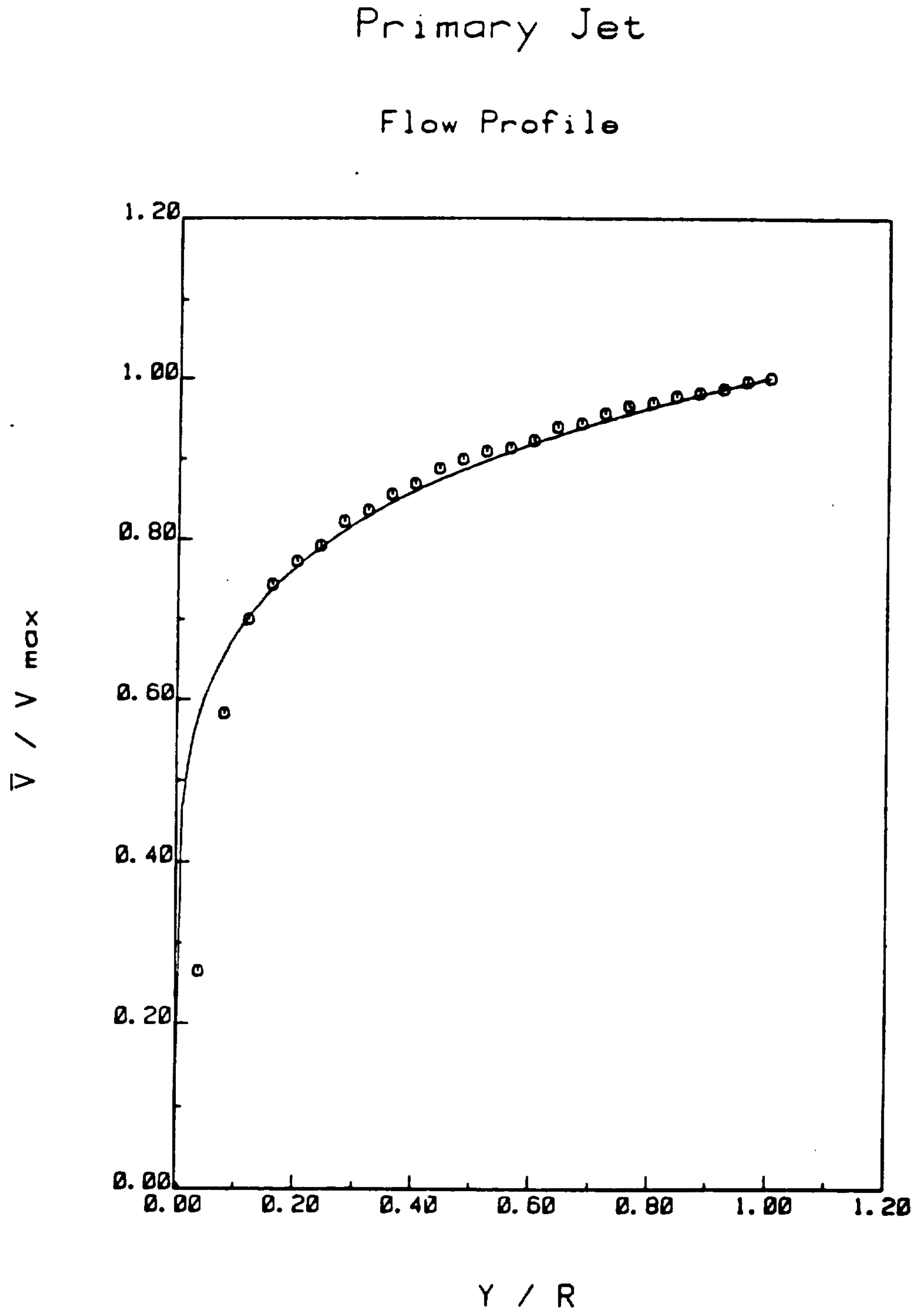

Figure A.2 Primary Jet Flow Profile

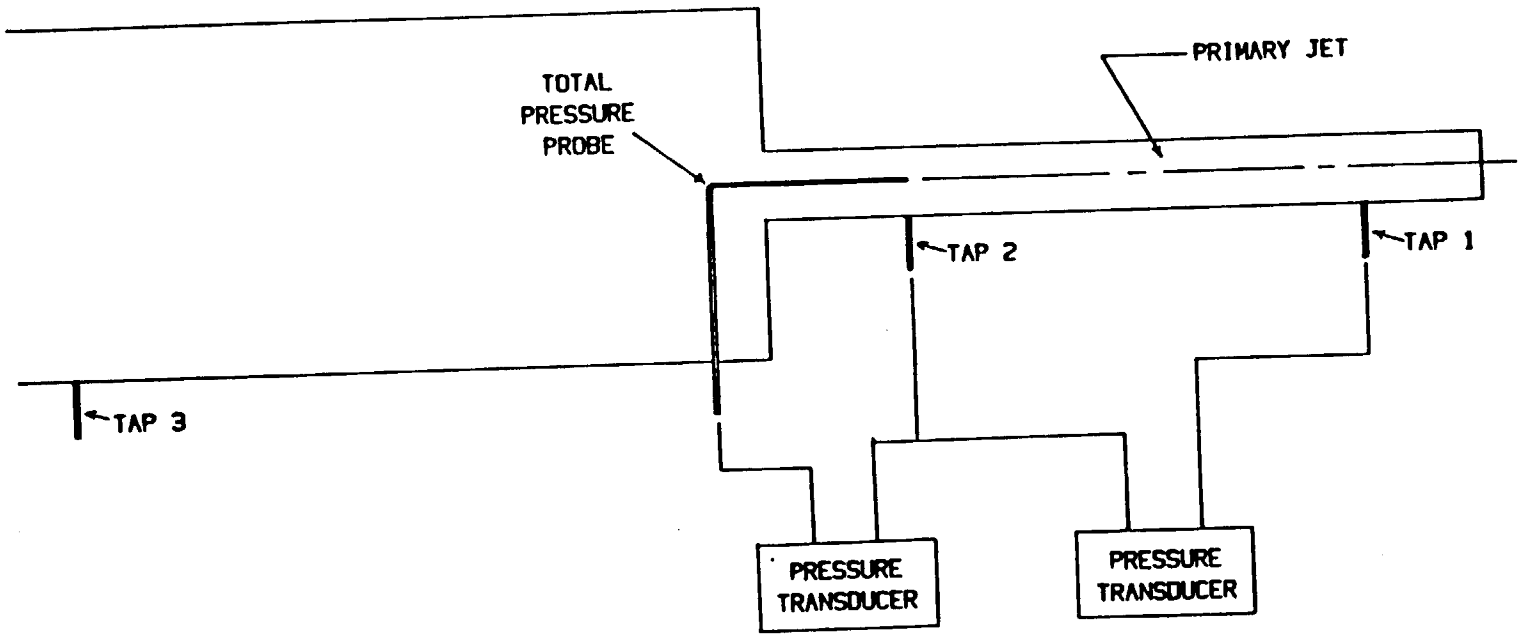

Figure A.3 Pressure Transducer Arrangement for Mass Flow Calibration of Primary Jet

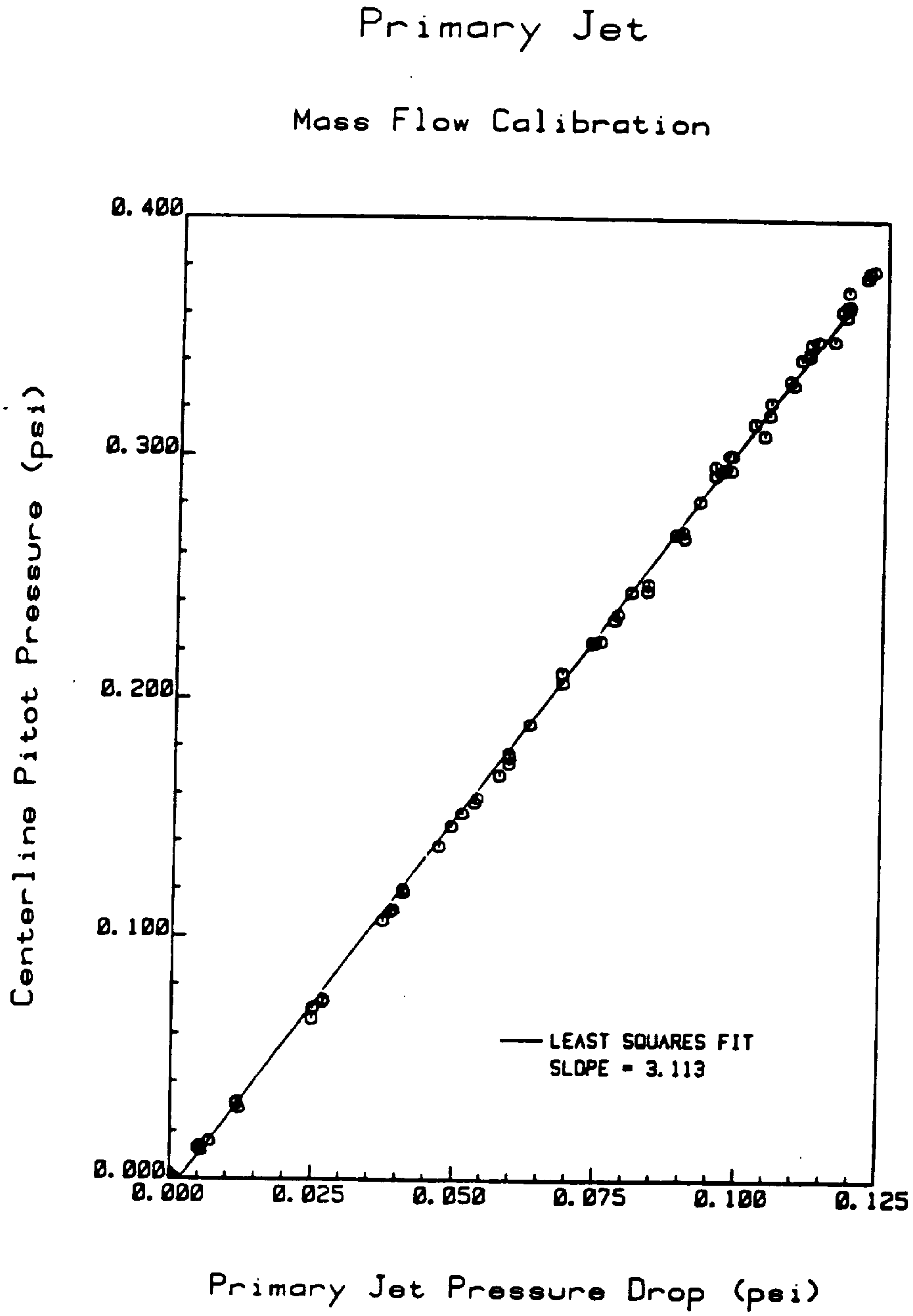

Figure A.4 Mass Flow Calibration Plot for Primary Jet

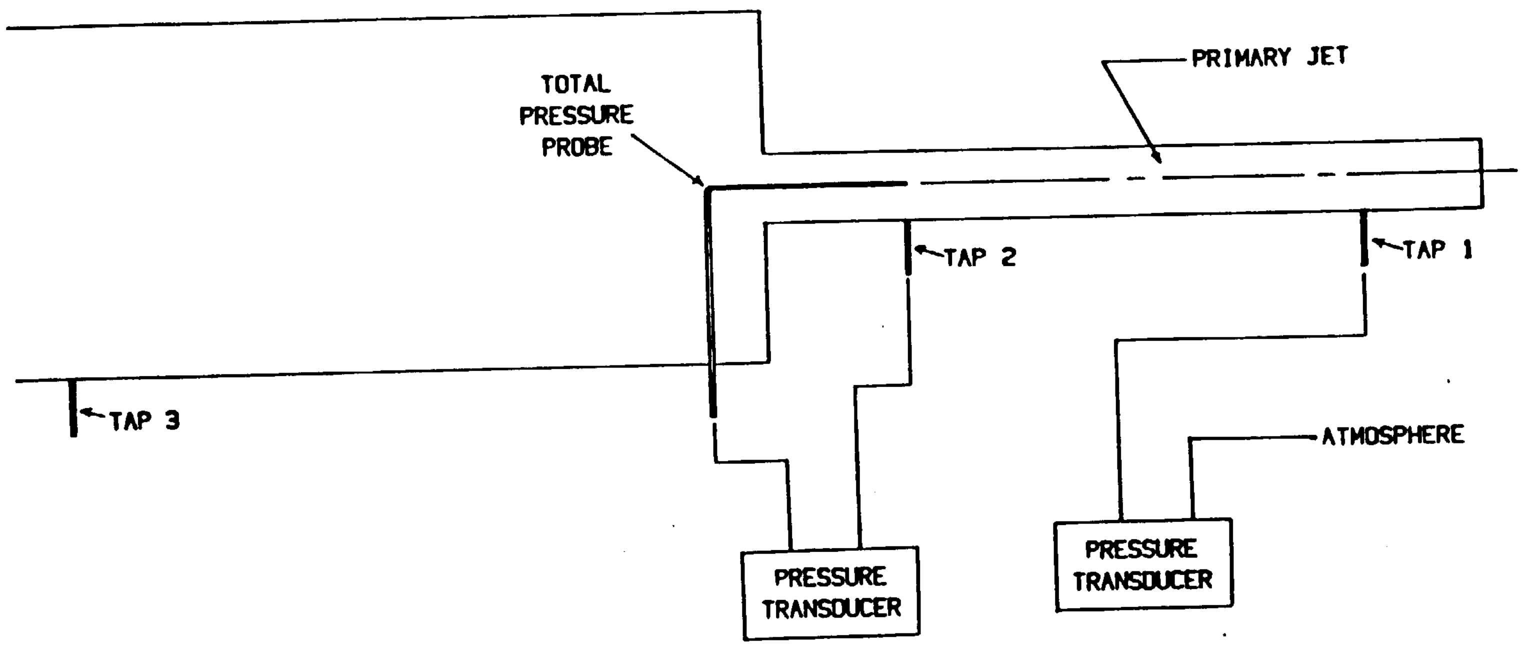

Figure A.5 Pressure Transducer Arrangement for Measurement of Primary Jet Inlet Loss

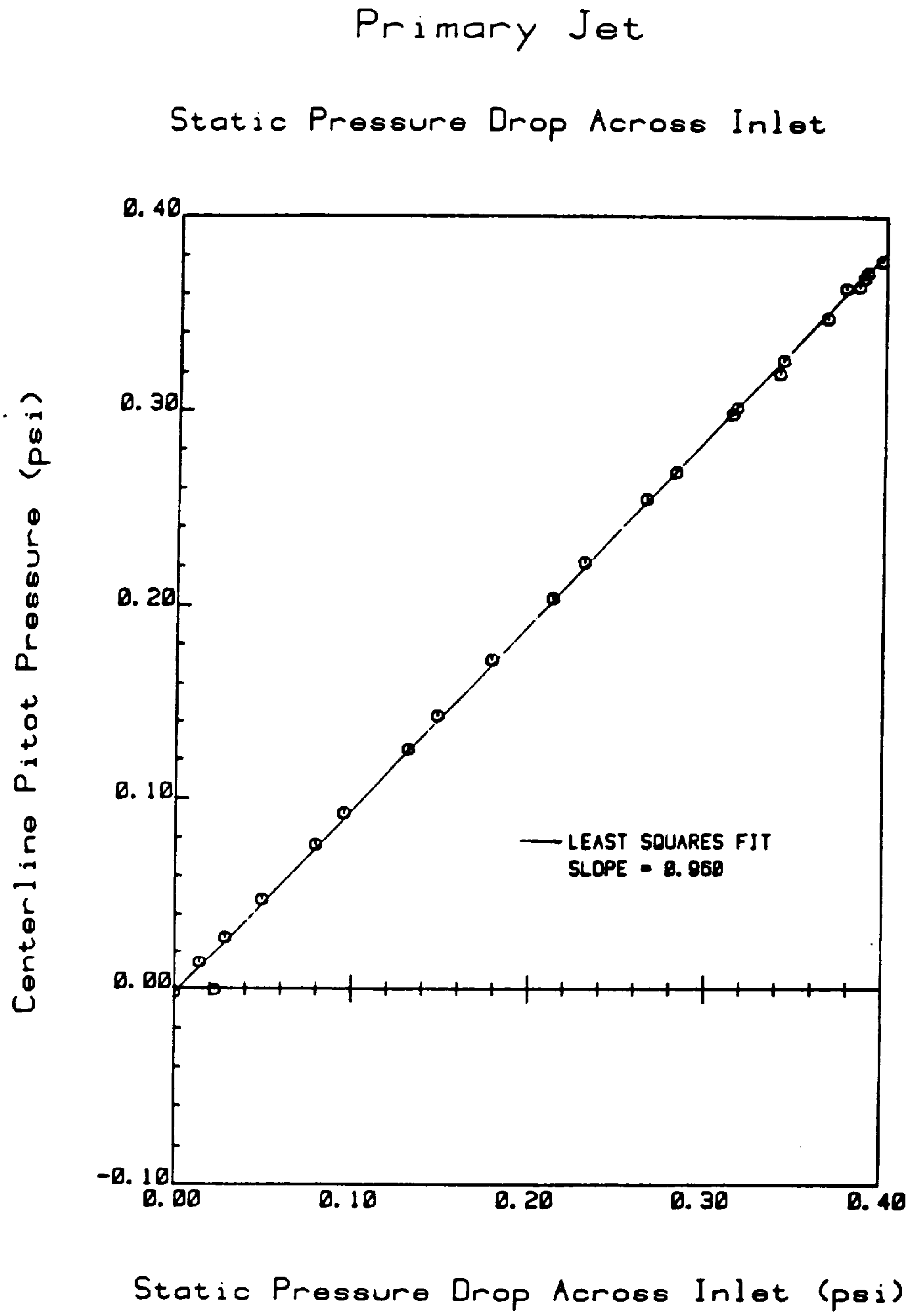

Figure A.6 Plot of Primary Jet Inlet Pressure Loss

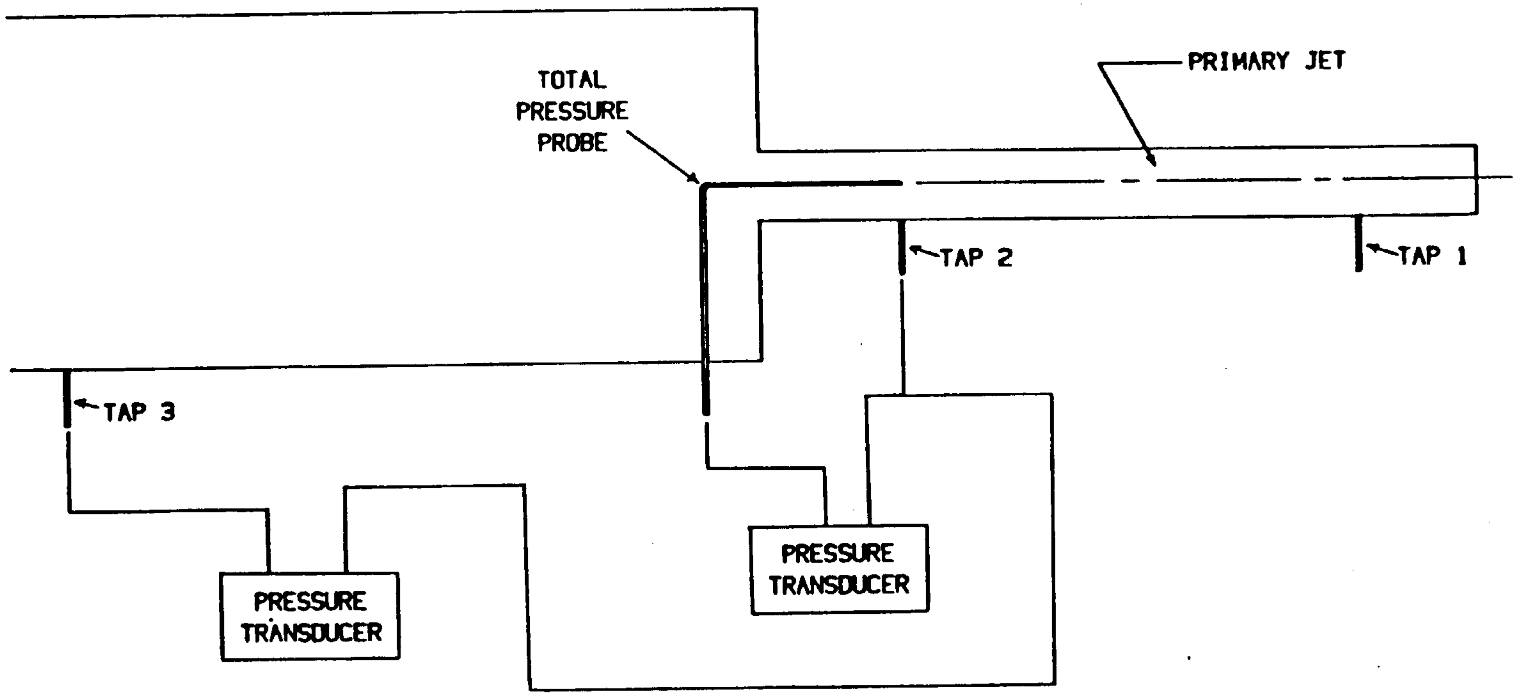

Figure A.7 Pressure Transducer Arrangement for Measurement of Primary Jet Exit Loss

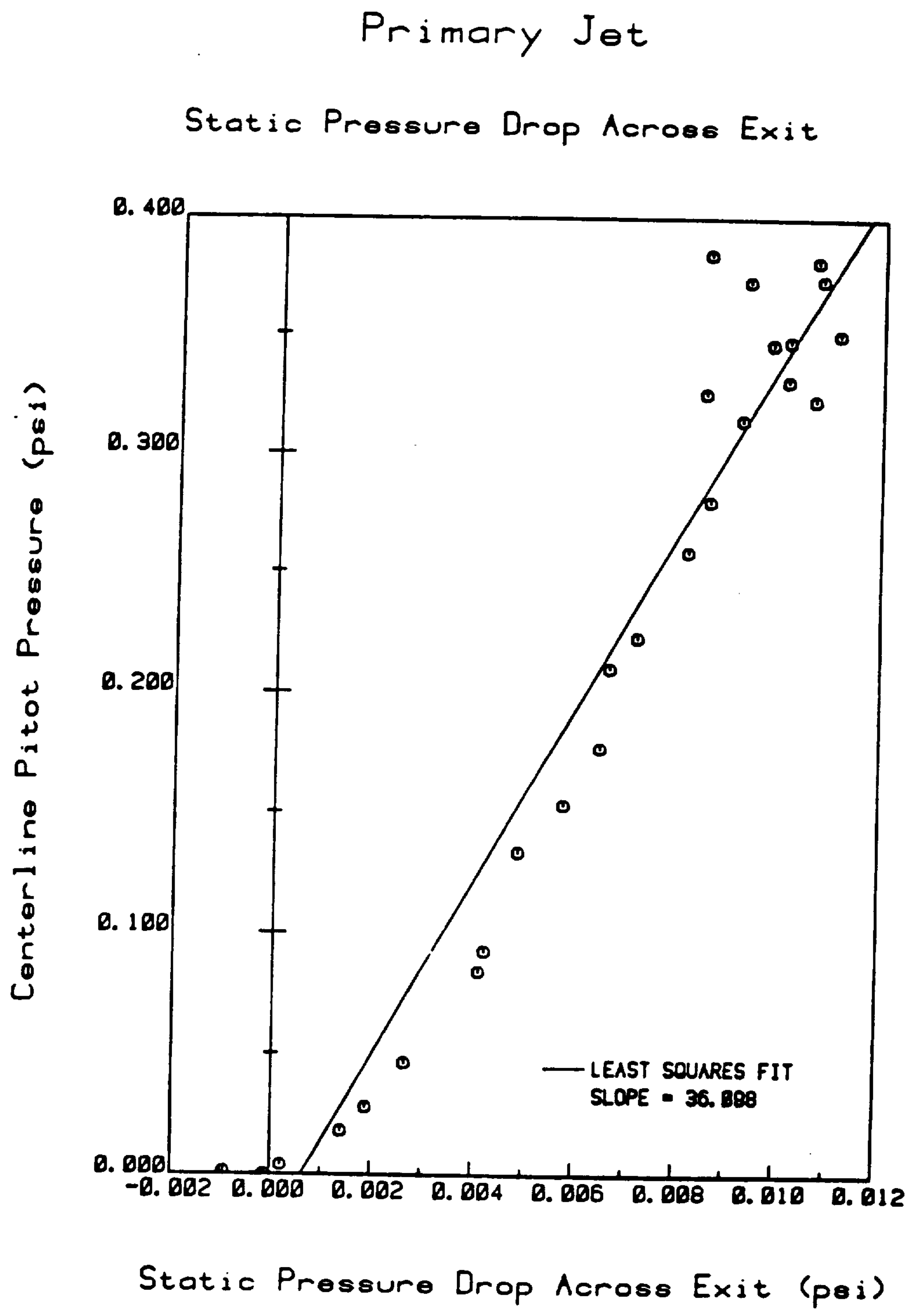

Figure A.8 Plot of Primary Jet Exit Pressure Loss

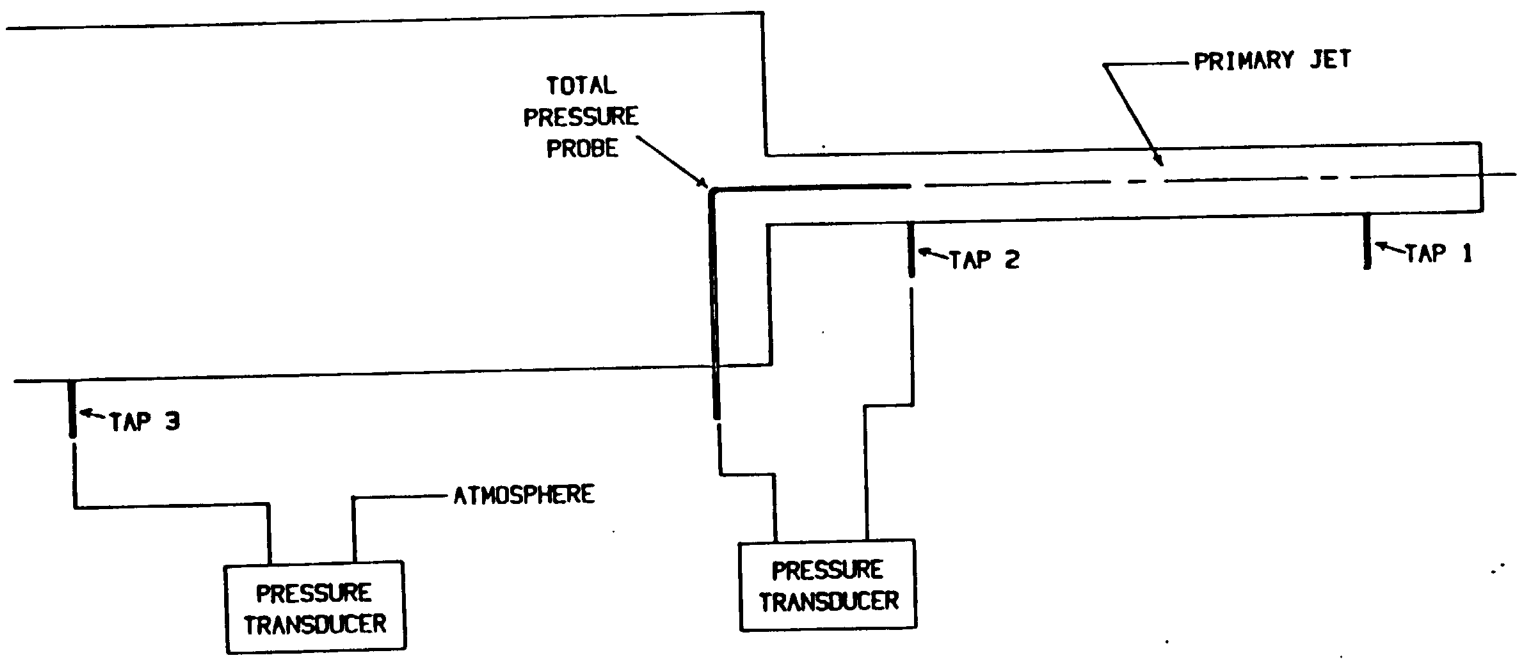

Figure A.9 Pressure Transducer Arrangement for Measurement of Primary Jet Pressure Loss

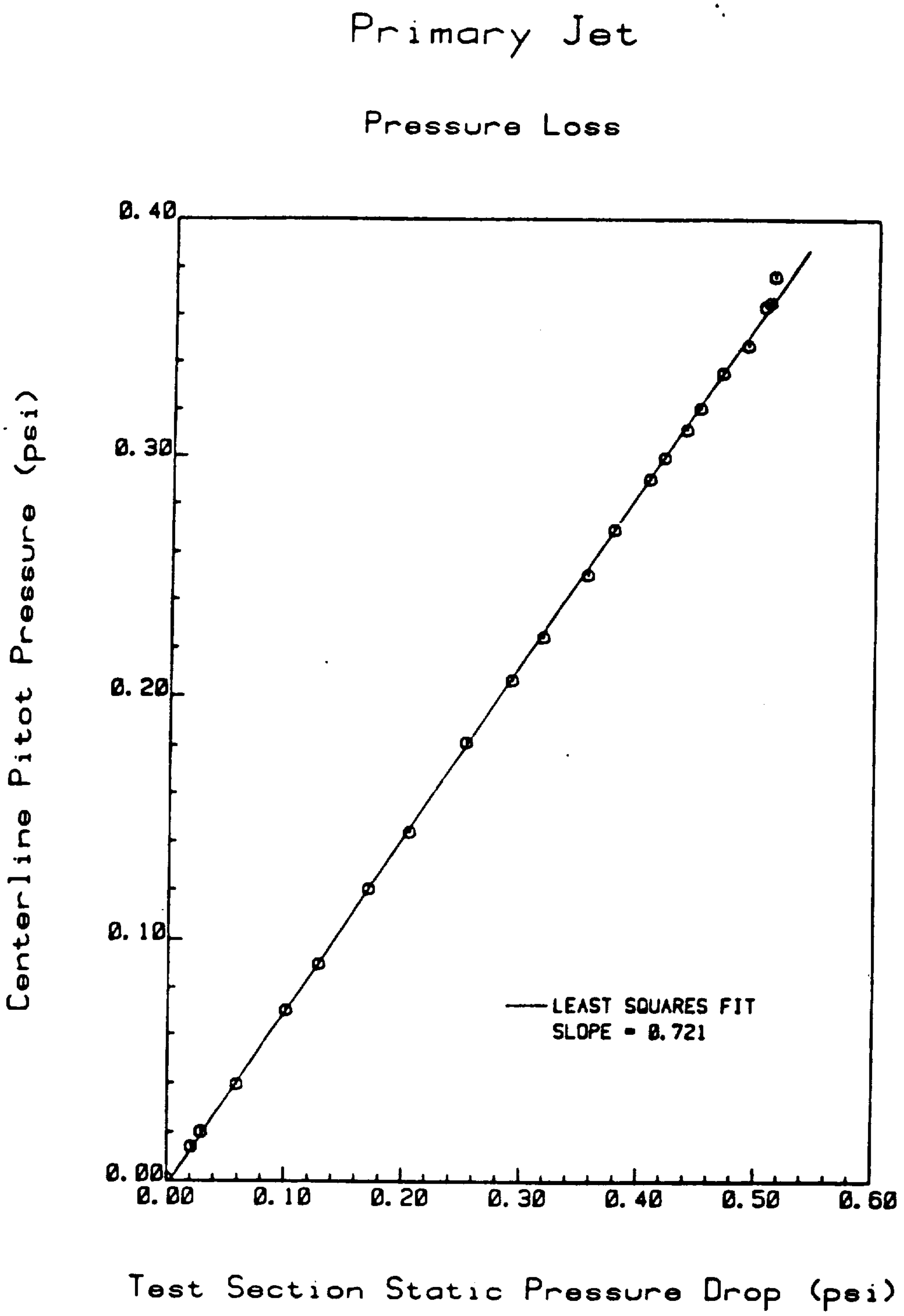

Figure A.10 Plot of Primary Jet Pressure Loss

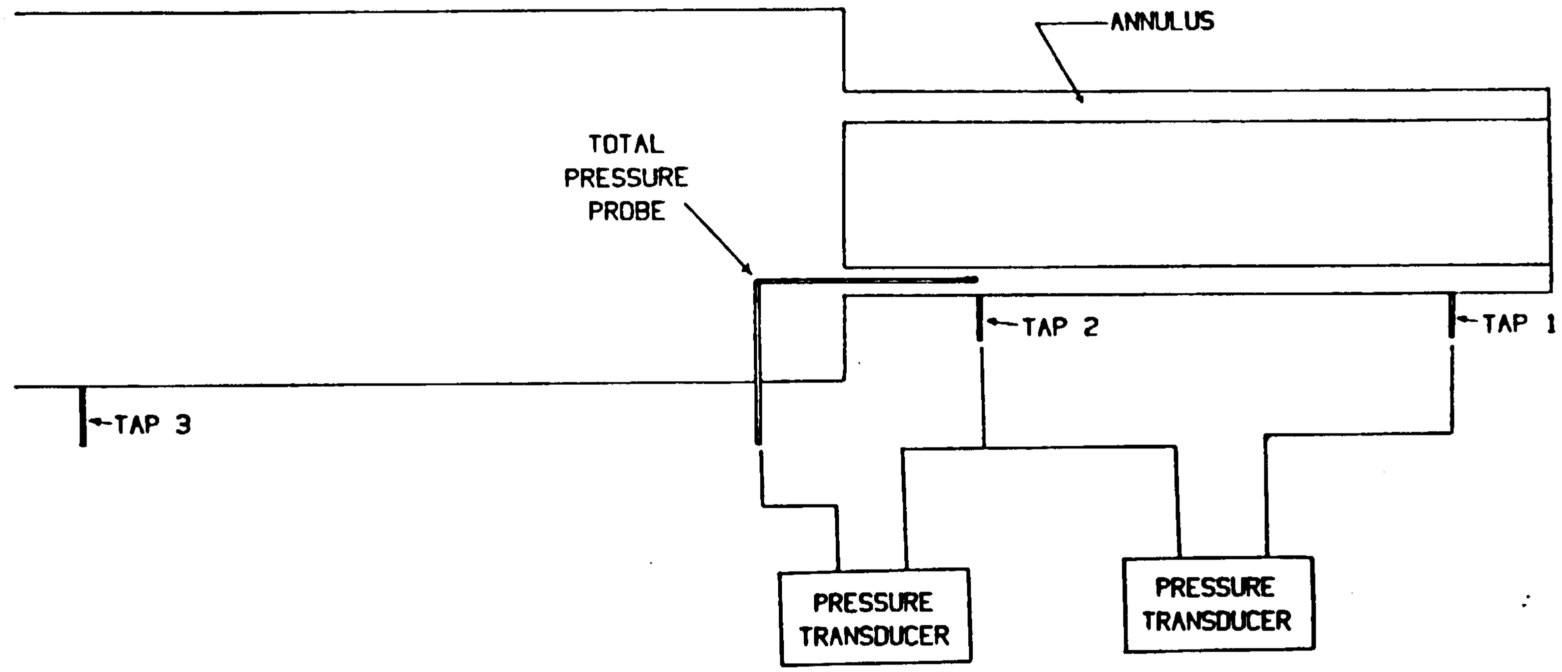

Figure A.11 Pressure Transducer Arrangement for Mass Flow Calibration of Annular Pipe

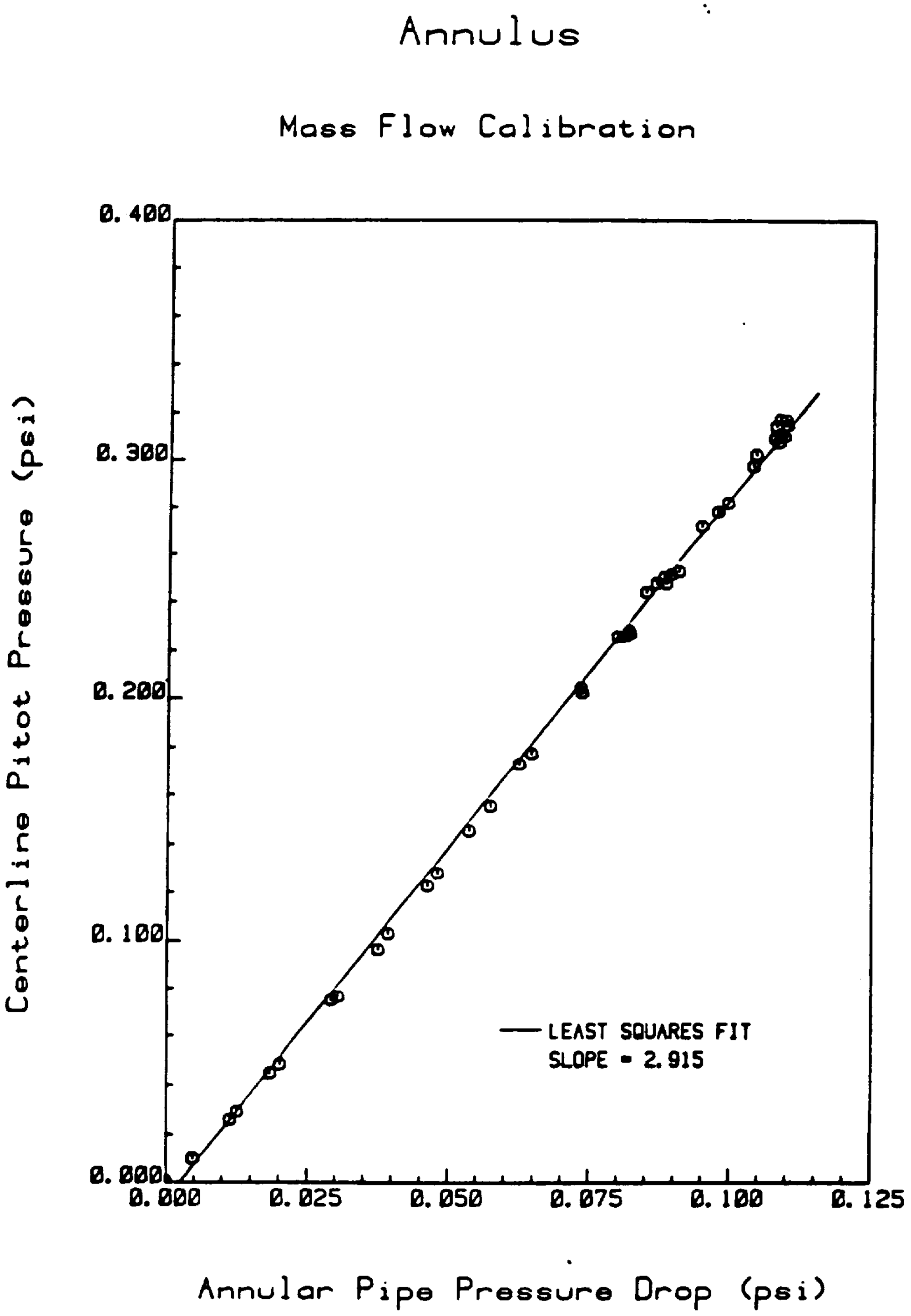

Figure A.12 Mass Flow Calibration Plot for Annular Pipe

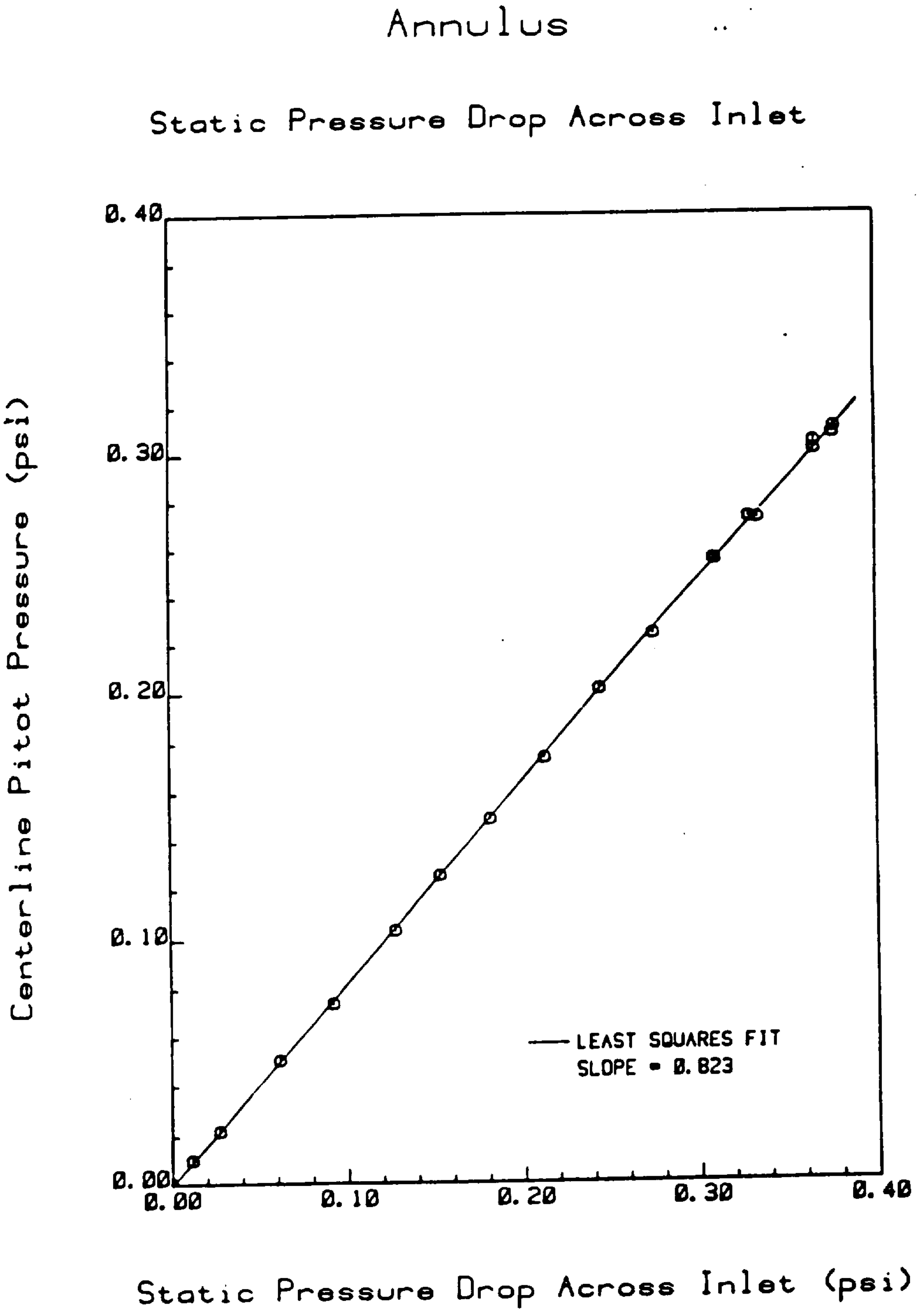

Figure A.13 Plot of Annular Pipe Inlet Pressure Loss

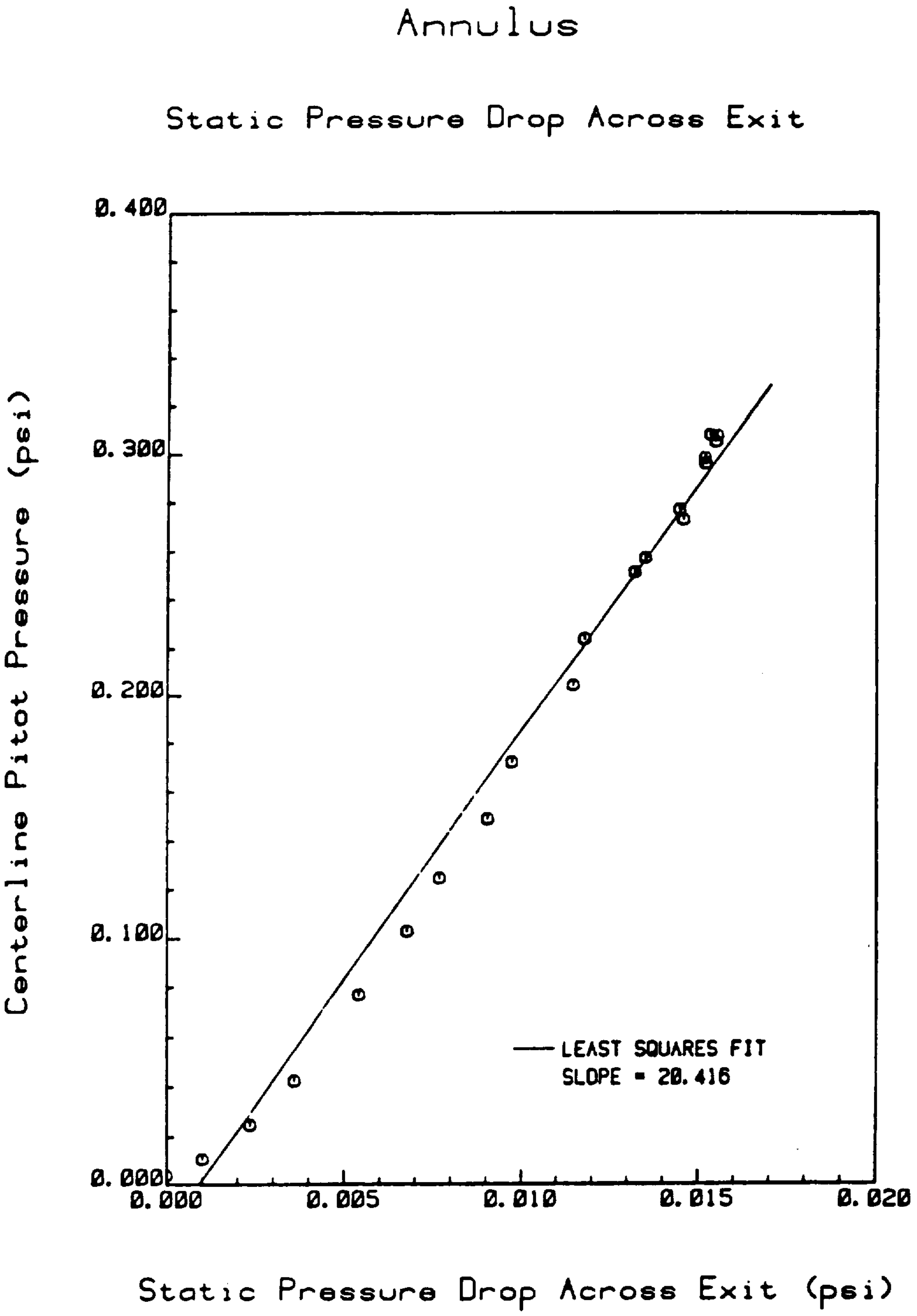

Figure A.14 Plot of Annular Pipe Exit Pressure Loss

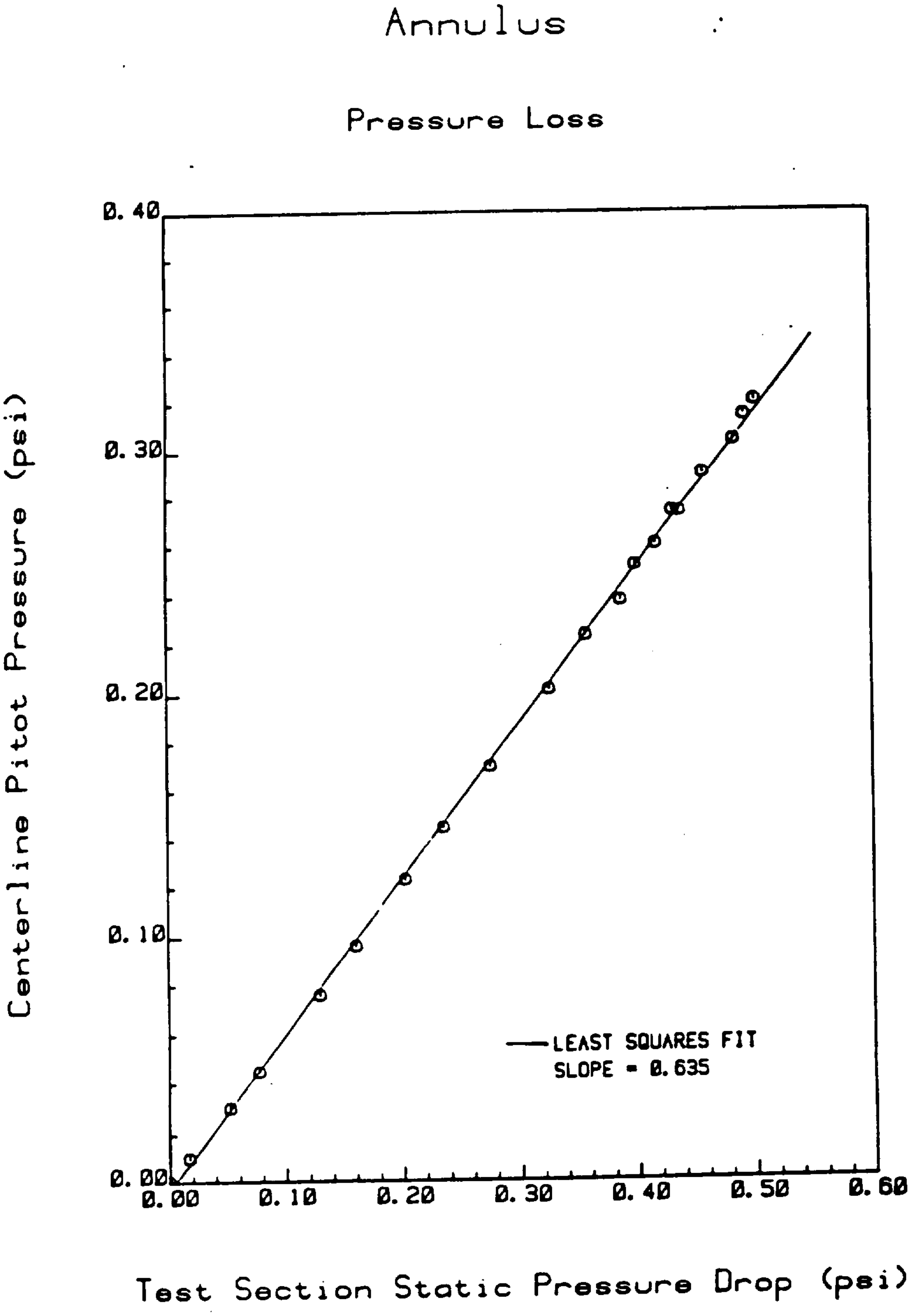

Figure A.15 Plot of Annular Pipe Pressure Loss

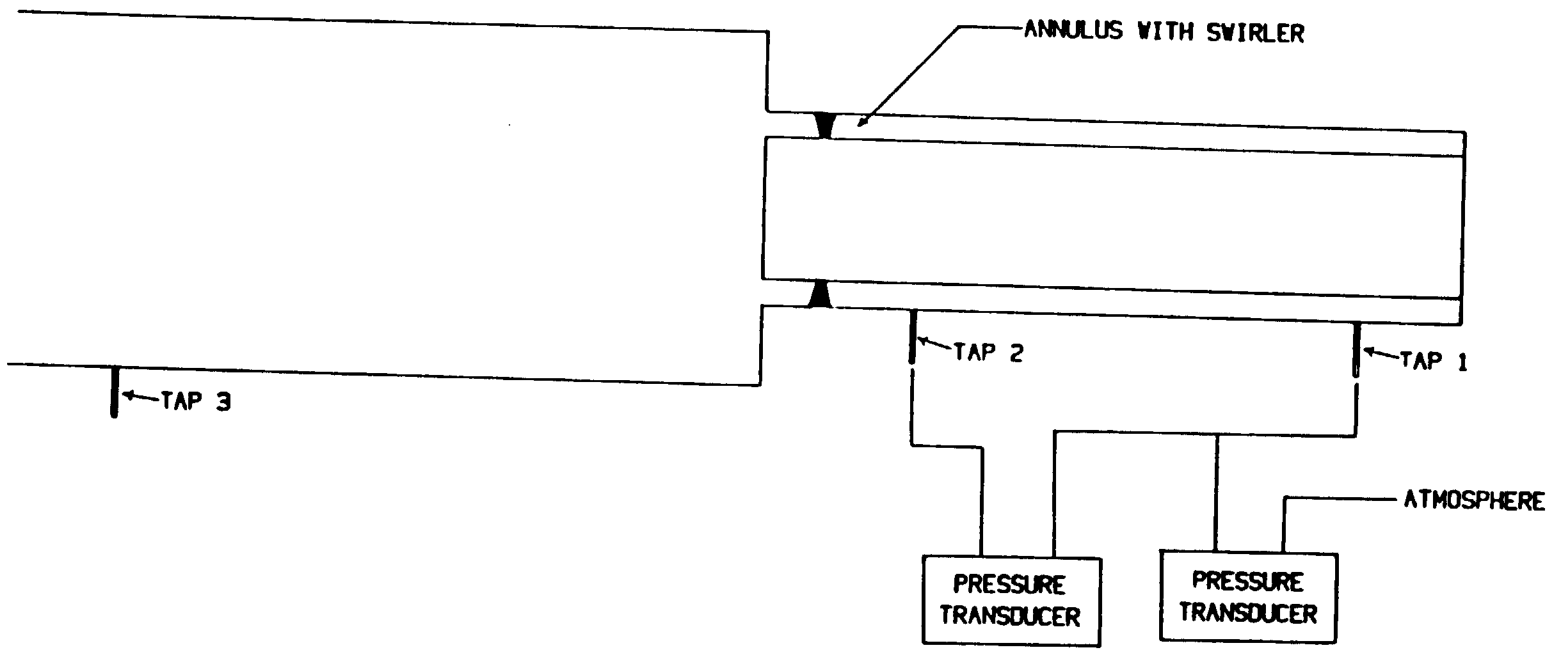

Figure A.16 Pressure Transducer Arrangement for Measurement of Swirler Inlet Loss

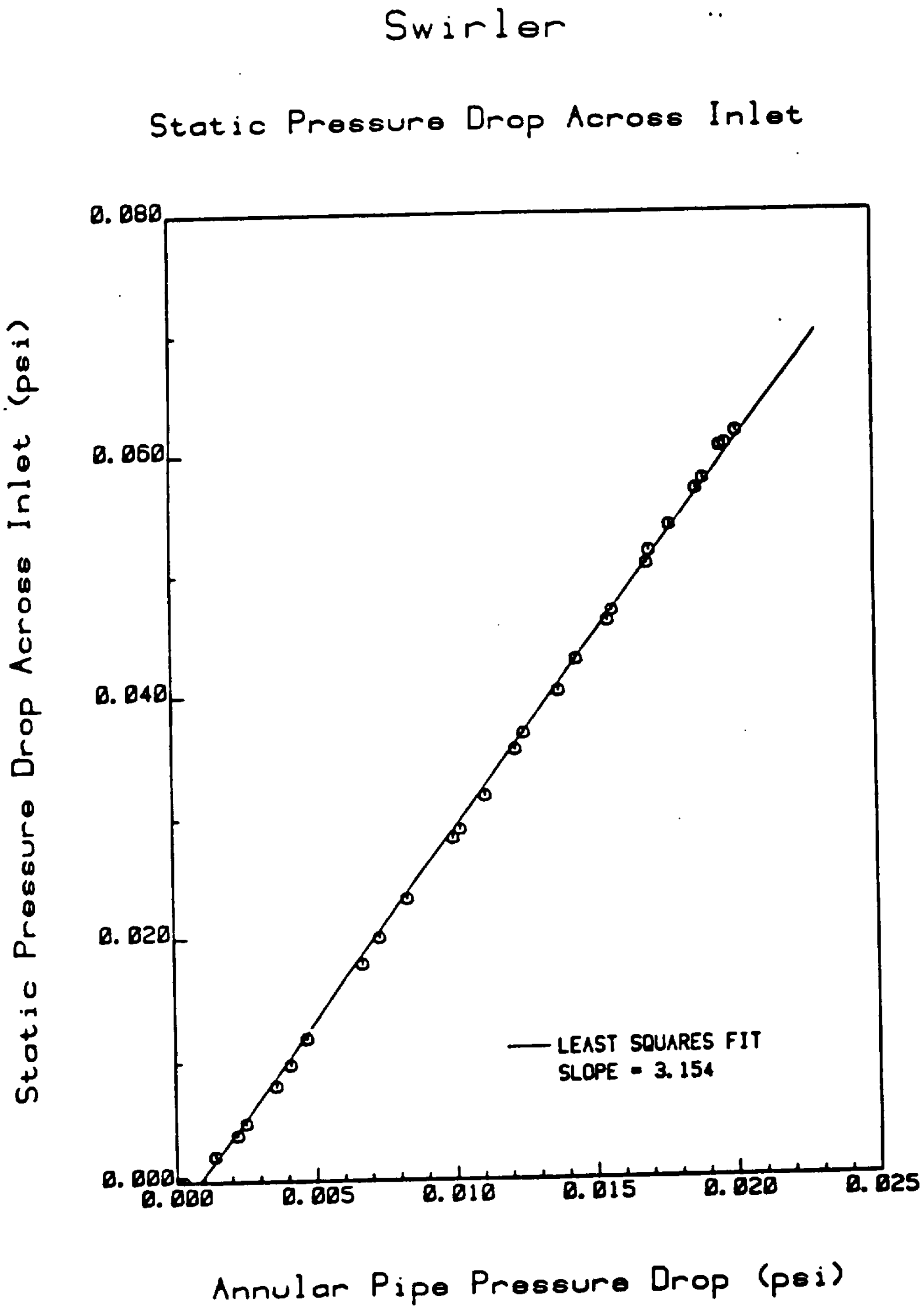

Figure A.17 Plot of Swirler Inlet Pressure Loss

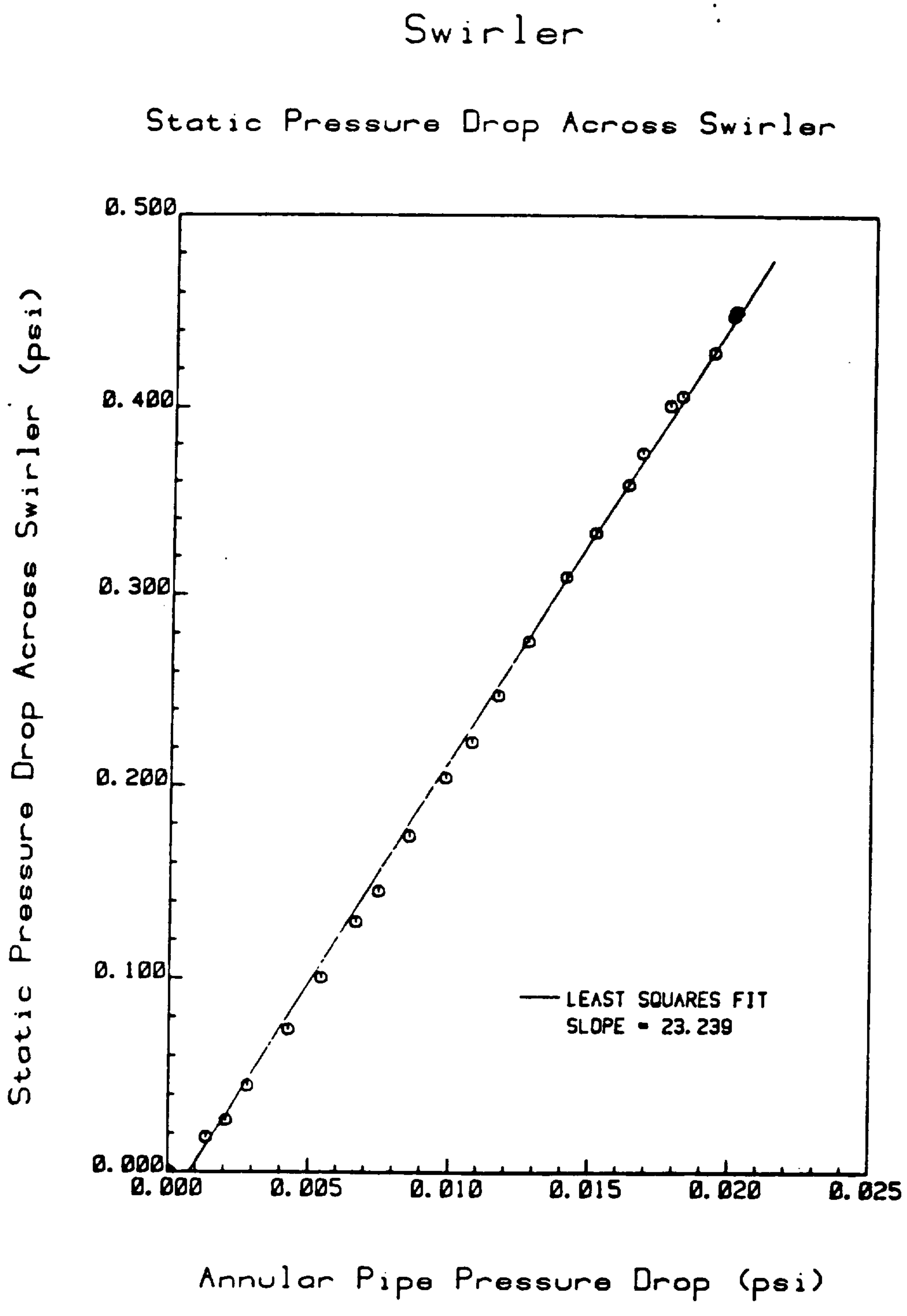

Figure A.18 Plot of Pressure Loss Across Swirler

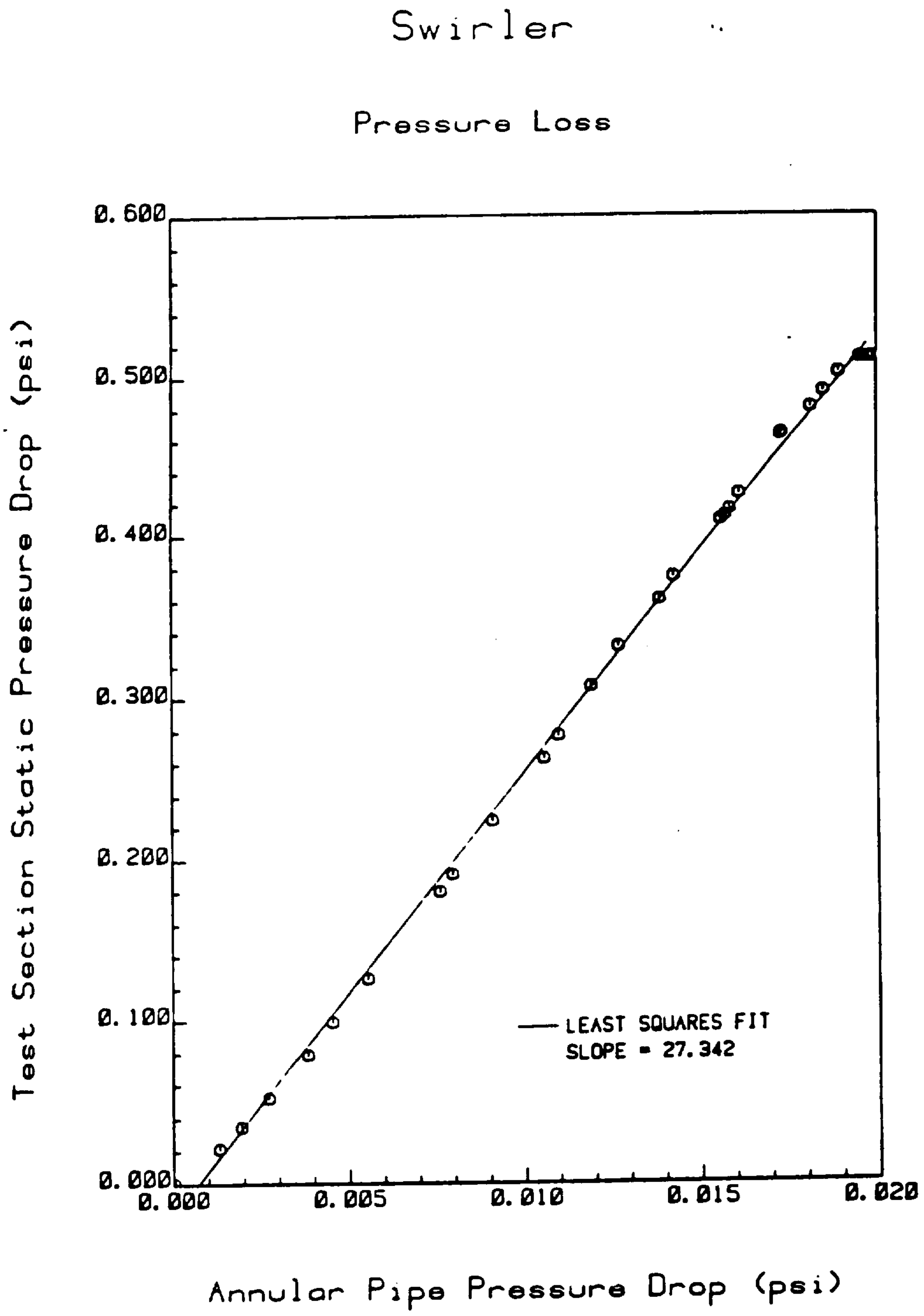

Figure A.19 Plot of Swirler Pressure Loss

REPORT DOCUMENTATION PAGE

Form Approved
OMB No. 0704-0188

1. AGENCY USE ONLY *(Leave blank)*

2. REPORT DATE
September 1996

3. REPORT TYPE AND DATES COVERED
Final Contractor Report

4. TITLE AND SUBTITLE
LDV Measurements in an Annular Combustor Model

5. FUNDING NUMBERS
WU–505–62–21
C–NAS3–24350

6. AUTHOR(S)
Dean A. Barron

7. PERFORMING ORGANIZATION NAME(S) AND ADDRESS(ES)
Purdue University
West Lafayette, Indiana 47907

8. PERFORMING ORGANIZATION REPORT NUMBER
E–9865

9. SPONSORING/MONITORING AGENCY NAME(S) AND ADDRESS(ES)
National Aeronautics and Space Administration
Lewis Research Center
Cleveland, Ohio 44135–3191

10. SPONSORING/MONITORING AGENCY REPORT NUMBER
NASA CR–182207

11. SUPPLEMENTARY NOTES

This report was submitted as a thesis in partial fulfillment of the requirements for the degree Master of Science in Aeronautics and Astronautics to Purdue University, West Lafayette, Indiana. Project Manager, J. Holdeman, Internal Fluid Mechanics Division, NASA Lewis Research Center, organization code 2650, (216) 433–5846.

12a. DISTRIBUTION/AVAILABILITY STATEMENT
Unclassified - Unlimited
Subject Category 07

This publication is available from the NASA Center for Aerospace Information, (301) 621–0390.

12b. DISTRIBUTION CODE

13. ABSTRACT ***(Maximum 200 words)***

This thesis covers the design and setup of a LDV system used to take velocity measurements in an annular combustor model. The annular combustor model is of contemporary design using 60 degree flat vane swirlers, producing a strong recirculation zone. Detailed measurements are taken of the swirler inlet air flow and of the downstream enclosed swirling flow. The laser system used is a two color, two component system set up in forward scatter. Detailed are some of the special considerations needed for LDV use in the confined turbulent flow of the combustor model. LDV measurements in a single swirler rig indicated that the flow changes radically in the first duct height. After this, a flow profile is set up and remains constant in shape. The magnitude of the velocities gradually decays due to viscous damping.

14. SUBJECT TERMS
Turbulent viscous flow; Laser diagnostics; LDV; Velocity measurements; Annular combustor; Swirler

15. NUMBER OF PAGES
159

16. PRICE CODE
A08

17. SECURITY CLASSIFICATION OF REPORT
Unclassified

18. SECURITY CLASSIFICATION OF THIS PAGE
Unclassified

19. SECURITY CLASSIFICATION OF ABSTRACT
Unclassified

20. LIMITATION OF ABSTRACT

NSN 7540-01-280-5500

Standard Form 298 (Rev. 2-89)
Prescribed by ANSI Std. Z39-18
298-102